THERMODYNAMICS OF METAL BINDING TO LIGAND-MODIFIED PNA

By

Zhijie Ma

A dissertation submitted in partial fulfillment of the requirements for the degree of

Doctor of Philosophy in Chemistry

Carnegie Mellon University

Pittsburgh, Pennsylvania

Feb 2011

ABSTRACT

"Thermodynamics of Metal Binding to Ligand-Modified PNA"

by Zhijie Ma

Advisor: Professor Catalina Achim

The research in this dissertation is about investigation of steric effect on the stablility of metal-containing peptide nucleic acid (PNA); thermodynamcs of metal binding to ligand-modified PNA studied by Isothermal titration calorimetry (ITC); incorporation of metal in 2,2'-bipyridine(Bpy) modified PNA triplexes and structural characterization of copper complexed 8-hydroxyquinoline (Q) modified PNA. All these research are necessary to further understand the coordination chemistry in PNA context, in comparison with the corresponding coordination of metal and simple ligand for the construction of hybrid inorganic-nucleic acid nanostructures.

The steric effect of ligand can be understood by using similar ligands that carry the same metal binding site, namely 8-hydroxyquinoline, but are attached differently to the PNA backbone and having incorporated them into PNA duplexes. We conclude that the incorporation of a metal complex with high stability constant into a PNA duplex is not a sufficient condition for the formation of stable hybrid metal-nucleic acid duplexes and that the steric relationship between the complex and the duplex must be considered in the design of metal-containing alternative base pairs.

Thermodynamic parameters of metal ions with ligand-containing PNA including Cu^{2+} with Q-PNA, Ni^{2+} and Cu^{2+} with Bpy-PNA have been studied by ITC. This study established that the previously proposed supramolecular chelate effect on metal binding to PNA duplexes exists and it is entropy-driven. Another major factor that influences

the binding affinity of ligand-containing PNA for transition metal ions is the steric interaction between the metal complex and the PNA. In addition, the sequence of the PNA, the base pair mismatches, and the position of ligands in the PNA also influence the stability constants of metal complexes formed with ligand-modified PNAs.

The incorporation of metal ions in PNA triplexes is observed and confirmed by spectroscopic methods and mass spectrometry. The formations of Ni-tsPNA and Co-tsPNA are stable. Electron paramagnetic resonance(EPR) results show that in the PNA triplex, the coordination environment of Cu^{2+} is similar to those of $[Cu(Bpy)_3]^{2+}$ or trans-$[Cu(Bpy)_2]^{2+}$.

A crystal structure of a 9-base pair PNA with a central Q ligand modification is obtained in the presence of excess Cu^{2+}. Due to the unfavorable condition of crystallization at pH 4.0 and with excess Cu^{2+}, metal coordination is outside the PNA duplex. An unusual Cu trinuclear cluster bridges two duplexes and excess Cu^{2+} is coordinated to terminal nucleobases. The similarity between the EPR parameters for the $[CuQ_2]$ complexes with 8-hydroxyquinoline and ipdq precluded us from distinguishing between the possible cis- or trans-geometry of the complex formed by Cu^{2+} with Q-modified PNA duplexes.

Future research includes investigation of thermodynamics by differential scanning calorimetry (DSC); analysis of kinetics of ITC results and identification of the intermediates; further characterization of the right-handed PNA induced by hydrogen bonding and structural characterizations of metal-containing PNA.

Acknowledgement

First, I have to thank to my advisor Dr. Achim, who is a great mentor, always offers to help me with my research and give me useful advices especially I was new in the lab.

Second, I have to thank to my committee members, Dr. Ly and Dr. Hendrich. Dr. Ly is an expert in bioorganic chemistry and helped me with the organic chemistry of nucleic acids. Dr. Hendrich is an expert in EPR spectrospcopy and gave me some useful feedbacks about my research. I have to thank to Dr. Waldeck to serve as my thesis committee member and Dr. Jin as my research proposal committee. Both of them gave me some advices concerning my thesis and my proposal.

Finally, I have to appreciate Joshua and Rupal for helping me take all the EPR spctra. I have to thank all Achim group members including Richard, Wei, Silvia, Arnie, Jing, Meimei, Kurt, Andrew, Gorana, Priyanka for their help in the past few years and all the undergraduate students envolved in my research, Mark and Frank for the ITC project, Andy for the triplex project and Avanti for some organic synthesis. In addition, I also need to thank all Dr. Ly, Armitage and Das group members for their kindness to let me use their instruments and Susan, Lenny, Gloria for helping me with my TA.

Contents

Scheme List

Figure List

Table List

ABBREVIATIONS AND SYMBOLS

A	Adenine
Aeg	N-(2-aminoethyl) glycine
Bpy	2,2-bipyridine
C	Cytosine
CD	Circular Dichroism
DNA	Deoxyribonucleic Acid
DSC	Differential Scanning Calorimetry
ds	Double Stranded
EPR	Electron Paramagnetic Resonance (Spectroscopy)
ESI	Electrospray Ionisation (Mass Spectrometry)
G	Guanine
GNA	Glycol Nucleic Acid
HPLC	High-performance Liquid Chromatography
ipdq	2,2'-isopropylidenedi-8-quinolinol
ITC	Isothermal Titration Calorimetry
LNA	Locked Nucleic Acid
MALDI	Matrix-assisted laser desorption/ionization Time of Flight
NMR	Nuclear magnetic resonance
PNA	Peptide Nucleic Acid
Py	Pyridine
Q	8-Hydroxyquinoline
RNA	Ribonucleic Acid
SPR	Surface Plasmon Resonance
ss	Single Stranded
T	Thymine
TFA	Trifluoroacetic Acid
TFMSA	Trifluoromethanesulfonic Acid
Tm	Melting Temperature
ts	Triple Stranded
UV-Vis	Ultraviolet-Visible

Chapter 1 Introduction

1.1 Metal-containing ligand-modified PNA

The interaction between nucleic acids and transition metal ions can be used to create molecules that have potential applications in nano- and bio-technology and molecular electronics.[1-3] One of the strategies for the incorporation of metal ion in nucleic acid duplexes was first proposed by Tanaka and Shionoya in 1999.[4] In this strategy, natural nucleobases are replaced by ligands having a higher affinity for metal ions than natural nucleobases do (Figure 1.1). The metal complexes formed with the ligands within the duplexes play the role of metal-mediated alternative base pairs. If the ligands are aromatic and the geometry of the complex is planar, the complex can have π stacking interactions with the adjacent base pairs. This strategy makes possible the incorporation of metal ions at specific positions in a nucleic acid duplex as well as the creation of arrays of different metal ions within the duplex. In the last decade, numerous ligands have been introduced into DNA, RNA and peptide nucleic acid (PNA) oligomers and a variety of metal ions have been incorporated into the ligand-modified duplexes formed by these oligomers.[2]

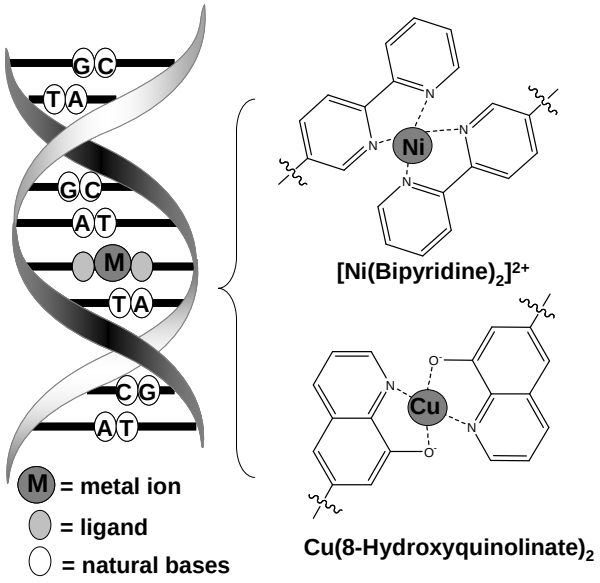

Figure 1.1. Cartoon representation of a metal-containing, ligand-modified nucleic acid duplex

The research in Achim lab is focused on using PNA as a scaffold for metal ions. In our past research, transition metal ions such as Ni^{2+}, Co^{2+} and Cu^{2+} have been incorporated into 2,2'-bipyridine- (**Bpy**) or 8-hydroxyquionline- (**Q**) modified PNA duplexes (Figure 1.1).[5-7] Our previous studies identified two major factors that affect the stability of the metal-containing PNA. One factor is the stability constant of the complexes formed by metal ions with the ligands incorporated in PNA. For example, the melting temperatures of **Bpy**-containing PNA duplexes with different metal ions correlated with the stability constants of the complexes of metal ions with free **Bpy** ligands.[5] Given the empirical relationship between stability of metal complexes and the stability of nucleic acid duplexes in which ligands have been incorporated,[8] ligands with high affinity for the metal ions have been consistently chosen in the design of metal-containing nucleic acids. Our studies have indicated that the counterpart of the aforementioned relationship is the effect of the duplex on the stability constants of the nucleic acid-incorporated, metal complexes. Specifically, a duplex-induced, supramolecular chelate effect influences the strength of the interaction between the metal ions and the ligands introduced in the nucleic acid structures. For example, the stability constants of complexes of Ag^+ with pyridine (**Py**) are very small and an $[Ag(\mathbf{Py})_2]^+$ complex does not form in solutions containing micromolar concentrations of Ag^+ and **Py**.[8] Nevertheless, in the same concentration range, a $[Ag(\mathbf{Py})_2]^+$ complex formed within DNA duplexes that contained a pair of **Py** in complementary positions. This result can be attributed to a duplex induced supramolecular chelate effect.[9]

We also found that another factor that influences the effect of a metal complex on the stability of the duplex is the position where the ligands are introduced in nucleic acid duplexes. Specifically, metal-containing PNA duplexes with a **Bpy** modification close to the end of the duplex showed significantly higher thermal stability than the duplexes in which the **Bpy** ligands were situated at the center of the duplex. We attributed this effect to the fact that the terminal base pairs have a higher tendency of fraying than the central ones.

In addition to these two factors, the steric interaction between the metal complex formed in the duplex and the rest of the duplex, mostly the adjacent nucleobase pairs, is likely to significantly influence the thermal stability of metal-containing PNA. For example, the increase in the thermal stability of 8-hydroxyquinoline-modified PNA duplexes upon coordination of Cu^{2+} to 8-hydroxyquinoline was very different when the ligands were introduced in PNAs with comparable length but different sequences.

1.2 Nucleic Acid Analogues

In the past twenty years, several nucleic acids analogues such as peptide nucleic acid (PNA), locked nucleic acid (LNA) and glycol nucleic acid (GNA) have been discovered (Figure 1.2). Some of these analogues form heteroduplexes with DNA and RNA that are more stable than homoduplexes of DNA or RNA.[2] The increased stability of the heteroduplexes makes the analogues excellent candidates for nucleic acid-based nanotechnology and biomedical applications.

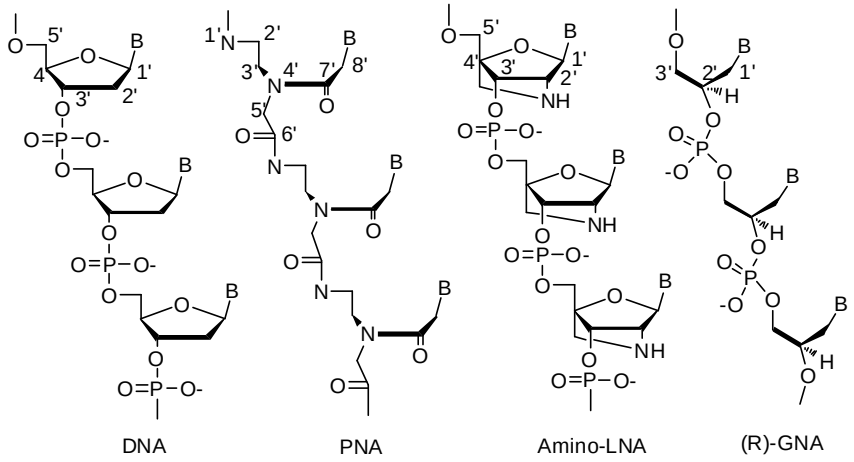

Figure 1.2. DNA and DNA analogues with different backbones

PNA, which was developed in 1991, is one of the most successful synthetic analogues of DNA.[10] PNA exhibits a higher affinity for DNA and RNA than DNA or RNA themselves because PNA has a neutral backbone based on N-(2-aminoethyl)-glycine (Aeg), and consequently, there is no electrostatic

repulsion between the two strands of heteroduplexes formed with PNA. It is noteworthy that PNA's pseudopeptide backbone makes PNA resistant to degradation by enzymes such as nuclease.[11] All these advantages make PNA a good candidate for construction of functional nanostructures.

The X-ray crystal structure of a palindromic 6mer PNA duplex showed that the PNA duplex adopts a unique, P-form helical structure which resembles that of A-DNA but has different helical parameters.[12] Recently, we have reported the solution structure and the crystal structure of a palindromic 8-base pair PNA duplex, both of which adopt also a P-type helical structure.[13,14] We have also reported the crystal structure of a PNA duplex with **Bpy** modifications.[14] In this structure, the Bpy ligands bulged out of the duplexes and formed inter-duplex π-stacked Bpy pairs that connected adjacent PNA duplexes. Three crystal structures of metal-containing, ligand-modified DNA duplexes have been reported to date. [15-17] These structures showed that the metal complexes function indeed as alternative base pairs and exert very small perturbations on the structure of the DNA duplexes.

Locked nucleic acid (LNA) is a nucleic acid analogue developed in 1998. The ribose group of the sugar phosphate backbone of LNA contains a methylene bridge between the 2'-oxygen atom and the 4'-carbon atom (Figure 1.2).[18,19] This bridge pre-organizes the LNA monomers into a locked C3'-endo conformation similar to that observed in A•type DNA and thus reduces the entropic penalty for the formation of heteroduplexes of LNA with DNA or RNA. Consequently, LNA•LNA, LNA•DNA and LNA•RNA duplexes show a substantial increase in duplex stability when compared to DNA•DNA or DNA•RNA duplexes.

Recently, Meggers et al. have synthesized a new DNA analogue with a simplified backbone. Glycol nucleic acid has an acyclic three-carbon propylene glycol phosphodiester backbone.[20,21] Variable temperature UV spectroscopy was used to demonstrate that complementary 18-mer GNA oligomers that contain T and A bases form antiparallel, helical duplexes based on Watson-Crick base

pairing. These duplexes are more stable than the corresponding DNA or RNA homoduplexes.

1.3 Thermodynamics of the Formation of Nucleic Acid Duplexes

The thermodynamics of the formation of nucleic acid duplexes has been extensively studied because it is important for the understanding of the stability of nucleic acids structures in biology and for the design of new nucleic acid structures for research and technological applications. For example, the knowledge of thermodynamic parameters is used in the design of nucleic acid sequences for PCR and therapeutics.

The focus of this thesis is on the thermodynamics of metal binding to ligand-modified peptide nucleic acids. To put our studies in context, we briefly review in this section (*a*) methods for the study of the thermodynamics of reactions involving non-modified and modified nucleic acids, (*b*) thermodynamic parameters of binding of DNA analogues to themselves or to DNA and RNA to form heteroduplexes, and (*c*) thermodynamic parameters of binding of metal ions to different types of non-modified and ligand-modified nucleic acids.

1.3.a Techniques for determination of thermodynamic parameters

The thermodynamic parameters can be determined by direct or indirect methods. The enthalpy is directly measured by calorimetric methods such as isothermal titration calorimetry (ITC) or differential scanning calorimetry (DSC).[22] In indirect methods, the equilibrium constants are measured at different temperatures and the enthalpy is calculated from the temperature dependence of the equilibrium constants using the Van't Hoff equation.[11,23,24] The methods that can be used to determine equilibrium constants are fluorescence and UV/vis,[25] CD,[26] and NMR spectroscopy,[27] surface plasmon resonance (SPR),[28] analytical ultracentrifugation (AUC), stopped-flow[29] and radio-ligand binding assay[30]. Among them, the most widely used method to measure the equilibrium constant for the Watson-Crick hybridization of single stranded (ss) nucleic acid

duplexes into (ds) double stranded duplexes is by variable temperature UV spectroscopy that provides melting curves for the duplexes.[11,23,24] The melting curves have usually sigmoidal shape. Assuming that the duplex melting is a two-state process and if the heat capacity is temperature independent, one can apply the Van't Hoff equation to obtain the melting temperature (T_m) and the enthalpy and entropy change for the duplex formation. It should be noted the use of Van't Hoff equation to calculate enthalpy has some assumptions such as the independence of heat capacity with temperature and the binding being two-state process.

1.3.b Thermodynamics of the Formation of Nucleic Acid Duplexes

PNA can form PNA•PNA homoduplexes as well as PNA•DNA and PNA•RNA heteroduplexes. DNA·DNA duplexes have melting temperatures that are 7-20° lower than the melting temperatures of PNA·DNA duplexes with the same sequence. At low to medium salt concentration, the melting temperature of DNA•DNA and PNA•DNA duplexes is affected by the buffer concentration due to the negatively charged backbone of DNA.[31] In contrast, the melting temperature of PNA•PNA duplexes is not affected by the buffer concentration.

Thermodynamic parameters for the hybridization of DNA•DNA and PNA•PNA homoduplexes, and DNA•PNA heteroduplexes have been determined for the first time by Nielsen and coworkers by UV or fluorescence melting curves and ITC titrations.[32] The thermodynamic parameters determined indirectly by UV melting curves are consistent with those determined directly by ITC calorimetry. This agreement confirms that the dissociation of PNA duplexes is a two-state process. The thermodynamic parameters determined from fluorescence melting curves are slightly different from those measured by ITC or obtained from UV melting curves. The difference was ascribed to the fact that in the fluorescence experiments, the melting is indirectly monitored through the fluorescence of conjugated dyes docked in the nucleic acid duplexes.

Later on, thermodynamic parameters of PNA•DNA duplexes have been measured also by UV melting curves, ITC and DSC by Butler and Schwarz and their collaborators.[33,34] ITC measurements showed that the binding constants for PNA•DNA duplexes are higher than those for the corresponding DNA•DNA duplexes, a fact previously inferred from melting curves studies. In this case too, the agreement between the thermodynamic parameters measured by UV melting and DSC validated the two-state model for melting. Melting curves analysis for perfectly sequence-matched PNA•DNA duplexes of varying lengths (6-20 bp) indicated that the average free energy of binding ($\Delta G°$) is -6.5 ±0.3 kJ mol^{-1} bp^{-1}, which corresponds to a microscopic binding constant of ~14 $M^{-1}bp^{-1}$.[35] These values are comparable to those previously measured for DNA•DNA duplexes.[36]

Base pair mismatches affect importantly the stability of nucleic acid duplexes. Nielsen et al reported that melting temperatures of 9- and 12-mer PNA•DNA duplexes with a single mismatch is lower by 15-20°C than that of the corresponding, fully complementary PNA•DNA heteroduplexes. The free energy penalty for a mismatch is ~15 $kJ{\cdot}mol^{-1}{\cdot}bp^{-1}$, which is larger than the corresponding penalty for a mismatch in DNA•DNA duplexes. The mismatch decreased both the enthalpy and entropy change of the duplex formation, which is a manifestation of the enthalpy-entropy compensation principle.[35]

Thermodynamic parameters for the formation of DNA duplexes with one internal LNA nucleotide in one of the two strands of the duplex were determined by UV melting curves.[37] These studies showed that LNA pyrimidines contribute more to the duplex stability than LNA purines, but that the contribution of each LNA monomer depends on the context of the monomer. Both the 5′ and 3′ neighbors of the LNA monomer influence the size of the effect of the monomer, with the stabilization effect being larger when the monomer has purine neighbors. The enthalpy-entropy compensation was observed across different sequences and that LNA stabilizes the duplex by either preorganization or improved stacking, but not by both simultaneously.[37]

Thermodynamic parameters of GNA duplexes and of the corresponding DNA duplexes were determined by UV melting curves.[38] The entropic penalty for duplex formation was found to be significantly smaller for GNA than for DNA because the conformational preorganization of single stranded GNA and the stacking interactions favor the duplex formation.

1.3.c Thermodynamics of Metal Binding to Nucleic Acids

The coordination properties of the nucleobases have been reviewed by Houlton[39] and by Lippert.[40] The metal coordination properties of the nucleobases are correlated with the nucleobases' pK_a.[40] The stability constants of metal complexes with DNA or RNA nucleosides and nucleotides have been measured by spectroscopic methods and found to be relatively small (Log$K$ = 3-7).[41] Stability constants for metal complexes with single stranded nucleic acids have been also studied and they have been summarized recently.[42]

While the coordination properties of nucleobases, nucleosides, and nucleotides have been extensively studied and reviewed, the number of articles dedicated to the coordination properties of nucleic acids is significantly smaller.

ITC studies of the thermodynamics of Mg^{2+} binding to ss RNA poly(A) and poly(U) or duplexes poly(A)·poly(U) provided equilibrium constants of 4.2, 3.7 and 4.4, respectively.[43] For poly(A) and poly(A)·poly(U), the values of ΔS and ΔH were negative, which indicates that the Mg^{2+} binding to these RNAs is enthalpically driven. In contrast, for poly(U), the ΔS and ΔH values were positive and thus indicative of entropically-driven binding. These differences in thermodynamics were attributed to the distinct coordination modes of Mg^{2+} to the different RNAs; that is, Mg^{2+} binds to poly(A) and poly(A)·poly(U) through exothermic, outer-sphere complexation, while it binds to poly(U) by endothermic inner-sphere coordination to the phosphate groups of the nucleotide backbone. ITC studies of the thermodynamics of Al^{3+} binding to calf thymus DNA under various pH and temperature conditions showed that at pH 3.5-5.5, the binding

constants Log*K* are 6.8-7.3 and that the binding is entropy driven. At pH=6.0 and 7.0, Al^{3+} caused the precipitation of calf thymus DNA.

Duguid et al. conducted DSC measurements and reported that the enthalpy and entropy for the melting of DNA complexed with divalent main group and transition metal ions Sr^{2+}, Ba^{2+}, Mg^{2+}, Ca^{2+}, Mn^{2+}, Co^{2+}, Ni^{2+} and Cd^{2+} were 6.2-8.7 $kcal.mol^{-1}bp^{-1}$ and 17.5-24.7 $cal.K^{-1}mol\ bp^{-1}$, respectively.[44] Calorimetric and spectroscopic studies of the interaction of Calf thymus DNA with the transition metal ions Mn^{2+}, Co^{2+}, Ni^{2+}, Cu^{2+}, Zn^{2+} and Cd^{2+} showed that each metal ion has a characteristic metal binding mode that is influenced by the concentration of the metal ion in solution.[45]

The stability constants of complexes of Ag^{+} with DNA or RNA have been measured by capillary electrophoresis.[46] In DNA, Ag^{+} coordinates preferentially to guanine and adenine with binding constants Log*K* 4.9 and 4.2, respectively. In RNA Ag^{+} coordinates to the guanine bases with Log*K* of 5.2.

Lee et al. reported in 1993 that at high pH, the divalent metal ions, Zn^{2+}, Ni^{2+}, or Co^{2+} coordinate to the nucleobase pairs of calf thymus, bacterial, or synthetic DNA to form M-DNA.[47] ITC studies of the formation of Zn-DNA with Calf thymus DNA showed that the metal binding is endothermic and, consequently, that it is entropy-driven.[48]

1.4 Thesis Organization

Chapter 2 of this thesis presents a study of the effect of steric interactions between the metal complexes and the PNA duplexes on the stability of the modified PNA duplexes. For this study, we have synthesized two 8-hydroxyquinoline PNA monomers **Q_1** and **Q_2** that differ from each other in the way in which the ligand is attached to the PNA backbone (Figure 1.3). The metal complexes formed with PNAs that contain **Q_1** are more stable than those formed with **Q_2**-containing PNAs. Conversely, in the presence of Cu^{2+}, the thermal stability of **Q_1**-containing PNA duplexes is significantly higher than that of **Q_2**-

containing PNAs. We have found also that another factor that influences the effect of the metal complex that functions as alternative base pairs depends on the sequence of the PNA duplex in which it is introduced. Specifically, the thermal stability of a 8- and a 9-base pairs PNA duplexes both containing a central pair of 8-hydroxyquinoline ligands is affected very differently by the presence of Cu^{2+}. The stability of the former duplex is not affected at all by Cu^{2+} while that of the 9-base pair duplex increases drastically in the presence of Cu^{2+}. ITC studies of the interaction between the Cu^{2+} and the Q-modified PNA duplexes provided stability constants for the complexes formed by Cu^{2+} with Q-PNA that explain the trends inferred based on thermal melting studies. The trend in stability constants determined by ITC is in agreement with that deduced based on the apparent stability constants determined by simulations of UV titrations. The trend is also corroborated by EPR spectroscopy studies of the **Q_1**-PNA and **Q_2**-PNA duplexes in the presence of Cu^{2+}. Specifically, EPR spectra of **Q_1**-modified PNA duplexes annealed in the presence of Cu^{2+} showed superhyperfine features while the spectra of **Q_2**-modified PNA duplexes annealed in the presence of Cu^{2+} showed broad peaks with no superhyperfine features. This difference between the EPR spectra is compatible with the finding that the interaction between Cu^{2+} and **Q_1-**PNA is stronger than that between Cu^{2+} and **Q_2**-PNA. CD spectroscopy showed that the chiral effect of the C-terminus Lysine is transmitted through **Q_1**-containing PNA in the presence of Cu^{2+} to a much higher extent than through **Q_2**-PNA. We attribute this effect to the stronger interaction between Cu^{2+} and the ligand **Q_1** than between Cu^{2+} and **Q_2**.

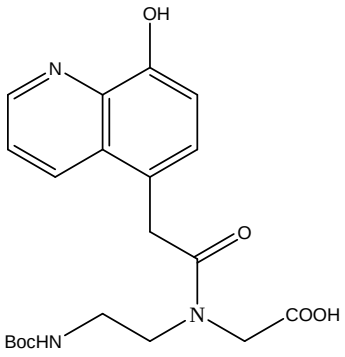

Q_1

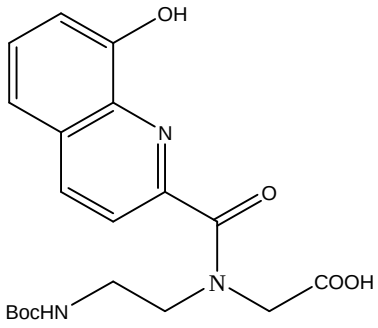

Q_2

Figure 1.3. PNA monomers 2-(*N*-(*tert*-Butyloxycarbonyl-2-aminoethyl)-2-(8-hydroxyquinolin-5-yl)-acetamido)acetic acid **Q_1** and 2-(N-(2-(*tert*-butoxycarbonyl)-ethyl)-8-hydroxyquinoline-2-carboxamido)acetic acid **Q_2**

Chapter 3 describes the results of ITC studies that provided binding constants and the corresponding contribution of enthalpy and entropy to the free energy for metal binding to a variety of ligands, and ligand-containing single stranded and double stranded PNAs. The absolute thermodynamic parameters independent of pH and buffer have been obtained by taking into account the pH of the solutions, the pK_a of the buffer, and the type of complexes that the metal ions form with the buffer and the ligand systems.[49] Analysis of the thermodynamic parameters measured by ITC indicate that the supramolecular chelate effect exerted by the PNA duplexes and the steric interactions are two major factors that influence the binding affinities of ligand-containing PNA for the metal ions. The supramolecular effect is entropy driven and stabilizes the metal complexes formed in PNA and the PNA, while the steric effect is enthalpy driven and destabilizes the complex and PNA. This effect is evident for the Cu^{2+} binding to **Q**-PNAs: the $[CuQ_2]$ complex formed with **Q_1**-PNA has a much larger stability constant than the corresponding complex formed with the free ligand 8-hydroxyquinoline, which in turn has a larger stability constant than the complex formed by Cu^{2+} with **Q_2**-containing PNA duplex. The steric effect is also manifested very strongly in the formation of Ni^{2+} complexes with **Bpy**-PNA, because Ni^{2+} forms only non-planar complexes with **Bpy**, and consequently,

these complexes are distorted and distort the PNA duplexes or triplexes in which they are incorporated.

The ITC results revealed also the formation of inter-duplex [CuQ_2] complexes with **Q_1**-PNA duplexes at a Cu^{2+}/**Q_1**-PNA duplex ration of ~0.5, which are transformed into intra-duplex [CuQ_2] complexes at a Cu^{2+}/**Q_1**-PNA duplex ratio of ~1.0. Our results suggest that the first binding is accompanied by a conformational change of PNA.

Chapter 4 describes our efforts to incorporate octahedral metal tris-ligand complexes such as $Ni(Bpy)_3$ in PNA triplexes. These PNA structures are formed from homopurine and homopyrimidine strands.[50] The formation of the **Bpy**-modified PNA triplexes was confirmed by UV Job plots and by CD spectroscopy. The coordination of Ni^{2+}, Co^{2+} and Cu^{2+} to the **Bpy-**PNA triplexes was confirmed by UV Job plots, UV-titrations, and ESI-mass spectrometry. The CD spectra of Ni^{2+}-containing **Bpy-**PNA triplexes suggest that both Δ and Λ complexes form in the PNA triplexes and that these complexes are determinant of the duplex's preferred handedness.

Chapter 5 presents the analysis of preliminary crystal structure of a **Q**-modified PNA duplex with the palindromic sequence $(H\text{-}GGCA\mathbf{Q}TGCC\text{-}Lys\text{-}NH_2)_2$ obtained in the presence of excess Cu^{2+}. This structure reveals the coordination of the Cu^{2+} to both the 8-hydroxyquinoline ligands, which are bulged out of the PNA duplex and the terminal guanine nucleobases (Figure 1.4). The trinuclear Cu^{2+} complex that forms between PNA duplexes contains 8-hydroxyquinolines that act as a bridge between the three Cu^{2+} ions, which is an unusual coordination mode for 8-hydroxyquinoline. There is no synthetic molecule that has a similar structure as this trinuclear complex.

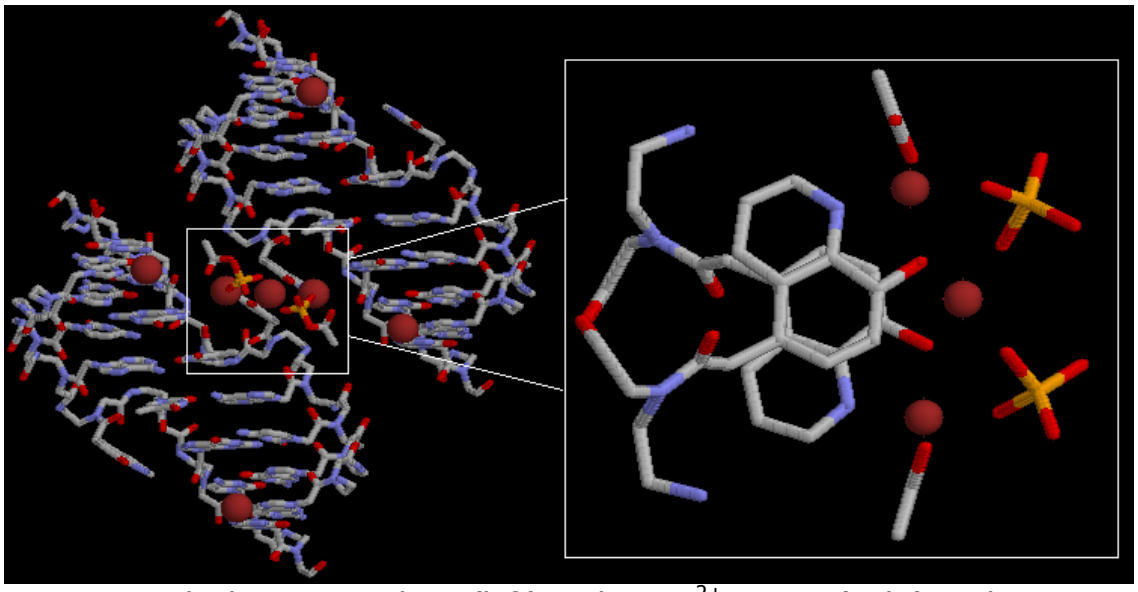

Figure 1.4. Inter-duplex **HQ** stacking (left) and tri-Cu^{2+} center (right) in the in the **HQ**-9mer PNA crystal.

References

(1) Clever, G. H.; Kaul, C.; Carell, T. *Angew. Chem. Int. Ed.* **2007**, *46*, 6226-6236.
(2) He, W.; Franzini, R. M.; Achim, C. *Prog. Inorg. Chem.* **2007**, *55*, 545-611.
(3) Mueller, J. *Eur. J. Inorg. Chem.* **2008**, 3749-3763.
(4) Tanaka, K.; Shionoya, M. *J. Org. Chem.* **1999**, *64*, 5002-5003.
(5) Franzini, R. M.; Watson, R. M.; Patra, G. K.; Breece, R. M.; Tierney, D. L.; Hendrich, M. P.; Achim, C. *Inorg. Chem.* **2006**, *45*, 9798-9811.
(6) Watson, R. M.; Skorik, Y.; Patra, G. K.; Achim, C. *J. Am. Chem. Soc.* **2005**, *127*, 14628-14639.
(7) Popescu, D.-L.; Parolin, T. J.; Achim, C. *J. Am. Chem. Soc.* **2003**, *125*, 6354-6355.
(8) Martell, A. E.; Smith, R. M. *Critical Stability Constants, Vol. 2.*; Plenum Press: New York and London, 1975.
(9) Tanaka, K.; Yamada, Y.; Shionoya, M. *J. Am. Chem. Soc.* **2002**, *124*, 8802-8803.
(10) Nielsen, P. E.; Egholm, M.; Berg, R. H.; Buchardt, O. *Science* **1991**, *254*, 1497-500.
(11) Nielsen, P. E.; Editor *Peptide Nucleic Acids: Protocols and Applications, Second Edition*, 2004.
(12) Rasmussen, H.; Kastrup, J. S.; Nielsen, J. N.; Nielsen, J. M.; Nielsen, P. E. *Nature Structural Biology* **1997**, *4*, 98-101.
(13) He, W.; Hatcher, E.; Balaeff, A.; Beratan, D.; Gil, R. R.; Madrid, M.; Achim, C. *J. Am. Chem. Soc.* **2008**, *130*, 13264-13273.
(14) Yeh, J. I.; Pohl, E.; Truan, D.; He, W.; Sheldrick, G. M.; Du, S. C.; Achim, C. *Chem. Eur. J.* **2010**, *16*, 11867-11875.
(15) Johannsen, S.; Megger, N.; Bohme, D.; Sigel, R. K. O.; Muller, J. *Nature Chem.* **2010**, *2*, 229-234.
(16) Schlegel, M. K.; Essen, L. O.; Meggers, E. *J. Am. Chem. Soc.* **2008**, *130*, 8158-+.
(17) Atwell, S.; Meggers, E.; Spraggon, G.; Schultz, P. G. *J. Am. Chem. Soc.* **2001**, *123*, 12364-12367.
(18) Obika, S.; Nanbu, D.; Hari, Y.; Andoh, J.; Morio, K.; Doi, T.; Imanishi, T. *Tetrahedron Letters* **1998**, *39*, 5401-5404.
(19) Singh, S. K.; Nielsen, P.; Koshkin, A. A.; Wengel, J. *Chemical Communications* **1998**, 455-456.
(20) Zhang, L.; Peritz, A.; Meggers, E. *Journal of the American Chemical Society* **2005**, *127*, 4174-4175.
(21) Zhang, L.; Meggers, E. *Journal of the American Chemical Society* **2005**, *127*, 74-75.
(22) Jelesarov, I.; Bosshard, H. R. *J. Mol. Recognit.* **1999**, *12*, 3-18.
(23) Puglisi, J. D.; Tinoco, I. *Method Enzymol.* **1989**, *180*, 304-325.
(24) Marky, L. A.; Breslauer, K. J. *Biopolymers* **1987**, *26*, 1601-1620.
(25) Gans, P.; Sabatini, A.; Vacca, A. *Talanta* **1996**, *43*, 1739-1753.

(26) Engman, K. C.; Sandin, P.; Osborne, S.; Brown, T.; Billeter, M.; Lincoln, P.; Norden, B.; Albinsson, B.; Wilhelmsson, L. M. *Nucleic Acids Res.* **2004**, *32*, 5087-5095.
(27) Ramstad, T.; Hadden, C. E.; Martin, G. E.; Speaker, S. M.; Teagarden, D. L.; Thamann, T. J. *Int. J. Pharm.* **2005**, *296*, 55-63.
(28) Myszka, D. G. *Curr. Opin. Biotechnol.* **1997**, *8*, 50-57.
(29) Green, D. B.; Lane, J.; Wing, R. M. *Appl. Spectrosc.* **1987**, *41*, 847-851.
(30) Wiesner, P.; Kayser, H. *J. Biochem. Mol. Toxicol.* **2000**, *14*, 221-230.
(31) Tomac, S.; Sarkar, M.; Ratilainen, T.; Wittung, P.; Nielsen, P. E.; Norden, B.; Graslund, A. *Journal of the American Chemical Society* **1996**, *118*, 5544-5552.
(32) Ratilainen, T.; Holmen, A.; Tuite, E.; Haaima, G.; Christensen, L.; Nielsen, P. E.; Norden, B. *Biochemistry* **1998**, *37*, 12331-12342.
(33) Schwarz, F. P.; Robinson, S.; Butler, J. M. *Nucleic Acids Research* **1999**, *27*, 4792-4800.
(34) Chakrabarti, M. C.; Schwarz, F. P. *Nucleic Acids Research* **1999**, *27*, 4801-4806.
(35) Ratilainen, T.; Holmen, A.; Tuite, E.; Nielsen, P. E.; Norden, B. *Biochemistry* **2000**, *39*, 7781-7791.
(36) SantaLucia, J.; Allawi, H. T.; Seneviratne, A. *Biochemistry* **1996**, *35*, 3555-3562.
(37) McTigue, P. M.; Peterson, R. J.; Kahn, J. D. *Biochemistry* **2004**, *43*, 5388-5405.
(38) Schlegel, M. K.; Xie, X. L.; Zhang, L. L.; Meggers, E. *Angewandte Chemie-International Edition* **2009**, *48*, 960-963.
(39) Houlton, A. *Advances in Inorganic Chemistry* **2002**, *53*, 87-158.
(40) Lippert, B. *Coordination Chemistry Reviews* **2000**, *200-202*, 487-516.
(41) Izatt, R. M.; Christensen, J. J.; Rytting, J. H. *Chem. Rev.* **1971**, *71*, 439-82.
(42) Sigel, R. K. O.; Sigel, H. *Accounts of Chemical Research* **2010**, *43*, 974-984.
(43) Ohyama, T.; Cowan, J. A. *Journal of Biological Inorganic Chemistry* **1996**, *1*, 83-89.
(44) Duguid, J. G.; Bloomfield, V. A.; Benevides, J. M.; Thomas, G. J. *Biophysical Journal* **1995**, *69*, 2623-2641.
(45) Souza, H. K. S. *Thermochim. Acta* **2010**, *501*, 1-7.
(46) Arakawa, H.; Neault, J. F.; Tajmir-Riahi, H. A. *Biophysical Journal* **2001**, *81*, 1580-1587.
(47) Lee, J. S.; Latimer, L. J. P.; Reid, R. S. *Biochemistry and Cell Biology* **1993**, *71*, 162-8.
(48) Wettig, S. D.; Wood, D. O.; Lee, J. S. *J. Inorg. Biochem.* **2003**, *94*, 94-99.
(49) Grossoehme, N. E.; Spuches, A. M.; Wilcox, D. E. *J. Biol. Inorg. Chem.* **2010**, *15*, 1183-1191.
(50) Wittung, P.; Nielsen, P.; Norden, B. *J. Am. Chem. Soc.* **1997**, *119*, 3189-3190.

Chapter 2 Metal Binding to Ligand-containing PNA

2.1 Introduction

The interaction between nucleic acids and transition metal ions can be used to create molecules that have potential applications in nanotechnology and molecular electronics.[1] A strategy for metal ion incorporation into nucleic acid duplexes first proposed by Tanaka and Shinoya in 1999 involves the replacement of the natural nucleobases by ligands that have a higher affinity for metal ions than the natural nucleobases (Scheme 2.1).[2] The metal complexes formed with these ligand-modified, nucleic acid duplexes can function as metal-mediated, alternative base pairs. If the ligands are aromatic and the geometry of the metal complex is planar, the complexes can participate in π stacking interactions with adjacent nucleobase pairs. This strategy allows the incorporation of metal ions at specific positions in a nucleic acid duplex,[1,3,4] as well as the creation of arrays of metal ions within a duplex.[5] In the last decade, numerous ligands have been introduced into DNA, RNA, LNA and PNA oligomers and a variety of metal ions have been incorporated into the ligand-modified duplexes formed by these oligomers.[1,3,4]

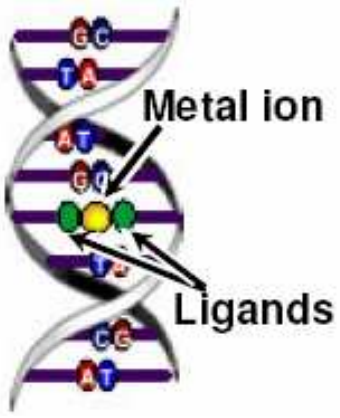

Scheme 2.1. Cartoon representation of a metal-containing, ligand-modified nucleic acid duplex

Work in our lab focuses on the use of PNA as a scaffold for metal ions. PNA is a synthetic analogue of DNA that commonly has a backbone based on N-

(2-aminoethyl)-glycine (Aeg).[6] PNA exhibits a remarkable affinity for complementary DNA and RNA, because its backbone is neutral. In our previous research, methyl bipyridine, bipyridine (Bipy), and 8-hydroxyquinoline (Q) have been introduced into PNA oligomers that formed PNA duplexes containing Ni^{2+}, Co^{2+}, or Cu^{2+}.[7-9] We determined that the thermal stability of the metal-containing, bipyridine-PNA duplexes correlates with the stability constant of the corresponding metal complexes,[7] which is in agreement with results obtained in studies of metal incorporation into DNA duplexes.[10] For example, DNA duplexes containing 2'-deoxyribosyl-N9-[6-(2'pyridyl)-purine)](Pur^p) or 2'-deoxyribosyl-N1-[4-(2'pyridyl)-pyrimidinone)] (Pyr^p) have been stabilized in the presence of Ni^{2+} to approximately the same extent despite the fact that the geometry of the Ni^{2+}-Pur^p complex is likely to match closely that of the base pair in DNA, while the Ni^{2+}-Pyr^p complex has a geometry dissimilar from that of the base pair (Scheme 2.2a,b).[11] The high stability of the duplex that contains the Ni^{2+}-Pyr^p complex was attributed to the strong coordination bonds and the stacking interactions that occur between the ligands and base pairs and may compensate for the steric constraint exerted by the complex on the DNA duplex.[11]

In other metal-containing nucleic acid duplexes, the geometry of the metal complex appeared also to be a determinant of the stability of the metal-containing nucleic acid duplexes. For example, a PNA duplex in which a central AT base pair was replaced by a $[Ni(bipy)_2]^{2+}$ complex had a lower melting temperature (56°C) than that of the non-modified duplex (63°C). This difference in the stability of the duplex existed despite the fact that the overall stability constant β_2 for $[Ni(bipy)_2]$ (3.2×10^{13} M^{-1})[12] is several orders of magnitude higher than the binding constant for an AT base pair (3.3×10^{2} M^{-1}).[13] The relatively small stabilization of the duplex imparted by the metal complex may be because the $[Ni(bipy)_2]$ complex has a distorted square planar geometry in which the two bipyridine ligands are not coplanar.[14] The relative orientation of the ligand binding sites is also likely to affect the binding of metal ions to the modified nucleic acid. Indeed, the thermal stability of two DNA duplexes, each containing

different isomers of salicylaldehyde (Scheme 2.2c,d) in the same position of the duplex, was affected differently by one equivalent of Cu^{2+}.[15] Specifically, the thermal stability of the DNA duplex that contained 2'-deoxyribosyl-5-(2-hydroxybenzaldehyde) (Scheme 2.2c) was about the same regardless of the presence of Cu^{2+} (ΔT_m = +1°C). In contrast, the duplex that contained 2'-deoxyribosyl-4-(2-hydroxybenzaldehyde) (Scheme 2.2d) was significantly more stable in the presence of Cu^{2+} than in its absence (ΔT_m = +15°C).[15] This difference in the thermal stability of duplexes induced by metal coordination was attributed to the relative orientation of the metal binding sites of the ligand with respect to the DNA backbone, which influences the structural compatibility between the metal complex and the duplex.

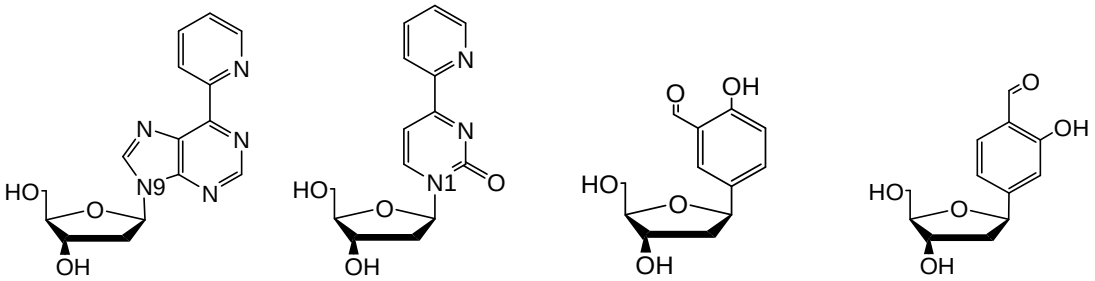

(a) (b) (c) (d)

Scheme 2.2. a. 2'-deoxyribosyl-N9-[6-(2'pyridyl)-purine)], Pur^p; b. 2'-deoxyribosyl-N1-[4-(2'pyridyl)-pyrimidinone)] Pyr^p; c. 2'-deoxyribosyl-5-(2-hydroxybenzaldehyde), Salen 1; d. 2'-deoxyribosyl-4- (2-hydroxybenzaldehyde), Salen 2.

Compared to the free ligands, the coordination mode of metal ions with the ligands incorporated into nucleic acid duplexes, as well as the stability constants of the corresponding complexes, can be very different due to the supramolecular chelate effect exerted by the duplex. For example, the stability constants of complexes of pyridine (Py) and Ag^+ are very small, and an $[Ag(Py)_2]^+$ complex does not form in solutions containing micromolar concentrations of Ag^+ and Py.[12] In contrast, at the same concentrations, a

$[Ag(Py)_2]^+$ complex formed within DNA duplexes that contained a pair of pyridines in complementary positions.[16] In another example, titrations of PNA duplexes containing one pair of 8-hydroxyquinolines led to the formation of $[CuQ_2]$ complexes at both low and high temperatures. These complexes transformed to [CuQ] complexes in the presence of excess Cu^{2+} only at high temperature, where the double stranded (ds) duplex dissociates in single strands (ss).[9]

The coordination of the metal ions to specific locations in the ligand-modified nucleic acid duplexes depends on the relative size of the binding constant of the metal ions to the ligands and to the nucleobases. This is because metal ions that are soft Lewis acids can coordinate not only to ligands incorporated into the nucleic acid but also to the nucleobases. Such binding was demonstrated for Ag^+ by UV-Vis, FTIR, and CD spectroscopy and by potentiometric titrations.[17-23] The binding mode of Ag^+ to nucleobases was seen to depend on pH and the ratio *r* between bound Ag^+ and the DNA nucleobase. If *r* is smaller than 1:5, Ag^+ coordinated to G-N7 ($K \sim 8 \cdot 10^4$ M^{-1}) and A-N7 ($K \sim 1.5 \cdot 10^4$ M^{-1}) and formed complexes termed type I. This coordination mode is predominant for DNA with G-rich sequences. For *r* ratios between 1:5 and 1:2, Ag^+ coordinated to GC and AT base pairs by replacing some of the protons to form N-Ag-N bridges between the AT and GC base pairs.[20,23]

The goal of the present research was to determine how steric factors affect the stability of a metal-containing PNA duplex. To achieve this goal, we incorporated into PNA duplexes a pair of 8-hydroxyquinoline ligands, which have been attached to the nucleic acid backbone at different positions and through different linkers (Scheme 2.3a, b). Our study shows that the interaction between the Q-PNA duplexes and Cu^{2+} depends on (*1*) the way in which a given ligand is attached to the PNA, and (*2*) the sequence and/or the structure of the PNA, and (3) the type of metal ion.

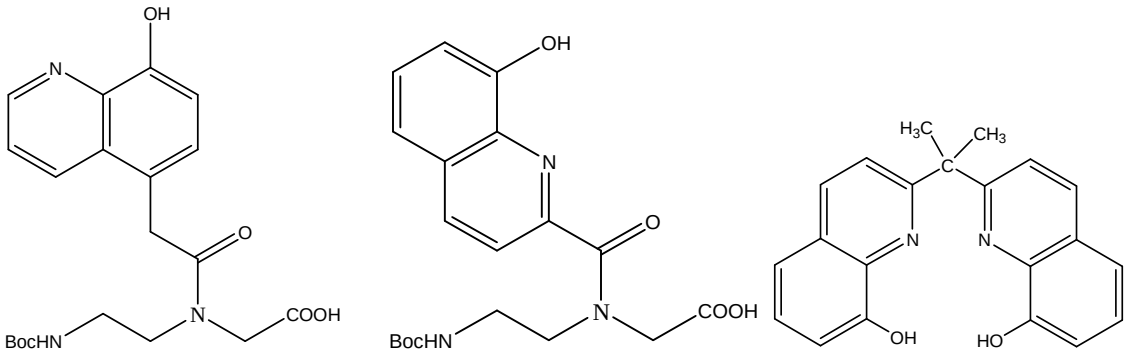

(a) (b) (c)

Scheme 2.3 Chemical structure of (a) 2-(*N*-(*tert*-Butyloxycarbonyl-2-aminoethyl)-2-(8-hydroxyquinolin-5-yl)-acetamido)-acetic acid Q_1; (b) 2-(N-(2-(*tert*-butoxycarbonyl-2aminoethyl)-8-hydroxyquinoline-2-carboxamido)-acetic acid Q_2; and (c) 2,2'-isopropylidenedi-8-quinolinol ipdq.

2.2 Results and Discussion

Two ligand-containing PNA monomers, Q_1 and Q_2, were synthesized (Scheme 2.3a,b). Both monomers contain the bidentate ligand 8-hydroxyquinoline, but the attachment of the ligand to the PNA backbone differs in Q_1 and Q_2 (Scheme 2.3a,b). The monomer Q_1 was synthesized by previously published procedures.[9] The monomer Q_2 was prepared by coupling the acetic acid derivative of 8-hydroxyquinoline **2** with N-(2-(tert-butoxycarbonyl)-aminoethyl)-glycinate **1** to obtain the ester **3**, which was next hydrolyzed (Scheme 2.4). The synthesis of PNA oligomers, some of which included the Q_1 and Q_2 monomers, was done by solid-phase peptide synthesis using the Boc-protection strategy.[24] For comparison purposes, we have also used published methods to synthesize the four-dentate ligand 2,2'-isopropylidenedi-8-quinolinol (ipdq), which contains two 8-hydroxyquinolines covalently connected to each other through a dimethyl-methylene linker (Scheme 2.3c).[9,25,26]

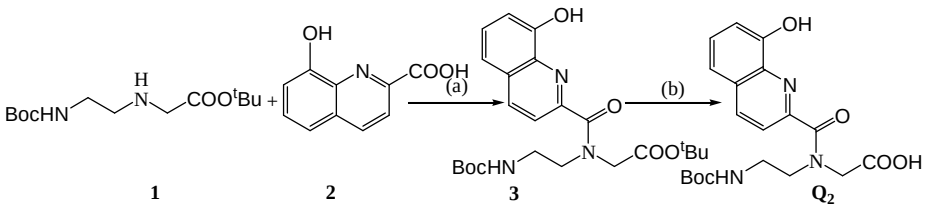

Scheme 2.4. Synthesis of monomer acid Q_2 . a. DCC, DhbtOH; b. NaOH, MeOH.

2.2.1 PNA sequences

The sequences of the non-modified and Q-PNA oligomers synthesized for this study are listed in Table 2.1. The 8-hydroxyquinoline monomers **Q_1** and **Q_2** have been inserted in the middle of a self-complementary PNA oligomer **X_1** to create the **Q_1**- or **Q_2**-containing oligomers **Q_1-X_1** or **Q_2-X_1**, respectively, which in turn can each form a palindromic PNA duplex **Q_1-X_1•X_1** or **Q_2-X_1•X_1**, respectively. A pair of **Q_1** or **Q_2** ligands has also been introduced in complementary positions in the middle of a PNA duplex based on two complementary PNA oligomers **X_2** and **X_3** to create the **Q**-modified, PNA duplexes **Q_1-X_2•X_3** or **Q_2-X_2•X_3**, respectively. All PNA oligomers had a terminal L-Lysine, which exerts a chiral induction effect on the duplexes in solution and improves the solubility of both the ss and ds PNA.

Table 2.1. Melting Temperatures T_m(°C), and Changes in the Melting Temperature ΔT_m for Non-modified and **Q**-PNA Duplexes in the Absence or Presence of Metal Ions[a].

Name	PNA Sequence	No M^{n+}	1 eq. Cu^{2+}	
		T_m[b]	T_m[b]	ΔT_m[c]
$\mathbf{X_1}$	H-GGCATGCC-Lys-NH_2	68	68	0
$\mathbf{X_4}$	Ac-GGCATGCC-Lys-NH_2	70	70	0
$\mathbf{Q_1}$-$\mathbf{X_1}$	H-GGCA$\mathbf{Q_1}$TGCC-Lys-NH_2	-	-	
$\mathbf{Q_2}$-$\mathbf{X_1}$	H-GGCA$\mathbf{Q_2}$TGCC-Lys-NH_2	-	-	
$\mathbf{X_5}$	Ac-GGCA$\mathbf{Q_2}$TGCC-Lys-NH_2	82	79	-3
$\mathbf{X_2}$ $\mathbf{X_3}$	H-GTAGTCACT-Lys-NH_2 NH_2-Lys-CATCAGTGA-H	63	63	0
$\mathbf{Q_1}$-$\mathbf{X_2}$ $\mathbf{Q_1}$-$\mathbf{X_3}$	H-GTAG$\mathbf{Q_1}$TCACT-Lys-NH_2 NH_2-Lys-CATC$\mathbf{Q_1}$AGTGA-H	46[9]	>79[9]	>33
$\mathbf{Q_2}$-$\mathbf{X_2}$ $\mathbf{Q_2}$-$\mathbf{X_3}$	H-GTAG$\mathbf{Q_2}$TCACT-Lys-NH_2 NH_2-Lys-CATC$\mathbf{Q_2}$AGTGA-H	38	37	-1

a The overall concentration of ss PNA in each sample was 10 μM. Solutions have been prepared in pH 7 10 mM sodium phosphate buffer;

b The precision for the T_m is ±1°C;

c ΔT_m was calculated as the difference between the melting temperature of the duplex formed in the presence and absence of the metal ion.

2.2.2 Properties of ligand-modified PNAs in the absence of transition metal ions

The UV spectra of the non-modified PNAs $\mathbf{X_1 \bullet X_1}$ and $\mathbf{X_2 \bullet X_3}$ are dominated by a strong absorption band at 260 nm (red line in Figure 2.1a,b). The spectrum of 8-hydroxyquinoline has an absorption band at 239 nm (black lines in Figure 2.1). The 260 nm and 293 nm bands correspond to $\pi-\pi^*$ transitions of the nucleobases and of 8-hydroxyquinoline, respectively. These transitions contribute also to the UV spectra of the $\mathbf{Q_1}$-modified PNAs $\mathbf{Q_1}$-

X_1•X_1 and **Q_1-X_2•X_3**, which showed two absorption bands at 260 nm and 247 nm, and of the **Q_2**-modified PNAs **Q_2-X_1•X_1** and **Q_2-X_2•X_3** (green lines in Figure 2.1), which showed a broad band at 253 nm (blue lines in Figure 2.1).

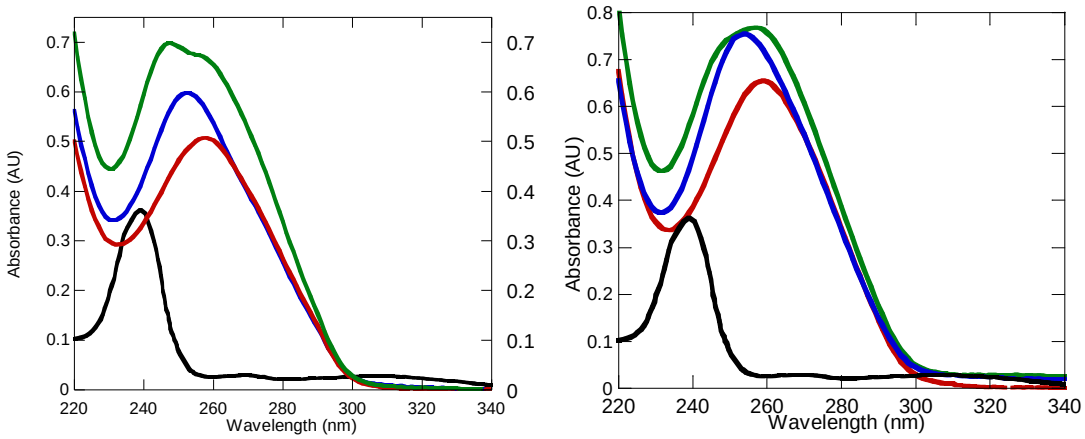

(a) (b)

Figure 2.1. UV absorption spectra of non-modified and 8-hydroxyquinoline-containing PNA duplexes in pH = 7.0 10 mM sodium phosphate buffer at 25 °C. (a) 5 μM palindromic duplexes 8-base pair duplex **X_1•X_1** (red); 5 μM **Q_2**-PNA duplex **Q_2-X_1•X_1** (blue); 5 μM **Q_1**-PNA duplex **Q_1-X_1•X_1** (green); 10 μM 8-hydroxyquinoline (black). (b) 5 μM non-palindromic duplexes **X_2•X_3** (red); 5 μM **Q_2**-PNA duplex **Q_2-X_2•X_3** (blue); 5 μM **Q_1**-PNA duplex **Q_1-X_2•X_3** (green); 10 μM 8-hydroxyquinoline (black).

The melting curves of the PNA duplexes monitored at 260 nm provided information on their thermal stability (Figure 2.2 and Table 2.1). The palindromic 8-bp PNA duplex **X_1•X_1** was slightly more stable than the 9-bp PNA duplex **X_2•X_3**, which we attribute to the higher GC content of the former duplex. A smaller and abrupt cooperative hyperchromicity change was seen for the melting of the shorter **X_1•X_1** PNA duplex than for the longer PNA duplex **X_2•X_3** (Figure 2.2). Acetylation of the N-terminus of the PNA oligomer **X_1** had a small stabilization effect (ΔT_m = +2°C) on the palindromic duplex **X_1•X_1** (Figure 2.3).

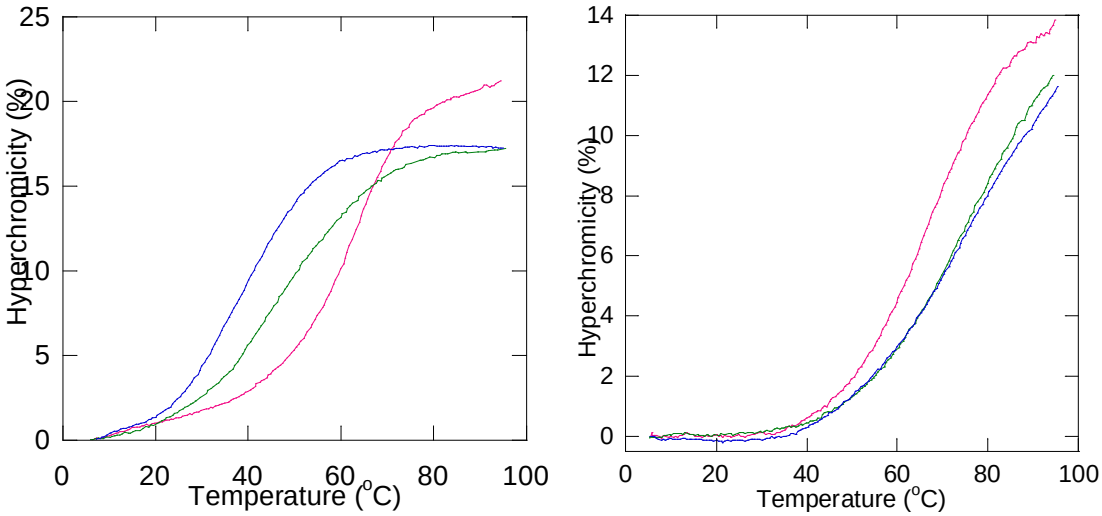

Figure 2.2. Denaturation profiles measured at 260 nm for a. 5 μM **X_2•X_3** (red), 5 μM **Q_1-X_2•X_3** (green), 5 μM **Q_2-X_2•X_3** (blue); b. 5 μM **X_1•X_1** (red), 5 μM **Q_1-X_1•X_1** (green), 5 μM **Q_2-X_1•X_1** (blue) in pH = 7.0 10 mM sodium phosphate buffer.

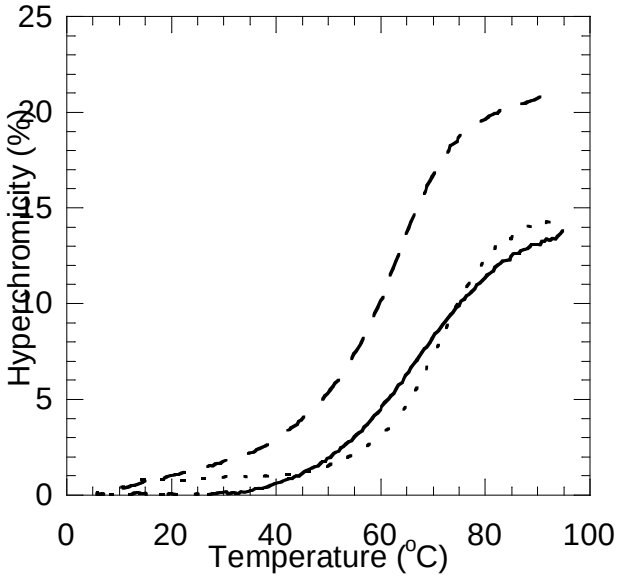

Figure 2.3. Denaturation profiles measured at 260 nm for 5 μM **X_1•X_1** (solid), **X_4•X_4** (dotted) **X_2•X_3** (dashed) in pH = 7.0 10 mM sodium phosphate buffer.

Incorporation of a pair of 8-hydroxyquinoline ligands in the middle of the 9-base pair PNA duplex **X_2•X_3** to form **Q_1-X_2•X_3** or **Q_2-X_2•X_3** significantly destabilized the duplex (Figure 2.2a and Table 2.1). Incorporation of the same pair of ligands into the 8-bp palindromic duplex **X_1•X_1** to form **Q_1-X_1•X_1** or **Q_2-X_1•X_1** had an even stronger destabilization effect than it did on **X_2•X_3**. An increase in absorbance was observed at temperatures above 40°C for **Q_1-X_1•X_1** and **Q_2-X_1•X_1**, but this increase was not sigmoidal as is typical for cooperative melting (Figure 2.2b). On the other hand, the CD spectra of annealed solutions of **Q_1-X_1•X_1** and **Q_2-X_1•X_1** at 20°C (Figure 2.4) showed features characteristic of left-handed PNA duplexes (Figure 2.4). Based on the combination of results of melting temperature and CD spectroscopy experiments, we conclude that at 20°C the **Q_1-X_1•X_1** and **Q_2-X_1•X_1** duplexes are formed.

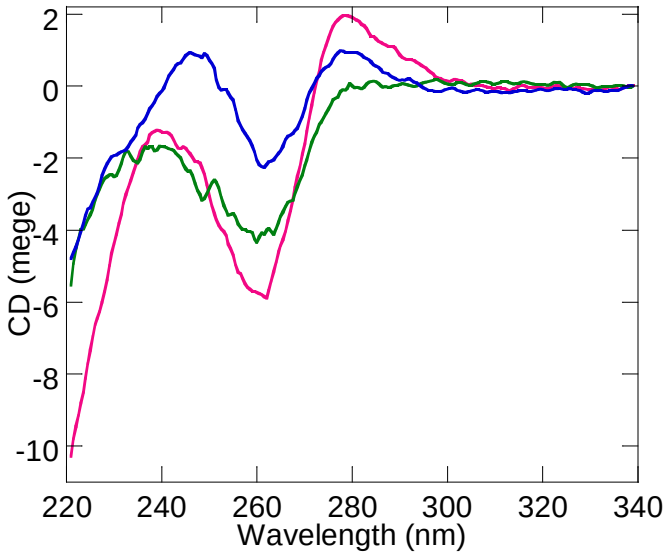

Figure 2.4. CD spectra of 10 μM **X_1•X_1** (red) and of 10 μM **Q**-PNA **Q_1-X_1•X_1** (green) and 10 μM **Q_2-X_1•X_1** (blue) in pH = 7.0 10 mM sodium phosphate buffer, 20 °C.

The UV and CD spectra and the melting curves indicate that the effect of ligand modification on PNA duplexes depends both on the duplex sequence, and

possibly the secondary structure of the PNA, as well as on the way in which the ligand is attached to the PNA backbone.

2.2.3 Interaction between Cu^{2+} and ligand-modified PNA

UV-monitored, thermal denaturation of the PNA duplexes was also performed in the presence of Cu^{2+}. No effect was observed on the melting temperature of the non-modified duplexes **X_1•X_1** and **X_2•X_3** by the presence of one equivalent of Cu^{2+} (Table 2.1). This observation indicates that Cu^{2+} interacts weakly, if at all, with the non-PNA duplexes. Our previous studies have shown that the **Q_1-X_2•X_3** PNA duplex was significantly stabilized by Cu^{2+} ions (ΔT_m > 30°C).[9] The effect of Cu^{2+} on the stability of the **Q_1-X_1•X_1** duplex was smaller than its effect on the stability of the **Q_1-X_2•X_3** duplex (Figure 2.5a and Table 2.1). This difference indicates that the effect of one and the same metal complex on the ligand-modified duplex stability depends on the duplex sequence and length. The stability of the **Q_2-X_1•X_1** and **Q_2-X_2•X_3** PNA duplexes was affected by Cu^{2+} to a much lesser extent than was the stability of the corresponding **Q_1**-PNA duplexes **Q_1-X_1•X_1** and **Q_1-X_2•X_3** (Figures 2.5b and 2.6). Comparison of the melting curves of **Q_2**-PNA duplexes in both the absence and presence of Cu^{2+} showed a negative effect of metal ions on the cooperativity of duplex formation.

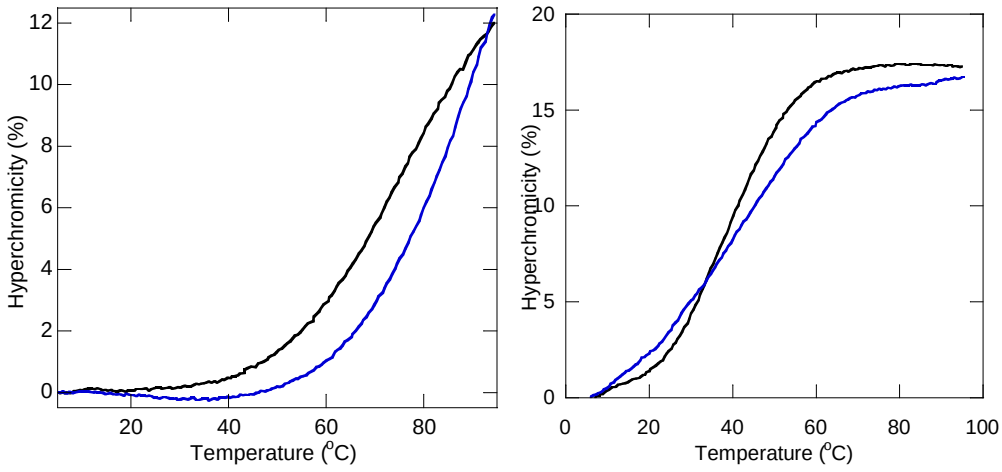

(a) (b)

Figure 2.5. Denaturation profiles measured at 260 nm for a. 5 μM **Q_1-X_1•X_1** , b.5 μM **Q_2-X_2•X_3** duplexes in the absence of metal ions (black) and in the presence of 5 μM Cu^{2+} (blue) in pH = 7.0 10 mM sodium phosphate buffer.

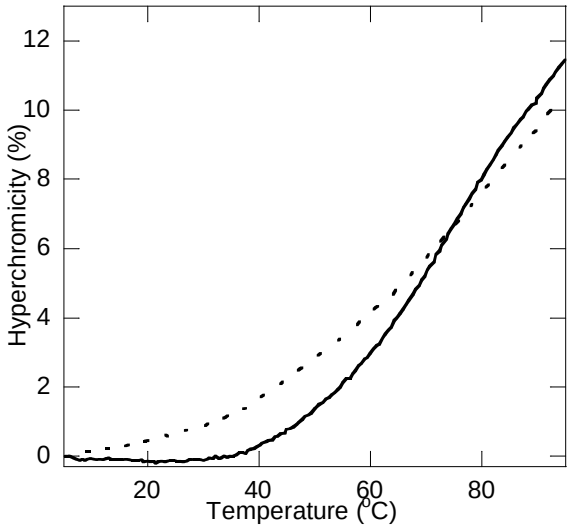

Figure 2.6. Denaturation profiles measured at 260 nm for 5 μM **Q_2-X_1•X_1** duplexes in the absence of metal ions (solid) and in the presence of 5 μM Cu^{2+} (dotted) in pH = 7.0 10 mM sodium phosphate buffer.

Titrations of the non-modified **X_1•X_1** PNA duplex with Cu^{2+} caused very small changes in absorption (Figure 2.7), which suggests that Cu^{2+} interacted very weakly with the **X_1•X_1** PNA duplex. In contrast, the titrations of all of the **Q**-PNA duplexes with Cu^{2+} led to major changes in the UV-Vis spectra of the duplexes, specifically the appearance of a metal-to-ligand charge-transfer band at about 400 nm, which is characteristic for the [CuQ_2] complex (Figures 2.8, 2.9, and 2.10).[9] The formation of [CuQ_2] was supported by the observation of isosbestic points for Cu^{2+}/**Q-PNA** duplex ratios of 0:0 to 1:1 and inflection points in the UV-vis titration curves at a Cu^{2+}/**Q-PNA** ratio of 1:1 (Figure 2.8c,d). The apparent stability constants of the complexes formed between Cu^{2+} and the **Q-PNA** duplexes have been determined by simulations of the UV titrations (Table 2.2).[27] The constants decreased in the order **Q_1-X_2•X_3** > **Q_1-X_1•X_1** > **Q_2-**

$X_2 \bullet X_3$ ≈ **Q_2-$X_1 \bullet X_1$**, which corroborates the fact that these constants depend on (*1*) the way in which the ligand is attached to the backbone, with **Q_1-**PNAs forming more stable complexes than **Q_2-PNAs**, and (*2*) the sequence of the PNAs, with **Q-$X_2 \bullet X_3$** PNA duplexes forming complexes more stable than the corresponding **Q-$X_1 \bullet X_1$** duplexes.

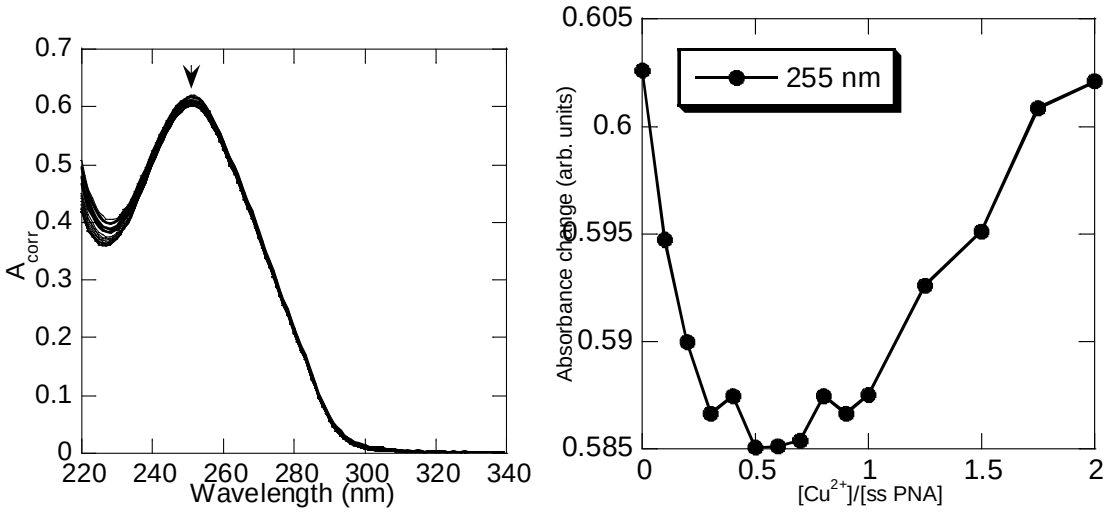

(a) (b)

Figure 2.7. Spectrophotometric titration of a 5μM **$X_1 \bullet X_1$** solution in pH 7.0 10 mM phosphate buffer with 0.5 mM $Cu(NO_3)_2$ solution, T=25 ^oC.

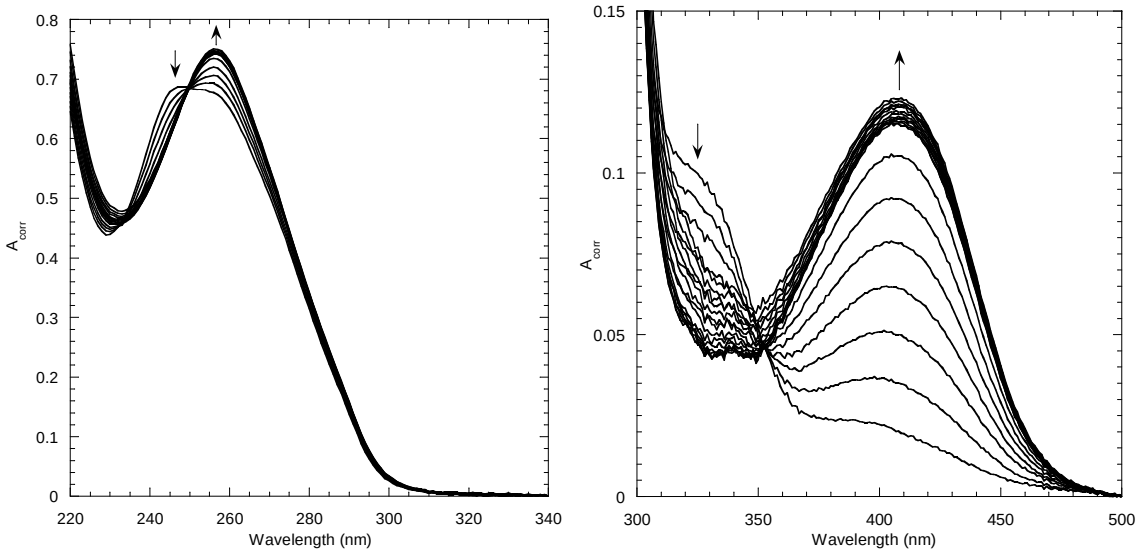

(a) (b)

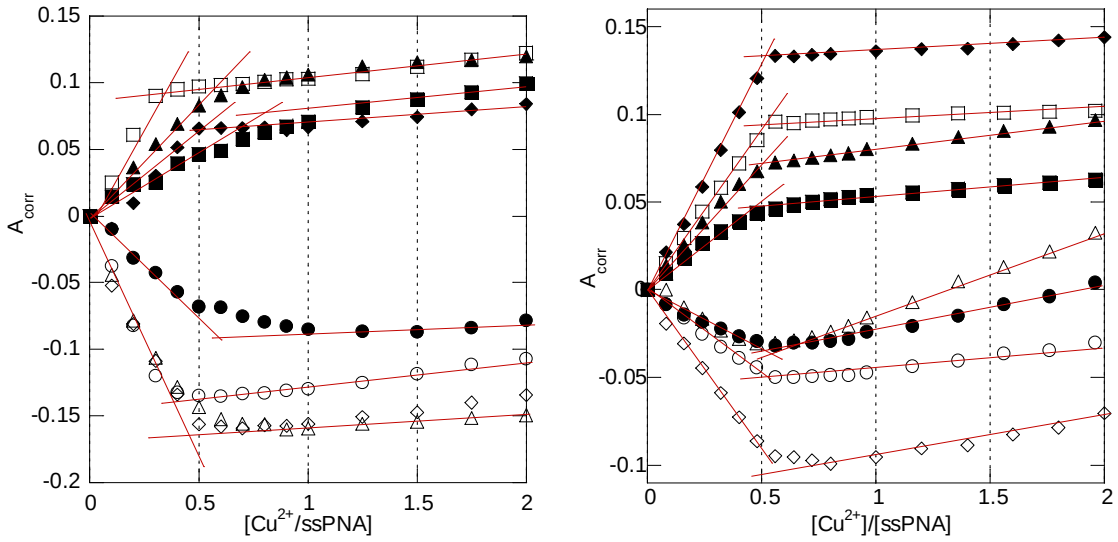

(c) (d)

Figure 2.8. Spectrophotometric titration of a 5 μM (a) and 25 μM (b) **Q_1-X_1•X_1** solution in pH = 7.0 10 mM sodium phosphate buffer with a 0.5 mM or 2.0 mM $Cu(NO_3)_2$ solution in water at 25 ^oC; (c) Titration curves at 260 nm (empty squares) and 244 nm (empty circles) for **Q_1-X_1•X_1** and at 274 nm (filled squares) and 250 nm (filled circles) for **Q_2-X_1•X_1** and at 260 nm (filled rhombus) and 247 nm (empty rhombus) for **Q_1-X_2•X_3** and at 272 nm (filled triangle) and 247 nm (empty triangle) for **Q_2-X_2•X_3**;(d) Titration curves at 410 nm (empty squares) and 332 nm (empty circles) for **Q_1-X_1•X_1** and at 403 nm (filled squares) and 342 nm (filled circles) for **Q_2-X_1•X_1** and at 412 nm (filled rhombus) and 320 nm (empty rhombus) for **Q_1-X_2•X_3** and at 403 nm (filled triangle) and 345 nm (empty triangle) for **Q_2-X_2•X_3**.

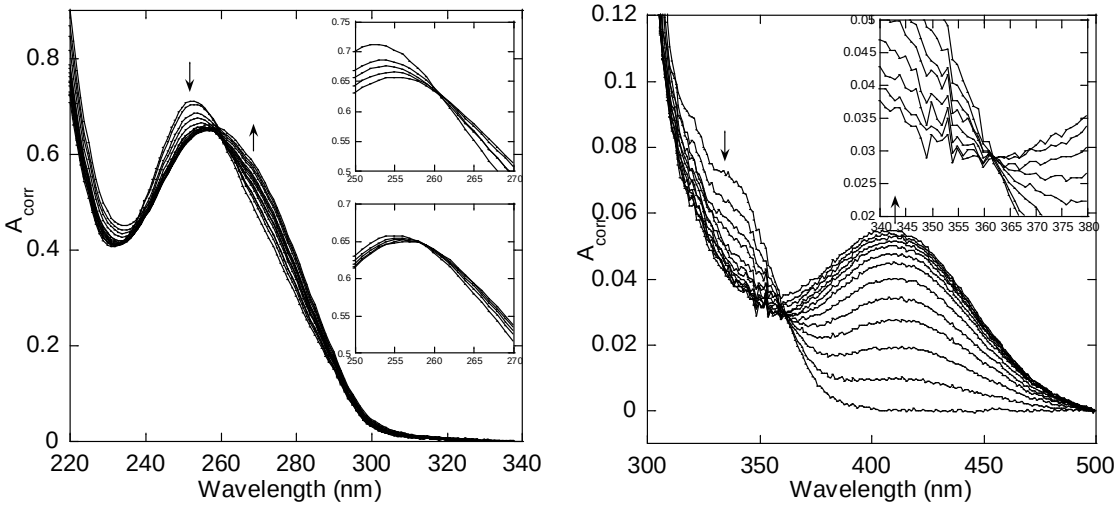

(a) (b)

Figure 2.9. Spectrophotometric titration of a 5 μM (a) and 25 μM (b) **Q_2-X_1•X_1** solution in pH 7.0 10 mM sodium phosphate buffer with a 0.5 or 2.0 mM $Cu(NO_3)_2$ solution in water, T=25 °C. Insets show spectra obtained for $[Cu^{2+}]$/[ss PNA] ratios of 0-0.5 (a and b) and 0.5-1.0 (a).

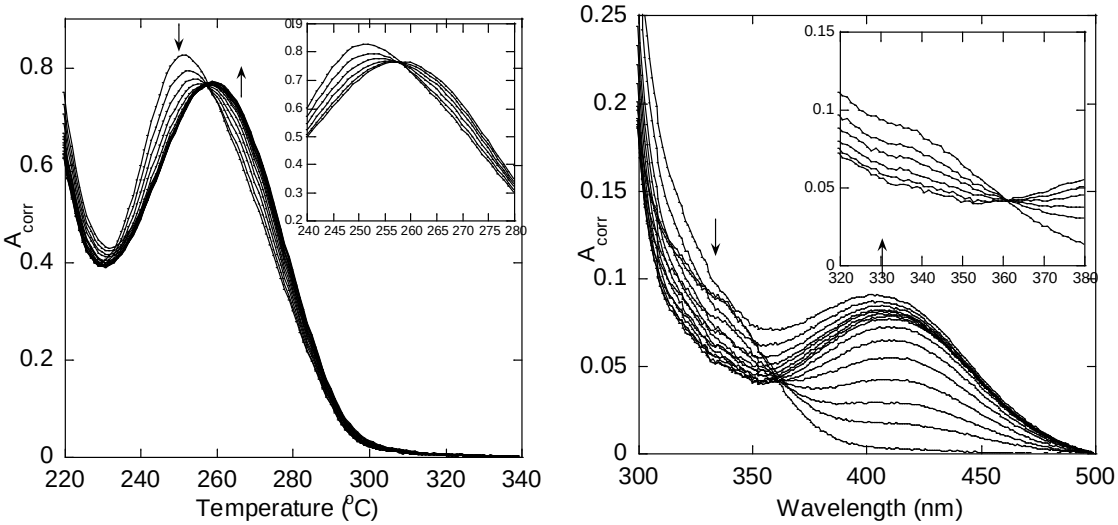

(a) (b)

Figure 2.10. Spectrophotometric titration of a 5 μM (a) and 25 μM (b) **Q_2-X_2•X_3** solution in pH = 7.0 10 mM sodium phosphate buffer with a 0.5 or 2.0 mM $Cu(NO_3)_2$ solution in water, T=25 °C. Insets show isosbestic points.

Table 2.2. Apparent stability constants of the [CuQ_2] complexes within Q-PNA determined from UV titrations in pH = 7.0 10 mM phosphate buffer.

Q-PNA duplex	Wavelengths range used for calculations	β_2'	RSD	Logβ_2'±SD	χ^2
Q_1-X_1•X_1	400-420	5.1×10^9	0.48	9.7±0.2	5.63
Q_1-X_2•X_3	400-420	4.4×10^{10}	0.36	10.6±0.2	5.31
Q_2-X_1•X_1	400-420	6.2×10^8	0.21	8.79±0.09	22.3*
Q_2-X_2•X_3	400-420	5.4×10^8	0.11	8.74±0.05	6.58

*Should be less than 12.6 @ 95% confidence level.

At Cu^{2+}/**Q-PNA** duplex ratios between 1:1 and 1:2, a new isosbestic point at 258 nm was observed for the **Q_2**- but not for **Q_1**-PNA duplexes (insets in Figure 2.9a). This observation indicates that in the case of **Q_2**-modified PNA, the [CuQ_2] complexes are converted by excess Cu^{2+} to complexes in which each Q ligand coordinates a Cu^{2+} ion. This difference further supports the conclusion that the [CuQ_2] complex formed between Cu^{2+} and **Q_2-PNA** is less stable than that formed between Cu^{2+} and **Q_1-PNA**.

We used isothermal titration calorimetry (ITC) to directly measure the thermodynamic parameters for the formation of Cu^{2+} complexes with the free ligand **Q**, the bitopic ligand ipdq, and **Q**-PNA in Tris buffer. This buffer was chosen because it is known that Cu^{2+} forms well characterized $Cu(Tris)_4^{2+}$ complexes,[28] whereas Cu^{2+} forms polynuclear complexes in phosphate buffers. Acetonitrile or methanol was added to the solutions of 8-hydroxyquinoline and ipdq to aid in their solubilization. The results of ITC titrations of 8-hydroxyquinoline, ipdq, **Q_1-X_1•X_1**, **Q_2-X_1•X_1**, **Q_1-X_2•X_3** and **Q_2-X_2•X_3** with Cu^{2+} are shown in Figures 2.11 and 2.12 and the thermodynamic data are compiled in Table 3.3.[29,30] The stability constant for the [CuQ_2] complex formed between Cu^{2+} and 8-hydroxyquinoline is in good agreement with the one

obtained previously by solubility measurements.[31] The stability constant of the [Cu(ipdq)] complex was four orders of magnitude larger than that of the corresponding [CuQ_2] complex formed between Cu^{2+} and 8-hydroxyquinoline, which is due to the chelate effect exerted by the covalent binding of two 8-hydroxyquinoline ligands to each other. We have hypothesized that the chelate effect will also manifest when two 8-hydroxyquinoline ligands are brought into close proximity of each other by the Watson-Crick hybridization of two complementary, **Q-PNA** strands. The ITC results indicate that this hypothesis is correct because the stability constants of the [CuQ_2] complexes formed between Cu^{2+} and **Q_1-X_1•X_1** and **Q_1-X_2•X_3** are two and four orders of magnitude larger, respectively, than the stability constant for the corresponding complex of Cu^{2+} and 8-hydroxyquinoline. The enthalpy changes ΔH for the formation of [CuQ_2] complexes are similar to those for the complexes with 8-hydroxyquinoline, ipdq or **Q_1**-PNA. However, a much larger positive entropy change was observed for the formation of Cu^{2+} complexes with ipdq or **Q_1**-PNA than for the complex formed with 8-hydroxyquinoline, which confirms the existence of a chelate effect.

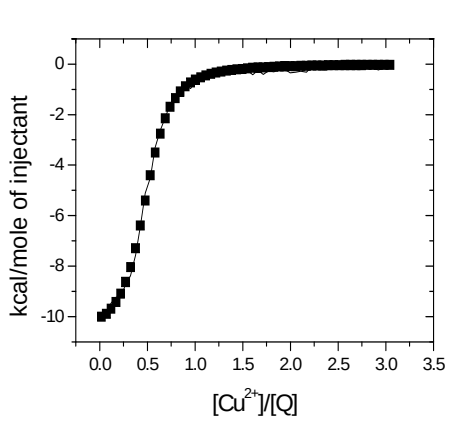

(a)

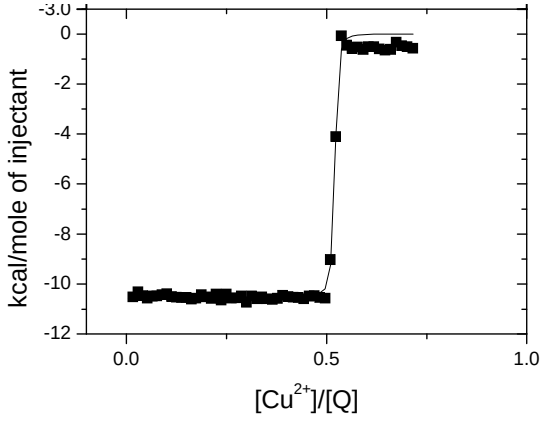

(b)

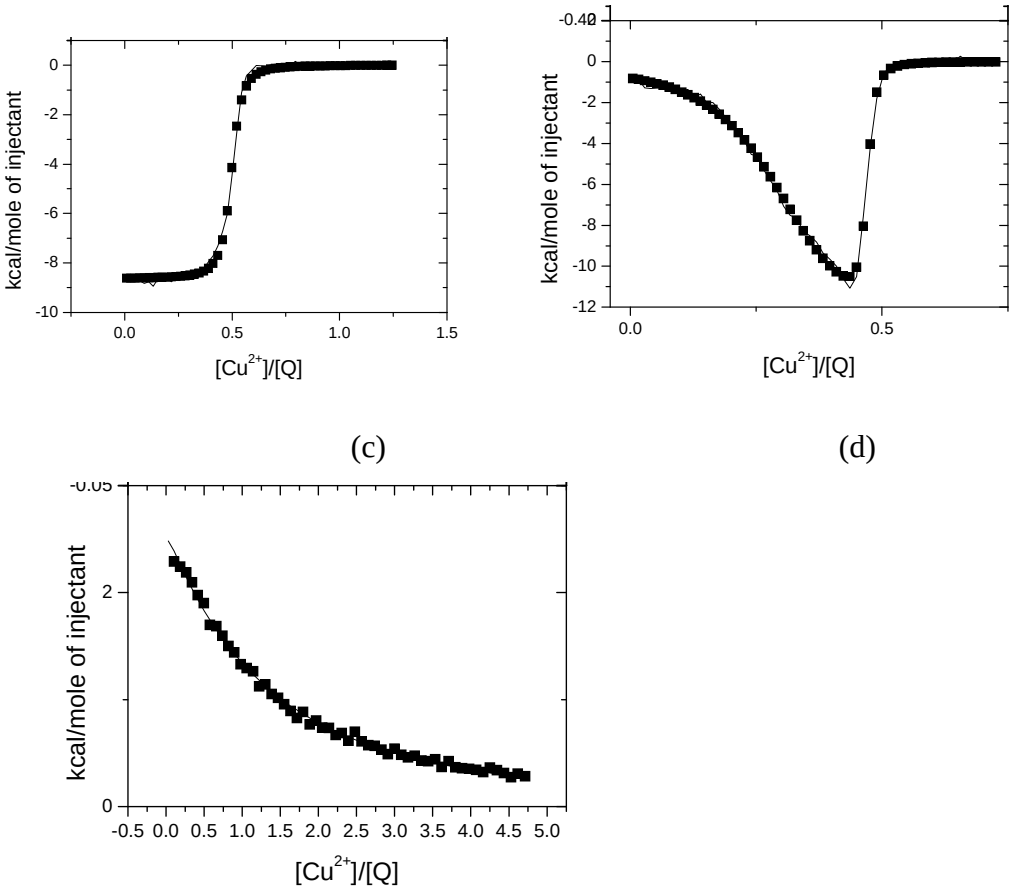

Figure 2.11. ITC titrations at 25 °C (a) 0.03 mM 8-hydroxyquinoline with 0.44mM $Cu(NO_3)_2$ in pH 8.1 3:1 100mM Tris buffer/acetonitrile; (b) 0.2 mM ipdq with 1.47 mM $Cu(NO_3)_2$ in 1:1 pH 8.1 100mM Tris buffer/methanol; (c) 0.03 mM **Q_1-X_1•X_1** with 0.36mM $Cu(NO_3)_2$ in pH 8.1 100mM Tris buffer; (d). 0.06 mM **Q_1-X_2•X_3** with 0.44mM $Cu(NO_3)_2$ in pH 8.1 100mM Tris buffer; (e). 0.06 mM **Q_2-X_2•X_3** with 1.30 mM $Cu(NO_3)_2$ in pH=8.1 100 mM Tris buffer.

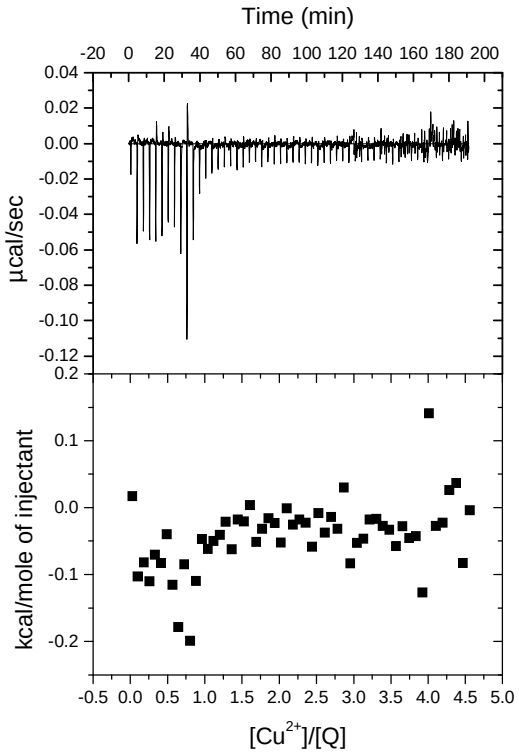

Figure 2.12. ITC titration of 0.06 mM dsPNA **Q_2-X_1•X_1** with 1.20 mM $Cu(NO_3)_2$ in pH 8.1 100mM.

Table 2.3. Stoichiometry and Thermodynamic Parameters for the Formation of Cu^{2+} Complexes with Ligands and **Q**-PNAs in pH=8.1 100 mM Tris buffer[a]

Ligand/Duplex	N	LogK_{ITC}	ΔH_{ITC} (kcal/mol)	Logβ_2	ΔH (kcal/mol)	ΔS (cal/mol/deg)	ΔG (kcal/mol)
8-HQ	1.98	5.8	-5.7	24.8	-22	40	-34
ipdq	1.95	7.7	-5.4	28.6	-22	57	-39
Q_1-X_1•X_1	2.02	6.8	-4.3	26.8	-19	60	-37
Q_1-X_2•X_3[b]	2.15	7.9	-4.1	29.0	-19	70	-40
Q_2-X_2•X_3	1.95	3.6	2.1	20.2	-7	70	-28

a. The transformation from apparent to absolute binding constants was done using the thermodynamic model described in the text. Error ranges for N, LogK and ΔH are 10%, 3% and 20% respectively.
b. Only the thermodynamic parameters of [CuQ_2] complex were listed.

Interestingly, ITC titrations of the **Q_1-X_2•X_3** PNA duplex showed a two-step binding process, with the first and second steps leading to complexes with the Cu^{2+}/**Q_1-X_2•X_3** stoichiometry of 1:2 and 1:1, respectively (Figure 2.11d). One possible explanation is that the first step involves the coordination of Cu^{2+} to two Q ligands from different duplexes to form inter-duplex [CuQ_2] complexes that bridge two **Q_1-X_2•X_3** PNA duplexes into dimers of duplexes, followed by the entropically-driven reorganization of the dimers of duplexes into **Q_1-X_2•X_3** PNA duplexes that contain an intramolecular [CuQ_2] complex. A detailed thermodynamic and kinetics study of these phenomena is under way in our lab.

The [CuQ_2] complex formed between Cu^{2+} and **Q_1-X_2•X_3** had a much higher stability constant than the Cu^{2+} complex with **Q_2-X_2•X_3**. ITC titrations of **Q_2-X_1•X_1** with Cu^{2+} (Figure 2.12) at PNA concentrations similar to the ones used in the titrations of **Q_1-X_1•X_1** and **Q_1-X_2•X_3** led to the observation of very weak features, which prevented us from determining the equilibrium constant and enthalpy change (Figure 2.12). The binding affinity of **Q_2-X_2•X_3** for Cu^{2+} is smaller because, in this system, the entropy increase does not compensate for the enthalpy increase. Hence, one can conclude that steric effects, such as those exerted by the change in the linker of the ligand to the PNA backbone, can have substantial effects on the overall stability of the complex formed between the metal and the ligand-PNA duplex. It is interesting to note at this juncture that Cu^{2+} increased the thermal stability of the **Q_1-X_2•X_3** duplex but not that of the **Q_1-X_1•X_1** or **Q_2-**PNAs.

EPR spectra have been recorded for 200 μM solutions of the PNA duplexes **Q_1-X_1•X_1**, **Q_2-X_1•X_1** or **Q_2-X_2•X_3** annealed in the presence of one equivalent of Cu^{2+} (Figure 2.13). The concentration of the coordinated Cu^{2+} in solutions of all Q-PNA duplexes determined by double integration of the EPR signal was 191, 202 and 190 μM, respectively, confirming that all Cu^{2+} was contained within [CuQ_2] complexes formed with **Q**-PNA duplexes. The spectra showed three g values $g_1 \sim g_2 < g_3$, which are very close to those previously measured for [CuQ_2] complexes (Table 2.4).[32] The EPR spectrum of the complex

formed by Cu^{2+} with the PNA duplex **Q_1-X_1•X_1** showed superhyperfine structure indicative of the coordination to Cu^{2+} of two nitrogen atoms, similar to the structure we have previously observed for **Q_1-X_2•X_3**.[9] In contrast, the EPR spectra of **Q_2**-modified PNAs **Q_2-X_1•X_1**-Cu^{2+} and **Q_2-X_2•X_3**-Cu^{2+} showed broad peaks with no superhyperfine features. This difference between the EPR spectra of **Q_1**-PNA and **Q_2**-PNA suggesting that there are slight differences between the environment of the [CuQ_2] complex formed with the **Q_2**-PNA or **Q_1**-PNA duplexes.

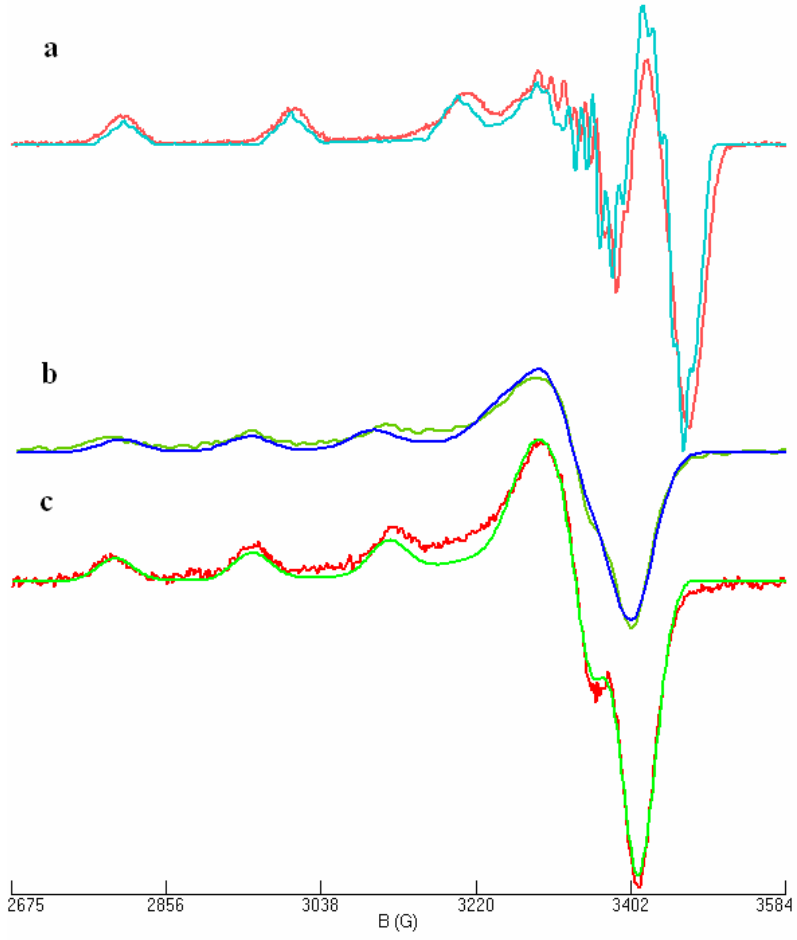

Figure 2.13. Perpendicular mode X-band EPR spectra of 200 μM solutions of (a) (**Q_1-X_1•X_1**)-Cu; (b) (**Q_2-X_1•X_1**)-Cu; (c). (**Q_2-X_2•X_3**)-Cu in pH 7.0 10 mM sodium phosphate buffer with 25% glycerol at 20 K, frequency 9.65 GHz, microwave power 0.02 mW, modulation amplitude 6.676 G. Simulations have been obtained using the parameters given in Table 2.4

Table 2.4. EPR Parameters for [CuQ_2] within PNA Context[a]

	$\mathbf{Q_1}$-$\mathbf{X_1}$•$\mathbf{X_1}$	$\mathbf{Q_1}$-$\mathbf{X_2}$•$\mathbf{X_3}$[1]	$\mathbf{Q_2}$-$\mathbf{X_1}$•$\mathbf{X_1}$	$\mathbf{Q_2}$-$\mathbf{X_2}$•$\mathbf{X_3}$	Cu$\mathbf{Q_2}$
$\mathbf{g_1}$	2.05	2.06	2.06	2.05	2.06
$\mathbf{g_2}$	2.06	2.05	2.07	2.08	2.06
$\mathbf{g_3}$	2.22	2.22	2.28	2.27	2.24
$\mathbf{A_1}$ (MHz)	77	72	63	62	72
$\mathbf{A_2}$ (MHz)	71	80	18	1	72
$\mathbf{A_3}$ (MHz)	611	611	474	522	530
$\mathbf{A_{1N}}$ (MHz)	32	39	-	-	39
$\mathbf{A_{2N}}$ (MHz)	40	32	-	-	33
$\mathbf{A_{3N}}$ (MHz)	38	36	-	-	33

a. A_i and A_{iN} are hyperfine coupling constants for copper and nitrogen nuclei, respectively.

PNA duplexes that have an aminoethyl glycine-based backbone, which is achiral, show a preferred handedness if a chiral amino acid is introduced into the PNA sequence. The chiral induction effect of the amino acid is transmitted through the GC and AT base pairs,[33] or through metal complexes contained within the PNA duplexes.[8,9] The CD spectra of all of the **Q**-PNA duplexes reported in this study have features indicative of left-handed structures, namely negative peaks at 220 nm and 255 nm (Figure 2.14). The small differences in the intensity of the spectra of duplexes that have the same sequence, but contain $\mathbf{Q_1}$ or $\mathbf{Q_2}$ ligands, as well as in the intensity of the spectra of the $\mathbf{Q_1}$-$\mathbf{X_1}$•$\mathbf{X_1}$ and $\mathbf{Q_1}$-$\mathbf{X_2}$•$\mathbf{X_3}$ duplexes annealed in the presence of Cu^{2+}, suggest the presence of some structural differences between these duplexes. Elucidation of the atomic level

details that lead to these differences must await the determination of the structures of these duplexes by NMR spectroscopy or X-ray crystallography.

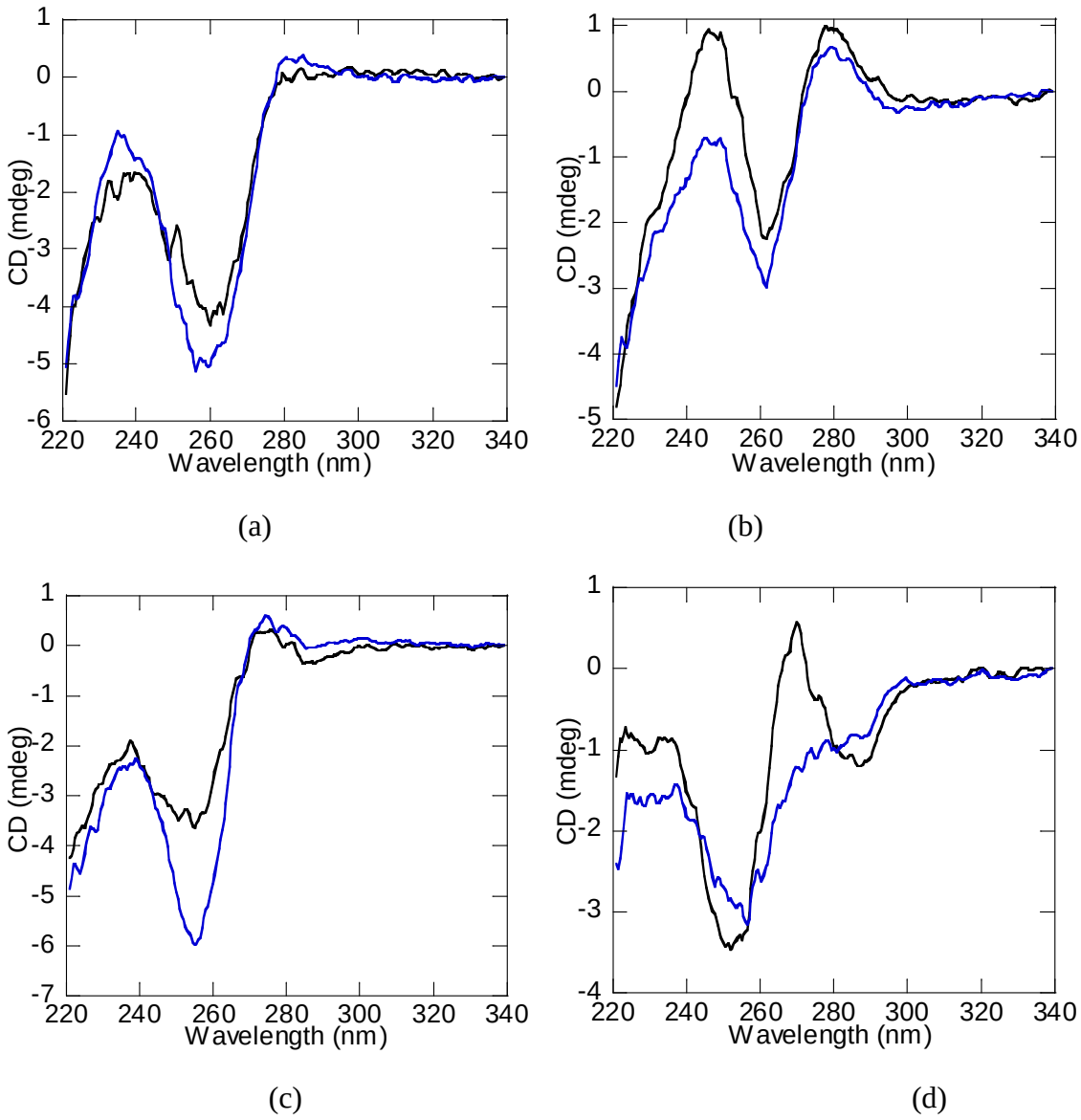

Figure 2.14. CD spectra of solutions Q-PNA a. $\mathbf{Q_1\text{-}X_1\bullet X_1}$ PNA; b. $\mathbf{Q_2\text{-}X_1\bullet X_1}$; c. $\mathbf{Q_1\text{-}X_2\bullet X_3}$ PNA; d. $\mathbf{Q_2\text{-}X_2\bullet X_3}$ PNA without (black) and with 1 eq. Cu^{2+} (blue). All samples are 20μM ss PNA in pH 7 10 mM sodium phosphate buffer, 20 °C.

2.2.4 Interaction of ligand modified PNA with Ag^+

UV-monitored thermal denaturation of ligand-modified PNA was performed in the absence and presence of Ag^+. All melting temperatures are listed in Table 2.5. The melting temperature of non-modified PNA duplexes **X_1•X_1** and **X_2•X_3** was not affected by one equivalent of Ag^+, which suggests that the metal ion interacts weakly if at all with the duplex. Both PNA duplexes **Q_1-X_1** and **Q_2-X_1** were slightly stabilized by Ag^+. The PNA duplex **Q_1-X_2•X_3** was much more stabilized by one eq. Ag^+ than the duplex **Q_2-X_2•X_3**.

Table 2.5. Non-modified and Q-modified PNA Oligomers, Melting Temperatures T_m(°C), and Changes in the Melting Temperature ΔT_m for Duplexes Formed in the Absence or Presence of Metal Ions[a]

Name	Sequence	No M^{n+}	Ag^+	
		T*m*[b]	T*m*[b]	ΔT*m*[c]
X_1	H-GGCATGCC-Lys-NH_2	68	67	-1
X_4	Ac-GGCATGCC-Lys-NH_2	70	73	+3
Q_1-X_1	H-GGCA**Q1**TGCC-Lys-NH_2			
Q_2-X_1	H-GGCA**Q2**TGCC-Lys-NH_2			
X_5	Ac-GGCA**Q2**TGCC-Lys-NH_2	82	83	+1
X_2 **X_3**	H-GTAGTCACT-Lys-NH_2 NH_2-Lys-CATCAGTGA-H	63	64	+1
Q_1-X_2 **Q_1-X_3**	H-GTAG**Q1**TCACT-Lys-NH_2 NH_2-Lys-CATC**Q1**AGTGA-H	46	61	+15
Q_2-X_2 **Q_2-X_3**	H-GTAG**Q2**TCACT-Lys-NH_2 NH_2-Lys-CATC**Q2**AGTGA-H	38	44	+6

(a) Samples were 10μM ss PNA in pH7 10 mM sodium phosphate buffer; (b) The precision for the T_m is ±1°C; (c) ΔT_m was calculated as the difference between the melting temperature of the duplex formed in the presence and absence of the metal ion.

Melting curves of **Q_1-X_2•X_3** and **Q_2-X_2•X_3** in the absence of Ag^+ and in the presence of Ag^+ were measured (Figure 2.15). **Q_1-X_2•X_3** was more stable in the presence of one equivalent Ag^+ than in the presence of excess Ag^+, but **Q_2-X_2•X_3** was more stable in the presence of two equivalents of Ag^+ than in the

presence of one equivalent. As shown in Figure 2.15, melting curves are more cooperative for **Q_1-X_2•X_3** than for **Q_2-X_2•X_3** in the presence of Ag^+, suggesting that the coordination of Ag^+ with PNA duplex **Q_2-X_2•X_3** is stronger than with **Q_1-X_2•X_3**.

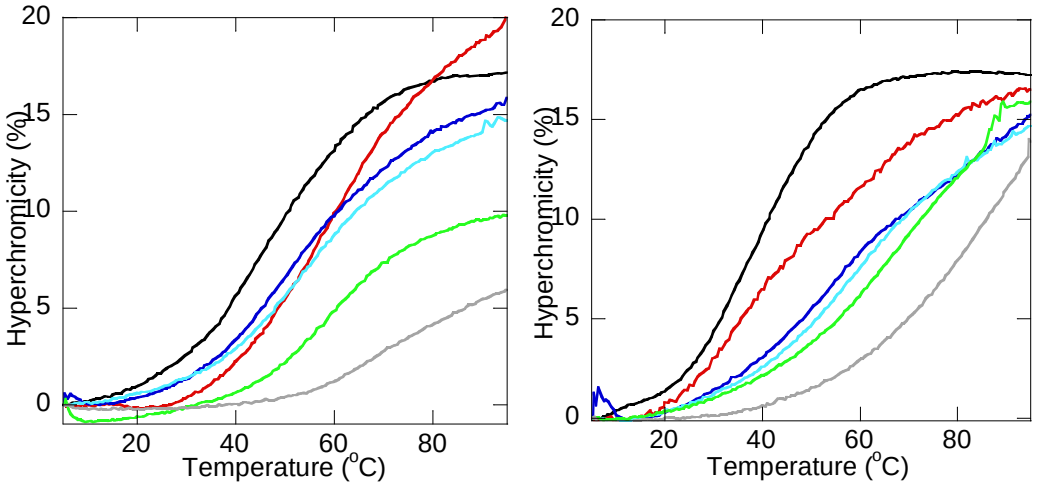

Figure 2.15. Melting curves of **Q_1-X_2•X_3** (a) and **Q_{12}-X_2•X_3** (b) in the presence of 0 (black), 1 (red), 2 (deep blue), 3 (light blue), 5 (green) and 10 (gray) equivalent Ag^+.

In titrations of non-modified PNAs **X_1•X_1**, **X_4•X_4** , and **X_2•X_3** with Ag^+ at pH 7, we observed a small decrease in the absorbance at 260 nm and several isosbestic points (Figures 2.16, 2.17 and 2.18). These changes are similar to those observed in UV titrations of nucleobases and of DNA with various GC/AT ratios with Ag^+ at pH 4-9, where changes in the absorbance were observed at 240-280 nm.[20,23] Based on these results, we conclude that Ag^+ coordinates to the nucleobases and possibly to the terminal lysine of the PNA.

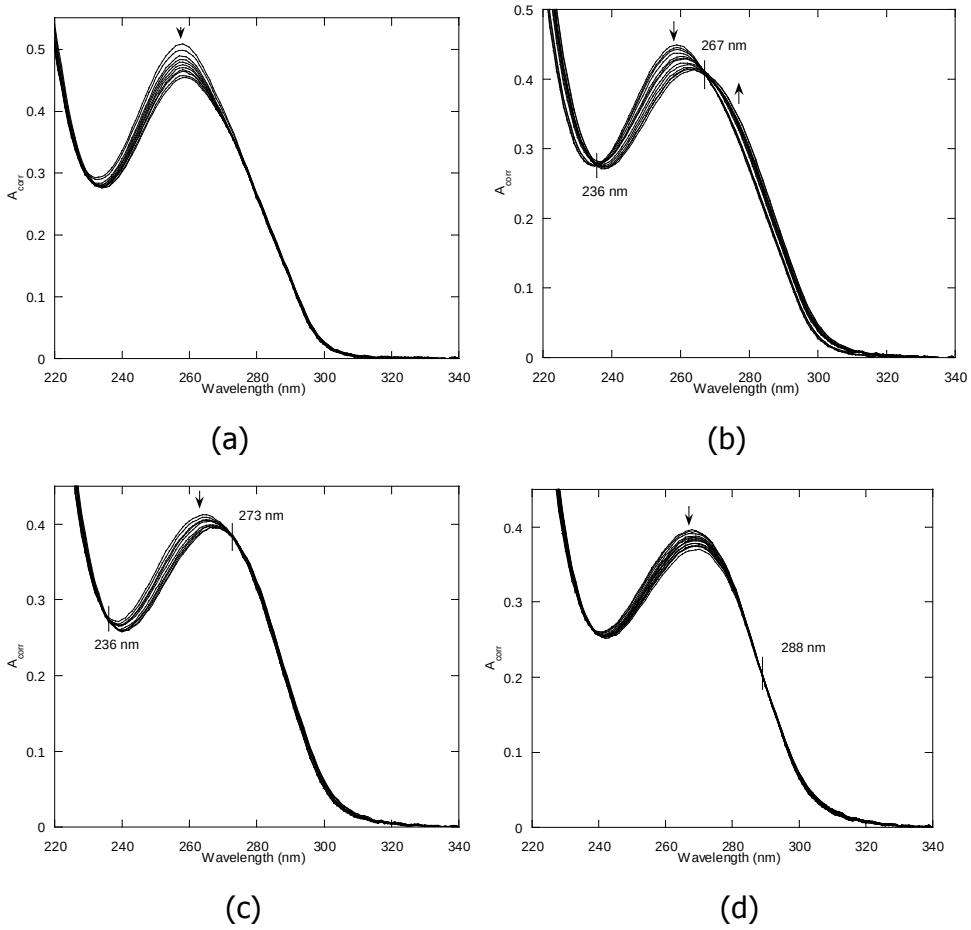

Figure 2.16. Spectrophotometric titration of a 5μM $\mathbf{X_1 \bullet X_1}$ solution in pH=7.0 10 mM phosphate buffer with 0.5 mM $AgNO_3$ solution, T=25°. a. Titration plot; b. $[Ag^+]/[ssPNA]=0\text{-}1.0$; c. $[Ag^+]/[ssPNA]=1.0\text{-}2.5$; d. $[Ag^+]/[ssPNA]=2.5\text{-}3.5$; e. $[Ag^+]/[ssPNA]=3.5\text{-}5.0$.

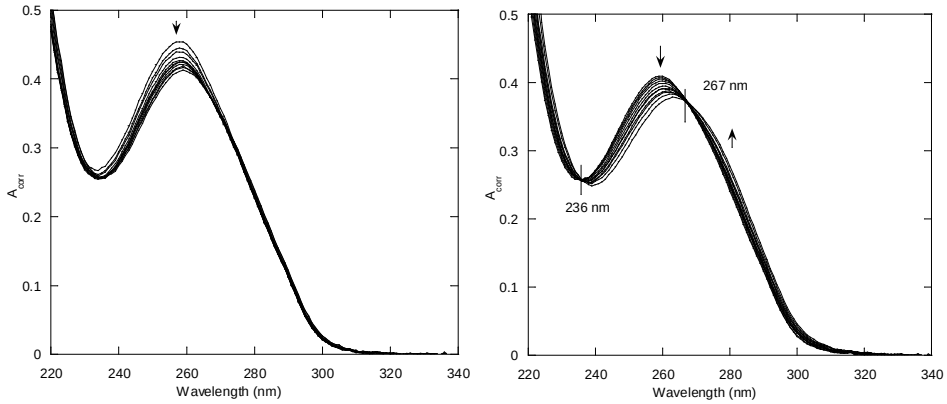

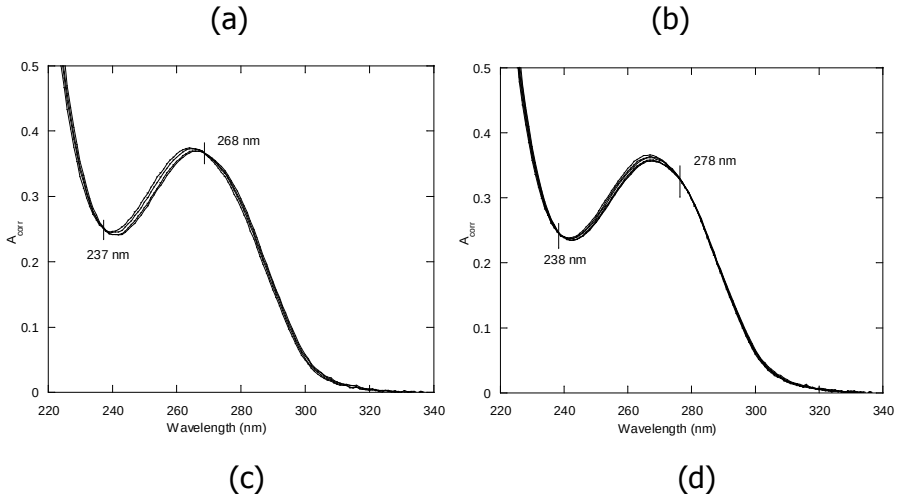

Figure 2.17. Spectrophotometric titration of a 5μM **X_4•X_4** solution in pH=7.0 10 mM phosphate buffer with 0.5 mM $AgNO_3$ solution, T=25°. a. $[Ag^+]$/[ssPNA]=0-1.0; b. $[Ag^+]$/[ssPNA]=1.0-2.5; c. $[Ag^+]$/[ssPNA]=2.5-3.5; d. $[Ag^+]$/[ssPNA]=3.5-5.0.

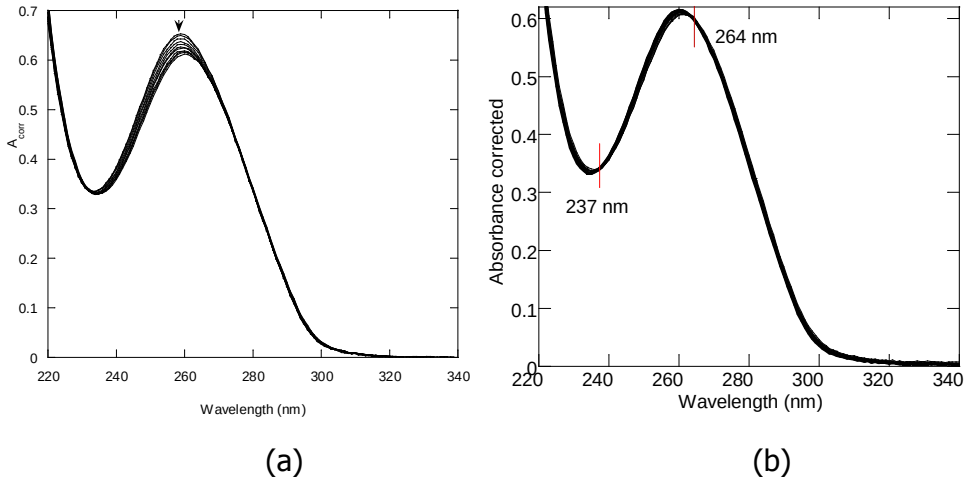

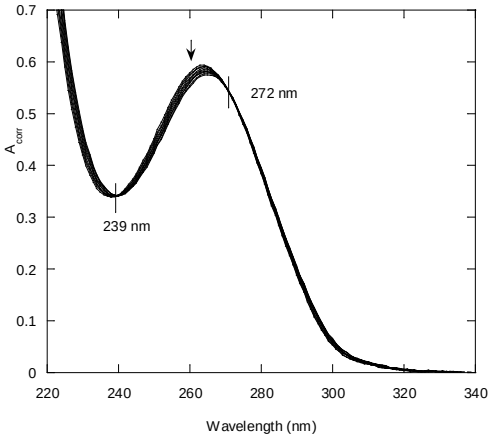

(c)

Figure 2.18. Spectrophotometric titration of a 5μM **X_2•X_3** solution in pH=7.0 10 mM phosphate buffer with 0.5 mM $AgNO_3$ solution, T=25°. a. Titration plot; b. $[Ag^+]$/[ssPNA]=0-1.0; c. $[Ag^+]$/[ssPNA]=1.0-3.0.

Titrations of 8-hydroxyquinoline with Ag^+ showed no change in the absorption spectrum of the ligand except for a small decrease in absorbance at 220 nm. This change at 220 nm is due to the formation of complexes between the metal ion and the phosphate present in the buffer (Figure 2.19a), and it indicates that at pH 7 and micromolar concentrations, Ag^+ does not coordinate to 8-hydroxyquinoline (Figure 2.19b).

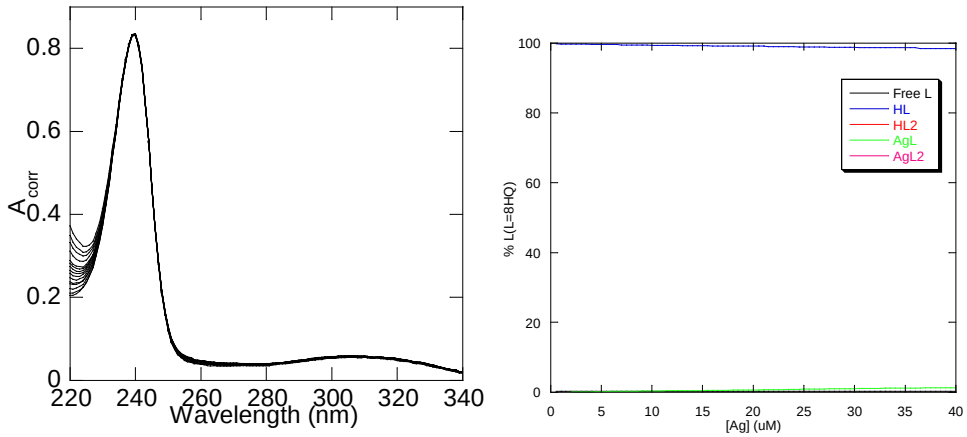

(a) (b)

Figure 2.19. a. Spectrophotometric titration of a 20μM 8-hydroxyquinoline solution in pH 7.0 10 mM phosphate buffer (25% MeCN) with 1.00 mM $AgNO_3$ solution, T=25°. b. Speciation diagrams for Ag-8HQ pH 7 solutions. The 8-hydroxyquinoline concentration was 20μM. Binding and acidity constants used in constructing the speciation diagrams were obtained from ref[12].

The UV titrations of PNA duplexes **Q_1-X_1•X_1**, **Q_2-X_1•X_1**, **Q_1-X_2•X_3**, and **Q_2-X_2•X_3** with Ag^+ are shown in Figures 2.20-Figure 2.23. All titrations show several isosbestic points at 230-280 nm, which indicates that Ag^+ coordinates to Q, the nucleobases and possibly to the terminal lysines of the PNA.

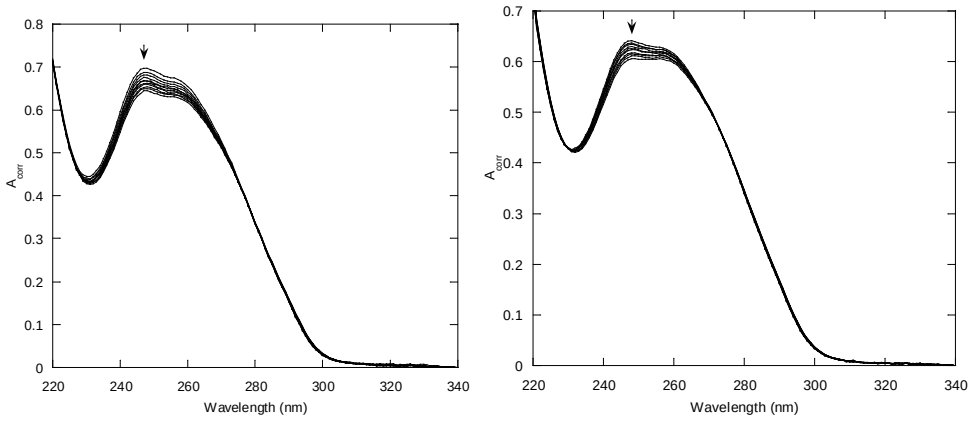

(a) (b)

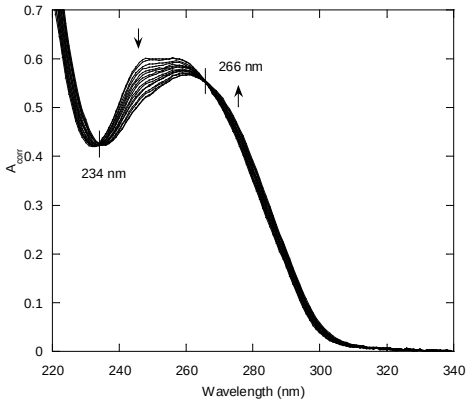

(c)

Figure 2.20. Spectrophotometric titration of a 5μM **Q_1-X_1•X_1** solution in pH=7.0 10 mM phosphate buffer with 0.5 mM $AgNO_3$ solution, T=25°. a. $[Ag^+]$/[ssPNA]=0-1.0; b. $[Ag^+]$/[ssPNA]=1.0-2.0; c. $[Ag^+]$/[ssPNA]= 2.0-6.0.

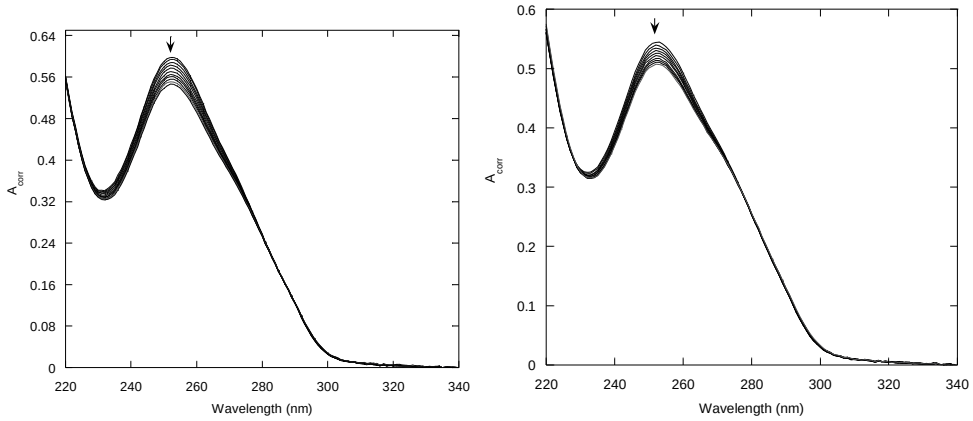

(a) (b)

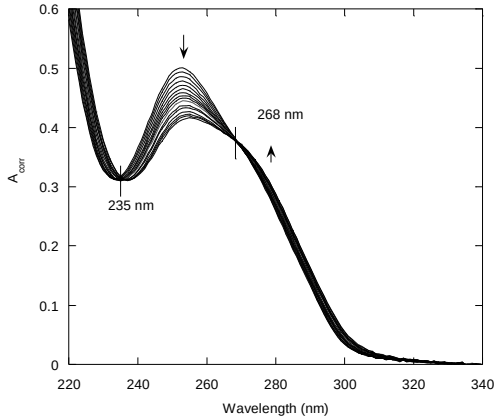

(c)

Figure 2.21. Spectrophotometric titration of a 5μM **Q_2-X_1•X_1** solution in pH=7.0 10 mM phosphate buffer with 0.5 mM $AgNO_3$ solution, T=25°. a. $[Ag^+]$/[ssPNA]=0-1.0; b. $[Ag^+]$/[ssPNA]=1.0-2.0; c. $[Ag^+]$/[ssPNA]=2.0-6.0.

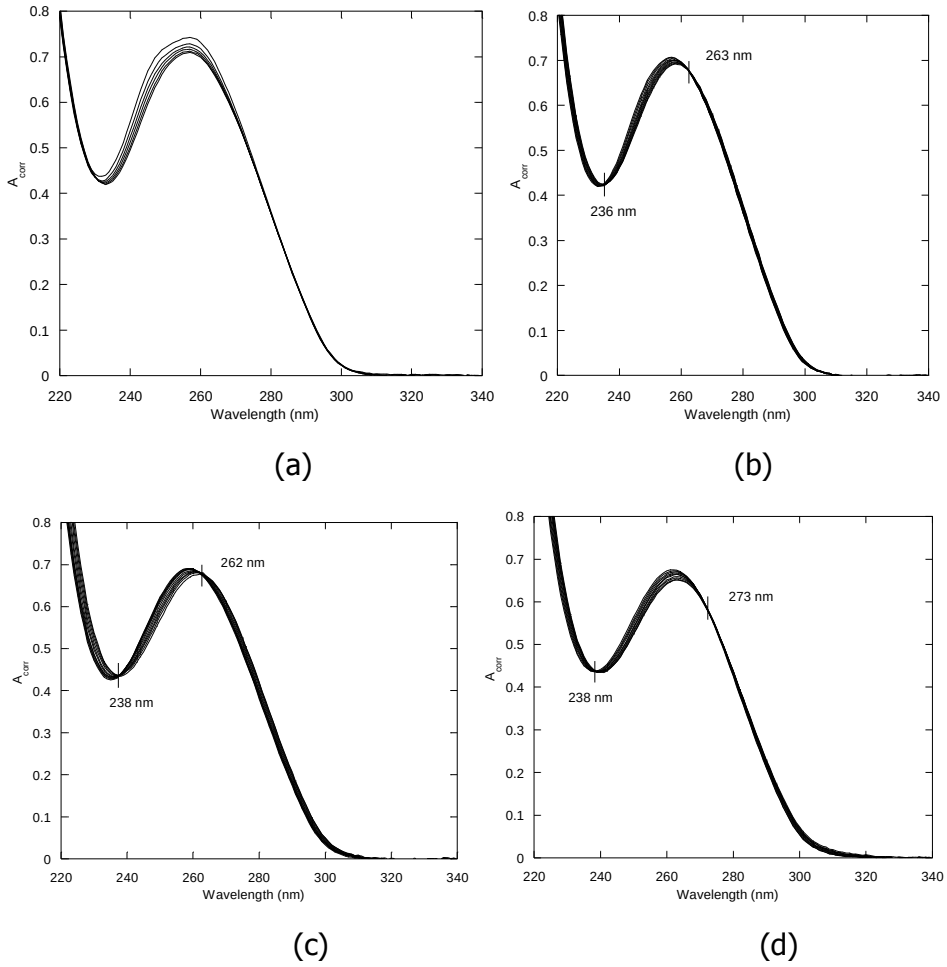

Figure 2.22. Spectrophotometric titration of a 5μM **Q_1-X_2•X_3** solution in pH=7.0 10 mM phosphate buffer with 0.5 mM $AgNO_3$ solution, T=25°. a. $[Ag^+]$/[ssPNA]=0-0.5; b. $[Ag^+]$/[ssPNA]=0.5-1.5; c. $[Ag^+]$/[ssPNA]=1.5-3.5; d. $[Ag^+]$/[ssPNA]=3.5-6.0.

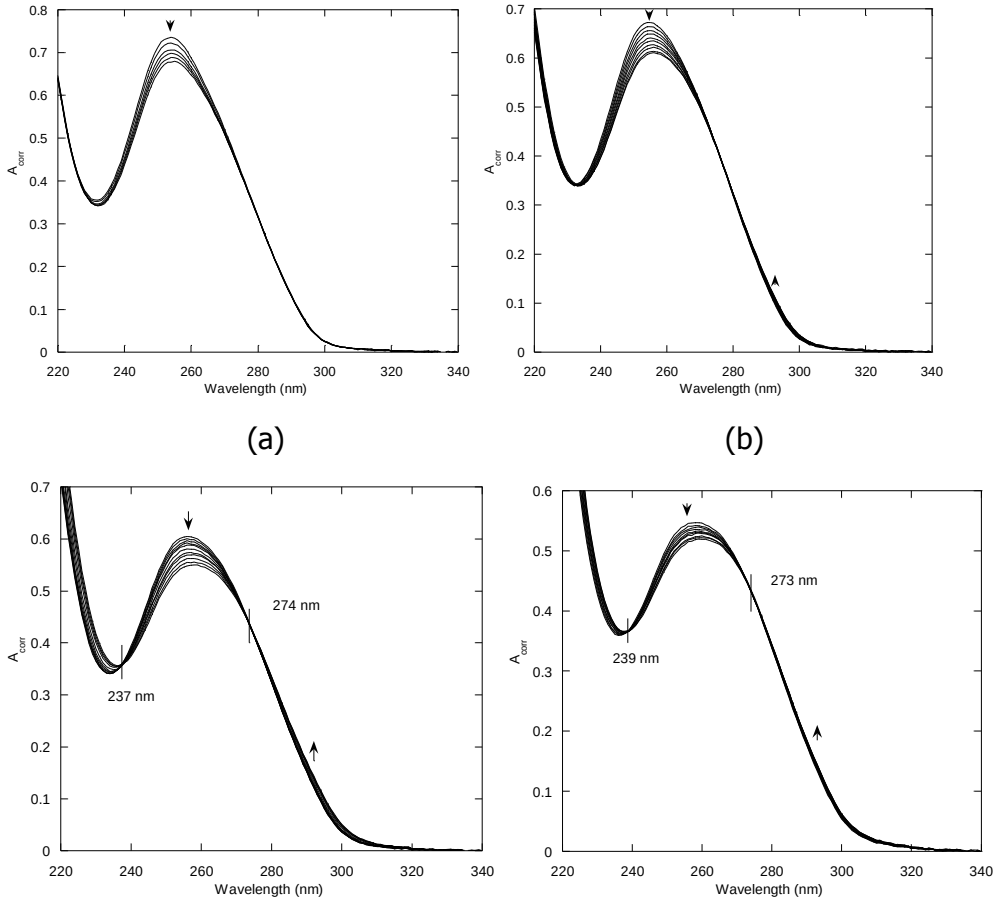

Figure 2.23. Spectrophotometric titration of a 5μM **Q_2-X_2•X_3**solution in pH=7.0 10 mM phosphate buffer with 0.5 mM $AgNO_3$ solution, T=25°. a. $[Ag^+]$/[ssPNA]=0-0.5; b. $[Ag^+]$/[ssPNA]=0.5-1.5; c. $[Ag^+]$/[ssPNA]=1.5-3.5; d. $[Ag^+]$/[ssPNA]=3.5-6.0.

Titrations of Q_1- and Q_2-containing PNA duplexes with Ag^+ showed a decrease in the absorbance at 230-280 nm, where there are absorption bands due to the π–π* transitions of the 8-hydroxyquinoline and nucleobases (Figure 2.24a and b). The absorbance changes at 260 nm are similar for **Q_1-X_2•X_3**, **Q_2-X_2•X_3** and **X_2•X_3** (Figure 2.25), as well as for **Q_1-X_1•X_1**, **Q_2-X_1•X_1** and **X_1•X_1** duplexes irrespective of the amount of Ag^+ added to the solutions (Figure 2.26). The relative change in absorption at 246 nm for **Q_1-X_2•X_3** and **Q_2-X_2•X_3** with

respect to that for **X_2•X_3** (Figure 2.24e) shows an inflection point at a 1:1 ratio between Ag^+ and ssPNA. These results suggest that the first two equivalents of Ag^+ bind to the two 8-hydroxyquinoline residues of each duplex and the subsequent equivalents bind to the nucleobases.

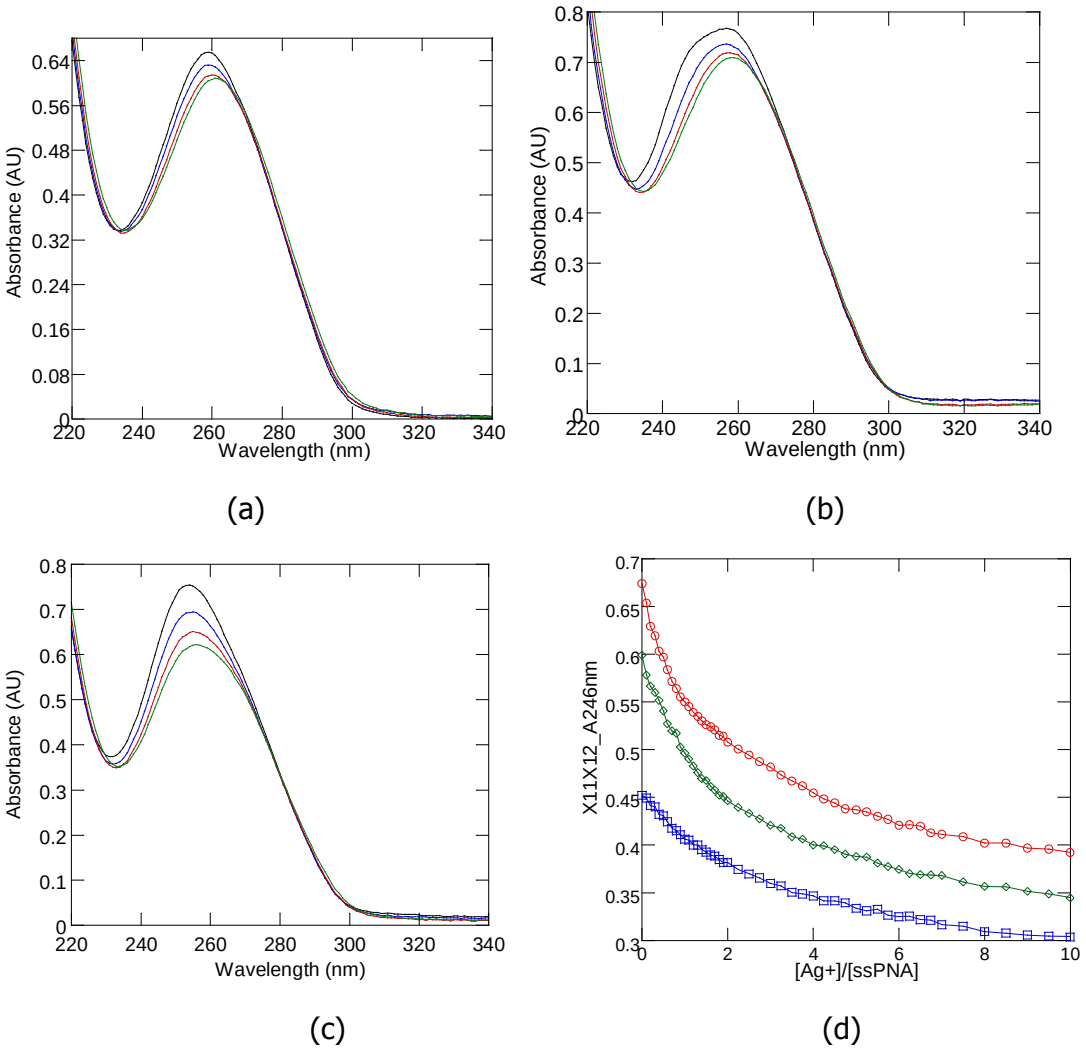

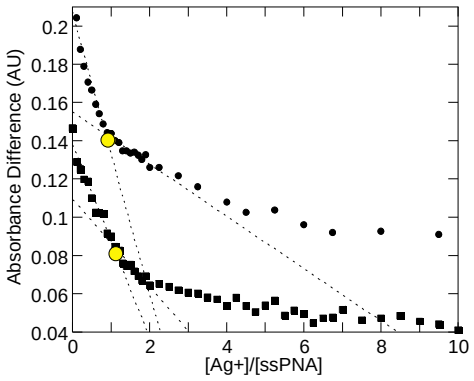

(e)

Figure 2.24. Absorption spectra for 10 μM solutions of a. $\mathbf{X_2 \bullet X_3}$ or b. $\mathbf{Q_1\text{-}X_2 \bullet X_3}$ c. $\mathbf{Q_2\text{-}X_2 \bullet X_3}$ in pH 7 10 mM sodium phosphate buffer in the presence of no Ag^+ (black), or 1 (blue), 2 (red) or 4 (green) equivalents of Ag^+; d. Absorbance 246 nm for $\mathbf{X_2 \bullet X_3}$ (blue), $\mathbf{Q_1\text{-}X_2 \bullet X_3}$ (red) and $\mathbf{Q_2\text{-}X_2 \bullet X_3}$ (green); e. Absorbance change at 246 nm for $\mathbf{Q_1\text{-}X_2 \bullet X_3}$ (circles) and $\mathbf{Q_2\text{-}X_2 \bullet X_3}$ (squares) with respect to $\mathbf{X_2 \bullet X_3}$.

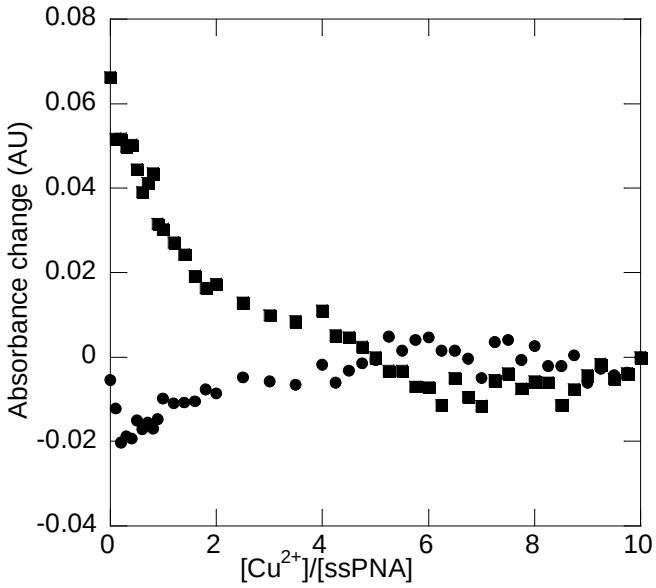

Figure 2.25. Absorbance change at 260 nm for $\mathbf{Q_1\text{-}X_2 \bullet X_3}$ (circle)and $\mathbf{Q_2\text{-}X_2 \bullet X_3}$ (square) with respect to $\mathbf{X_2 \bullet X_3}$.

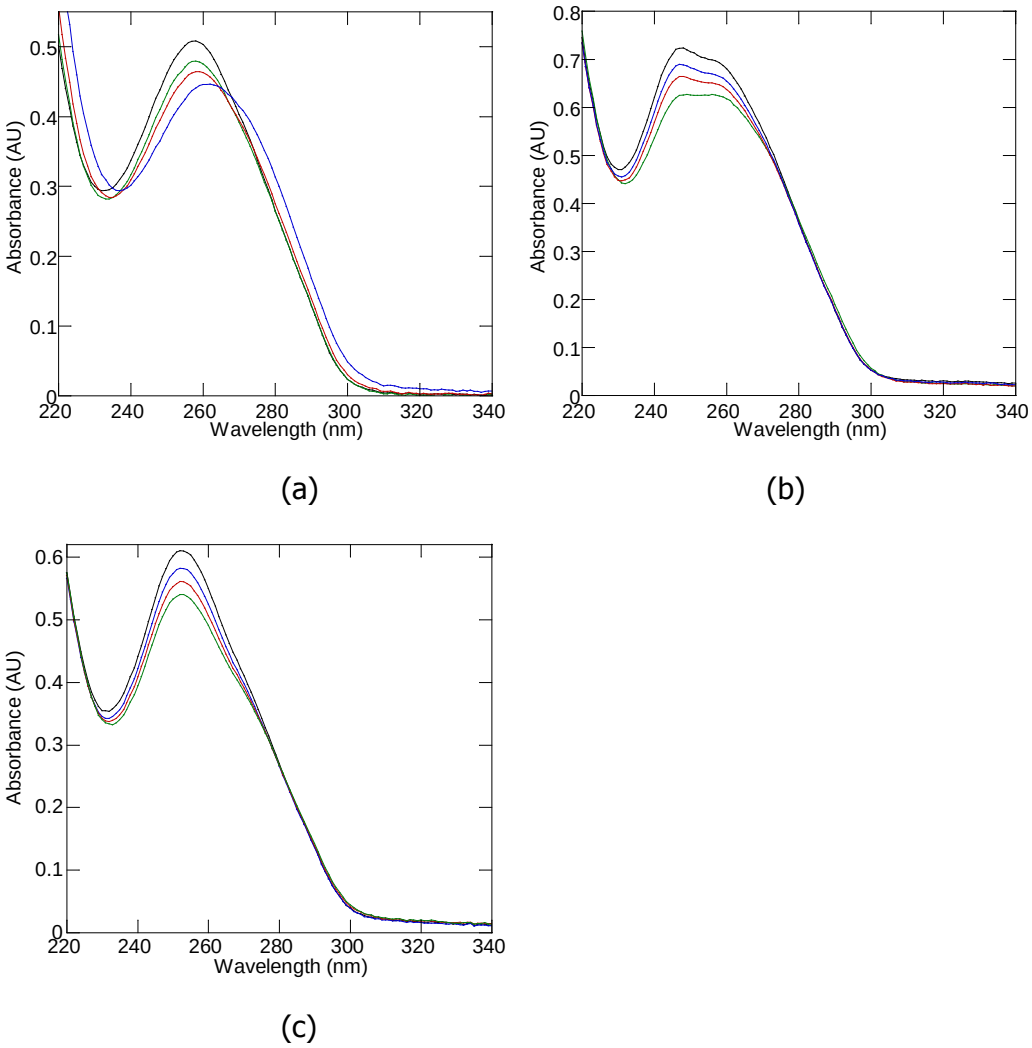

Figure 2.26. Absorption spectra for 10 μM solutions of a. $\mathbf{X_1 \bullet X_1}$ or b. $\mathbf{Q_1\text{-}X_1 \bullet X_1}$ or c. $\mathbf{Q_2\text{-}X_1 \bullet X_1}$ in pH 7 10 mM sodium phosphate buffer in the presence of no Ag^+ (black), or 1 (blue), 2 (red) or 4 (green) equivalents of Ag^+.

Conclusions

The possibility of synthesizing nucleic acid duplexes that contain both nucleobase pairs and transition metal complexes is attractive because these hybrid inorganic-nucleic acid structures have properties that are potentially useful for nanotechnology applications. Achieving this potential depends on knowledge of the factors that affect the formation and properties of the hybrid inorganic-nucleic acid structures. Our studies indicate that the propensity of a specific pair of metal ions and ligands to form a complex is maintained when the ligands are introduced into a PNA duplex.

The spectroscopy and thermodynamic studies led to the conclusion that the stability constants of Cu^{2+} complexes with **Q-PNA** decreased in the order **Q_1-X_2•X_3** > **Q_1-X_1•X_1** > **Q_2-X_2•X_3** ≈ **Q_2-X_1•X_1**, which corroborates the fact that these constants depend on (*1*) the way in which the ligand is attached to the backbone, with **Q_1-**PNAs forming more stable complexes than **Q_2-PNAs**, and (*2*) the sequence of the PNAs, with **Q-X_2•X_3** PNA duplexes forming complexes more stable than the corresponding **Q-X_1•X_1** duplexes. The apparent stability constants (Logβ_2) of the [CuQ_2] complexes formed between **Q_1-X_2•X_3**, **Q_1-X_1•X_1** and **Q_2-X_2•X_3** and Cu^{2+} are 10.6, 9.7 and 8.7, respectively, in phosphate buffer and 7.9, 6.8 and 3.6, respectively, in Tris buffer. The trend in the stability constants obtained by different methods in different buffers and the difference between the stability constants of the complexes formed with **Q_1-X_2•X_3** and **Q_1-X_1•X_1** are the same. However, the difference between the stability constants of complexes with **Q_1-X_1•X_1** and **Q_2-X_2•X_3** is about 1 for UV titrations in pH 7.0 10 mM sodium phosphate buffer and 3 for ITC in pH 8.10 100 mM Tris buffer. It is possible that the secondary structure of **Q_2-X_2•X_3** is affected by the buffer and pH, leading to differences in the strength of the interactions between Cu^{2+} and **Q_2-X_2•X_3**.

Our calorimetry studies showed quantitatively that the Watson Crick hybridization of two ligand-PNA strands into a duplex can increase the stability

constants of the metal complexes formed within the PNA by a few orders of magnitude when compared to the corresponding stability constants for complexes with free ligands. This effect occurs in a manner similar to that in which polytopic ligands form more stable complexes than the corresponding complexes with individual ligands that have the same binding motifs – it is an entropy-driven supramolecular chelate effect. On the other hand, steric constraints limit the supramolecular effect when the relative orientation of the ligands within the PNA duplex does not favor for the formation of a metal complex. This modulation effect, which is enthalpic in nature, can be induced both by the sequence/secondary structure of the PNA and by the way in which the ligand is attached to the PNA backbone.

We conclude that the incorporation of a metal complex with high stability constant into a PNA duplex is not a sufficient condition for the formation of stable hybrid metal-nucleic acid duplexes and that the steric relationship between the complex and the duplex must be considered in the design of metal-containing alternative base pairs.

2.3 Experiments

Materials. All reagents have been obtained from commercially available sources, have been of analytical grade quality, and have been used without further purification. ^{1}H NMR spectra have been recorded on a Bruker Cryospec WM 300. A Finnegan Mattson instrument was used for electrospray mass spectrometry (ES-MS). An Applied Biosystems Voyager Biospectrometry Workstation with Delayed Extraction was used for MALDI-TOF mass spectrometry. Tert-Butyl N-(2-Boc-aminoethyl)-glycinate **1** was prepared according to a published procedure [34].

Synthesis of *tert*-butyl 2-(N-(2-(tert-butoxycarbonyl)ethyl)-8-hydroxyquinoline -2-carboxamido)-acetate (3). 100 mg (0.53mmol) 8-hydroxyquinoline-2-carboxylic acid and 86 mg (0.53 mmol) DhbtOH have been dissolved in 10 ml DMF. 146 mg (0.53 mmol) Aeg dissolved in 15ml DCM was

added to the DMF solution. The resulting solution was cooled to 0°C and then 109 mg (0.53 mmol) DCC was added. The solution was stirred at 0°C for 2 h and then at room temperature for 24 h. The solution was filtered and then diluted with 30 ml DCM. The resulting solution was washed with a dilute aqueous solution of $NaHCO_3$ (25ml×3). The organic phase was dried over Na_2SO_4. The DCM was removed under vacuum. The solid obtained after solvent removal was suspended in 20 ml ethyl acetate. A yellow ethyl acetate solution was obtained after a white precipitate was filtered off. Removal of the ethyl acetate under vacuum led to **1** as orange solid. Yield: 121 mg, 51%. ^{1}H NMR(300 MHz, in d-acetone) : δ,8.44 (d, 1H); 7.92, 7.72 (dd, 1H); 7.55 (m, 1H); 7.47 (dd, 1H); 7.20 (dd, 1H); 4.57,4.23 (ss, 2H, N-CH_2-CO); 3.75 (tt, 2H, CH_2-N=); 3.36 (tt, 2H, CH_2-NHBoc); 1.40 (m, 18H, Boc+OtBu). ES-MS for $(M-H)^-$ (methanol): m/z=444.1 observed, 444.5 calculated.

Synthesis of 2-(N-(2-(*tert*-butoxycarbonyl)ethyl)-8-hydroxyquinoline-2-carboxamido)-acetic acid (4)

1.5 ml of a 6M NaOH solution was added drop wise with constant stirring to a solution of the 8-hydroxyquinoline monomer ester **3** (120.9 mg) in 30 ml 1:2 ethanol-water cooled to 0°C. The mixture was stirred for 4 hours at room temperature. The resulting solution was then filtered, acidified to pH = 4 by addition of 4 M HCl, and extracted with 3×30 ml ethyl acetate. The ethyl acetate fractions have been combined, dried over anhydrous Na_2SO_4, filtered and the solvent was removed under vacuum to obtain **4** as a yellow solid. Yield: 82 mg, 77%. ^{1}H NMR(300 MHz, in d-acetone): δ,8.44 (d, 1H); 7.92, 7.73 (dd, 1H); 7.55 (m, 1H); 7.47 (dd, 1H); 7.20 (dd, 1H); 4.58, 4.35 (ss, 2H, N-CH_2-CO); 3.78 (tt, 2H, CH_2-N=); 3.39 (tt, 2H, CH_2-NHBoc); 1.36 (d, 9H, Boc). ES-MS for $(M-H)^-$ (methanol): m/z=388.1 observed, 388.4 calculated.

PNA Sample Preparation and Storage. PNAs have been dissolved in nanopure water (>18.3 $M\tilde{\Omega}cm^{-1}$) and stored at -18 ^oC to avoid depurination reactions.

Solid-Phase PNA Synthesis. PNA oligomers have been synthesized using the Boc-protection strategy. PNA monomers have been purchased from Applied Biosystems and ASM Research Chemicals and used without further purification. After cleavage, PNA was precipitated using ethyl ether and was purified by reversed-phase HPLC using a C18 silica column on a Waters 600 Controller and Pump. Absorbance was measured with a Waters 2996 Photodiode Array Detector. Characterization of the oligomers was performed by MALDI-ToF mass spectrometry on an Applied Biosystems Voyager Biospectrometry Workstation with Delayed Extraction and an R-cyano-4-hydroxycinnamic acid matrix (10 mg/mL in 1:1 water: acetonitrile, 0.1% TFA). Calculated/found m/z for $(\mathbf{X_i}+H)^+$ $\mathbf{X_1}$ 2314.3/2314.6, $\mathbf{Q_1\text{-}X_1}$ 2600.5/2600.2, $\mathbf{Q_2\text{-}X_1}$ 2586.5/2586.5, $\mathbf{X_2}$ 2579.6/2579.8, $\mathbf{X_3}$ 2588.6/2588.7, $\mathbf{Q_1\text{-}X_2}$ 2865.8/2866.0, $\mathbf{Q_1\text{-}X_3}$ 2874.8/2875.0, $\mathbf{Q_2\text{-}X_2}$ 2851.8/2850.6, $\mathbf{Q_2\text{-}X_3}$ 2860.8/2860.8, $\mathbf{X_4}$ 2356.3/2356.6, $\mathbf{X_5}$ 2628.5/2628.2.

Physical Methods.

CD Spectroscopy. CD spectra have been measured for 20 μM total PNA concentration in pH 7.0 10 mM sodium phosphate buffer solutions. In the case where complementary PNA strands have been used, solutions have been equimolar in the two strands. CD measurements have been conducted on a JASCO J-715 spectropolarimeter equipped with a thermoelectrically controlled, single-cell holder. CD spectra have been collected using bandwidth 1 nm, response time 1 s, speed 50 nm/min, sensitivity 20 mdeg, and scan accumulation 20.

UV-Vis Spectroscopy. UV-vis experiments have been performed on a Varian Cary 3 spectrophotometer with programmable temperature block, in 10 mm quartz cells. PNA stock solutions have been prepared with nanopure water and have been stored at -18 °C. The concentration of PNA oligomers was determined by UV absorption at 95 °C using the sum of the extinction coefficients of the constituent nucleosides ε_{260} taken from the literature. The extinction coefficient for 8-hydroxyquinoline ε_{260} =2570 M^{-1} cm^{-1} (pH =7.0) was determined from the

slope of the calibration curve A_{260} versus concentration. PNA solutions for melting curves and titrations had concentrations in the micromolar range (5-25) and have been prepared in pH 7.0 10 mM phosphate buffer. UV-vis titrations have been carried out by addition of standard 0.5-2 mM $Cu(NO_3)_2$ or $AgNO_3$ solutions in water to PNA solutions. The absorbance A after each addition was corrected for dilution and for the contribution of $Cu(NO_3)_2$ and PNA. The PNA solutions for UV-Vis spectra have been 10 μM in ss PNA in pH 7 10 mM sodium phosphate buffer unless otherwise noted. The apparent stability constants were calculated from spectrophotometric titration curves by non-linear regression using the HYPERQUAD 2000 program.[35]

UV melting curves have been recorded in the temperature range 5-95 °C for both cooling and heating modes, at the rate of 1 °C/min. Prior to the measurement of the melting profiles, the solutions have been kept at 95 °C for at least 10 min. Melting curves have been measured at 260 nm. T_m is the inflection point of a sigmoidal function used to fit the melting curve. All measurements have been performed at least in triplicate.

EPR Spectroscopy. EPR spectra have been recorded on an X-band (9 GHz) Bruker ESP 300 spectrometer equipped with an Oxford ESR 910 cryostat. The microwave frequency was calibrated with a frequency counter and the magnetic field with a NMR gaussmeter. The temperature was calibrated using devices from Lake Shore Cryonics. Spectra have been collected under nonsaturating conditions. Samples have been prepared in pH 7.0 10 mM sodium phosphate buffer with 25% glycerol as glassing agent. Samples containing PNA and Cu^{2+} in appropriate molar ratio have been heated at 95 °C for 10 min, slowly cooled to room temperature, and then transferred into EPR tubes and frozen. EPR spectra have been simulated using the program SpinCount written by Prof. Michael P. Hendrich.[36] Spin quantitation was done relative to a 0.499 mM Na_2[Cu(edta)] standard, the copper concentration of which was determined by plasma emission spectroscopy.

ITC $Cu(NO_3)_2$ was bought from Alfa Aesar and was 99.999%. 8-Hydroxyquinoline and Tris(hydroxymethyl)-aminomethane (Tris) have been obtained from Aldrich and was 99% and 99.9+% pure respectively. Tris buffer solutions have been made by dissolving calculated amounts of solid in Nanopure water, and adjusting to the desired pH with HCl. The concentration of $Cu(NO_3)_2$ was corrected by Cu-EDTA ITC experiment.

A MicroCal VP-ITC was used for all ITC experiments. A solution of one of the solution was placed in the cell (volume 1.46 mL) and the titrant solution (about 281.5 μM) in a syringe with the stirring speed at 300 rpm. Typically 58 injections of 5 μL each and 210s apart have been made. The integrated peaks of the heat p have been plotted as a function of the molar ratio. With MicroCal Origin, the binding isotherms have been fitted to a one-site-binding or two-site-binding model, giving values of the enthalpy of binding (ΔH_{ITC}) and the binding constant (K_{ITC}). The binding constants were then corrected taking into consideration the $[Cu(Tris)_4]$ complex formation (α_{Cu}, β_4) and the protonation of 8-hydroxyquinoline (α_Q, K_{1H}, K_{2H}).[28]

Reference

(1) He, W.; Franzini, R. M.; Achim, C. *Prog. Inorg. Chem.* **2007**, *55*, 545-611.
(2) Tanaka, K.; Shionoya, M. *J. Org. Chem.* **1999**, *64*, 5002-5003.
(3) Clever, G. H.; Kaul, C.; Carell, T. *Angewandte Chemie, International Edition* **2007**, *46*, 6226-6236.
(4) Tanaka, K.; Shionoya, M. *Coord. Chem. Rev.* **2007**, *251*, 2732-2742.
(5) Tanaka, K.; Tengeiji, A.; Kato, T.; Toyama, N.; Shionoya, M. *Science* **2003**, *299*, 1212-1213.
(6) Nielsen, P. E.; Egholm, M.; Berg, R. H.; Buchardt, O. *Science* **1991**, *254*, 1497-500.
(7) Franzini, R. M.; Watson, R. M.; Patra, G. K.; Breece, R. M.; Tierney, D. L.; Hendrich, M. P.; Achim, C. *Inorg. Chem.* **2006**, *45*, 9798-9811.
(8) Popescu, D.-L.; Parolin, T. J.; Achim, C. *J. Am. Chem. Soc.* **2003**, *125*, 6354-6355.
(9) Watson, R. M.; Skorik, Y.; Patra, G. K.; Achim, C. *J. Am. Chem. Soc.* **2005**, *127*, 14628-14639.
(10) Clever, G. H.; Kaul, C.; Carell, T. *Angew. Chem. Int. Ed.* **2007**, *46*, 6226-6236.
(11) Switzer, C.; Shin, D. *Chem. Commun.* **2005**, 1342-1344.
(12) Martell, A. E.; Smith, R. M. *Critical Stability Constants, Vol. 2.*, 1976.
(13) Barawkar, D. A.; Kumar, R. K.; Ganesh, K. N. *Tetrahedron* **1992**, *48*, 8505-14.
(14) Milani, B.; Anzilutti, A.; Vicentini, L.; Santi, A. S.; Zangrando, E.; Geremia, S.; Mestroni, G. *Organometallics* **1997**, *16*, 5064-5075.
(15) Clever, G. H.; Soeltl, Y.; Burks, H.; Spahl, W.; Carell, T. *Chem. Eur. J.* **2006**, *12*, 8708-8718.
(16) Tanaka, K.; Yamada, Y.; Shionoya, M. *J. Am. Chem. Soc.* **2002**, *124*, 8802-8803.
(17) Arakawa, H.; Neault, J. F.; Tajmir-Riahi, H. A. *Biophys. J .* **2001**, *81*, 1580-1587.
(18) Arya, S. K.; Yang, J. T. *Biopolymers* **1975**, *14*, 1847-61.
(19) DiRico, D. E., Jr.; Keller, P. B.; Hartman, K. A. *Nucleic Acids Res.* **1985**, *13*, 251-60.
(20) Eichhorn, G. L.; Butzow, J. J.; Clark, P.; Tarien, E. *Biopolymers* **1967**, *5*, 283-96.
(21) Izatt, R. M.; Christensen, J. J.; Rytting, J. H. *Chem. Rev.* **1971**, *71*, 439-82.
(22) Jensen, R. H.; Davidson, N. *Biopolymers* **1966**, *4*, 17-32.
(23) Yamane, T.; Davidson, N. *Biochim. Biophys. Acta* **1962**, *55*, 609-21.
(24) Nielsen, P. E.; Editor *Peptide Nucleic Acids: Protocols and Applications, Second Edition*, 2004.
(25) Yamamoto, Y.; Miura, A.; Kawamata, A.; Miura, M.; Takei, S. *Bull. Chem. Soc. Jpn.* **1978**, *51*, 3489-95.
(26) Deraeve, C.; Boldron, C.; Maraval, A.; Mazarguil, H.; Gornitzka, H.; Vendier, L.; Pitie, M.; Meunier, B. *Chem.--Eur. J.* **2008**, *14*, 682-696.

(27) The inflection points in the titration curves for **Q_2-X_1•X_1** were not as sharp as for the other Q-PNAs, making the corresponding simulated stability constant less reliable.
(28) Zhang, Y.; Akilesh, S.; Wilcox, D. E. *Inorg. Chem.* **2000**, *39*, 3057-3064.
(29) Cu^{2+} interacts very weakly with the nucleobases and consequently an ITC titration of the 9-bp X_2•X_3 PNA duplex showed only mixing heat.
(30) The titration of PNA duplexes identical to Q_2-X_1•X_1 except for the N-terminus, which was acetylated, was very similar to that of Q_2-X_1•X_1, which indicates that the acetylation of the terminal amine of the PNA oligomers does not affect the coordination of Cu^{2+} to the Q_2-PNA and exclude the possibility that Cu^{2+} would coordinate to the terminal NH_2 group of the PNA in Q_2-X_1•X_1 rather than to the Q_2 ligands of the Q_2-X_1•X_1 duplex.
(31) Fresco, J.; Freiser, H. *Analytical Chemistry* **1964**, *36*, 372-375.
(32) Walker, F. A.; Sigel, H.; McCormick, D. B. *Inorg. Chem.* **1972**, *11*, 2756-63.
(33) Wittung, P.; Eriksson, M.; Lyng, R.; Nielsen, P. E.; Norden, B. *J. Am. Chem. Soc.* **1995**, *117*, 10167-73.
(34) Dueholm, K. L.; Egholm, M.; Behrens, C.; Christensen, L.; Hansen, H. F.; Vulpius, T.; Petersen, K. H.; Berg, R. H.; Nielsen, P. E.; Buchardt, O. *J. Org. Chem.* **1994**, *59*, 5767-73.
(35) Gans, P.; Sabatini, A.; Vacca, A. *Talanta* **1996**, *43*, 1739-1753.
(36) Hendrich, M. P.; Petasis, D.; Arciero, D. M.; Hooper, A. B. *J. Am. Chem. Soc.* **2001**, *123*, 2997-3005.

Chapter 3 Thermodynamics of Metal Binding to Ligand-modified PNA by ITC

3.1 Introduction

The incorporation of transition metal ions in nucleic acid duplexes by formation of alternative metal-based alternative base pairs has received intense interests recently due to the potential applications of hybrid inorganic-nucleic acid structures in molecular electronics.[1-3] The approach for metal incorporation in DNA by the substitution of nucleobase pairs with ligands that have high affinity for metal ions was first described by Tanaka et al.[4] The method has been successfully extended to Peptide Nucleic Acid (PNA), which is a synthetic analogue of DNA with a pseudo-peptide backbone.[5-7] The coordination of metal ions to ligands incorporated in nucleic acid duplexes is different from that to free ligands due to the effect of the duplex on the coordination. For example, the stability constant of the metal complex formed by pyridine (**Py**) and Ag^+ is small and an $[Ag(\mathbf{Py})_2]^+$ complex does not form in solutions containing micromolar concentrations of Ag^+ and **Py**.[8] Nevertheless, at this concentration range, a $[Ag(\mathbf{Py})_2]^+$ complex formed within DNA duplexes that contained a pair of **Py** in complementary positions and was attributed to a duplex-induced supramolecular chelate effect.[9] In another example of a chelate effect exerted by a duplex, titrations of PNA duplexes containing one pair of 8-hydroxyquinoline (**Q**) ligands lead to the formation of $Cu\mathbf{Q}_2$ complexes both at low and high temperature but these complexes can be transformed into Cu**Q** complexes in the presence of excess Cu^{2+} only at high temperature where the duplex is dissociated.[7]

The experimental results described above provide a qualitative view of the duplex-induced supramolecular chelate effect, which can be quantitatively assessed by examining the stability constants of metal-containing PNA and those of the corresponding metal ions and free ligand measured by isothermal

calorimetry (ITC). This method provides also the enthalpy and entropy change for the metal binding to the ligand-modified PNA.

Isothermal titration calorimetry as well as differential scanning calorimetry have been extensively used to determine the thermodynamic parameters for biochemical and biophysical studies[10] including those addressing interactions between metal ions and free ligands,[11] proteins[12] or nucleic acids[13,14]. ITC (and DSC) has two major advantages compared with other methods for studying thermodynamics such as spectroscopy (fluorescence, UV/vis, CD),[15] nuclear magnetic resonance (NMR),[16] surface plasmon resonance (SPR),[17] stopped-flow,[18] or radio-ligand binding assays.[19] First, it measures the enthalpy directly, independent of a model that describes the chemical process.[20,21] The other methods mentioned above directly measure equilibrium constants. The enthalpy of the reaction can be indirectly measured from the temperature dependence of the equilibrium constants using the van't Hoff equation or from the concentration dependence of the melting temperature and assuming in both cases a two-state model.[22-24] Second, ITC determines all thermodynamic parameters, including enthalpy, entropy and free energy, in a single experiment. ITC can only determine stability constants for which Log$K$ is in the range of 3-9.[10] However, it is possible to measure lower binding constants if the stoichiometry of the complexes and their concentrations are known.[25] Additionally, binding constants for which LogK is outside the 3-9 range can be measured by competition ITC.[26,27]

In this chapter, we report the results of an ITC study of the thermodynamics of metal binding to ligand-containing PNA. Our goal was to address in a quantitative manner the dependence of the stability constants for the metal complexes formed with ligand-modified PNAs on (*1*) the way in which the ligand is attached to the PNA backbone, and (*2*) the position of the ligand in the duplex. For the former effect, we chose to introduce in the PNA the 8-hydroxyquinoline (Q), which forms square planar complexes with Cu^{2+}, [CuQ_2]. This coordination geometry reduces steric interactions between the metal

complex and the adjacent nucleobase pairs. We have connected the ligand to the PNA backbone at either the 5- or the 2- position through either an acetyl or a keto linker, respectively. For the latter effect, we have introduced the ligand at different positions in two PNA duplexes, one whose sequence of eight nucleobase pairs was palindromic, and one which had nine base pairs. In addition, we have also investigated the thermodynamics for the metal complexes formed with Ni^{2+}, Cu^{2+} and 2,2'-Bypyridine (**Bpy**)-modified PNA.

3.2 Results

3.2.1 ITC of Cu^{2+} with Q ligands and Q-containing PNA

PNA Sequence

The non-modified and **Q**-modified PNA oligomers synthesized for this study are listed in Table 3.1. Duplexes $\mathbf{X_1 \bullet X_1}$ and $\mathbf{X_2 \bullet X_3}$ contain exclusively A, G T and C nucleobases and have been used in control experiments for the study of Cu^{2+} binding to non-modified PNA. 8-hydroxyquinoline ligands $\mathbf{Q_1}$ and $\mathbf{Q_2}$ (Scheme 3.1) were inserted in the middle of the self-complementary PNA oligomer $\mathbf{X_1}$ to create the $\mathbf{Q_i}$–containing oligomers $\mathbf{Q_i\text{-}X_1}$ (i = 1,2), which in turn form the palindromic Q-PNA duplexes $\mathbf{Q_i\text{-}X_1 \bullet X_1}$. The same two $\mathbf{Q_i}$ ligands were inserted in the middle of complementary PNA oligomers $\mathbf{X_2}$ and $\mathbf{X_3}$ to create the $\mathbf{Q_1}$- or $\mathbf{Q_2}$–containing oligomers $\mathbf{Q_i\text{-}X_2}$ and $\mathbf{Q_i\text{-}X_3}$, which in turn can form the **Q-**PNA duplexes $\mathbf{Q_i\text{-}X_2 \bullet X_3}$. The metal binding to PNA duplexes containing terminal ligands was investigated using the two Q-PNA duplexes $\mathbf{Q_1\text{-}X_2 \bullet X_3}$**-same** and $\mathbf{Q_1\text{-}X_2 \bullet X_3}$**-opp**. Upon Watson Crick hybridization of the two PNA strands of each of these duplexes, the former duplex contains the two $\mathbf{Q_1}$ ligands at the same end of the duplex while the latter one contains them at opposite ends. To evaluate the possibility of using metal complexes as a synthetic equivalent of multiple-way junctions, we have studied the metal binding to single stranded Q-PNA $\mathbf{Q_1\text{-}X_4}$,

Q_1-X_2, and **Q_1-X_3** and to the **Q_1C-X_2•X_3** duplex, which contains one **Q_1** ligand only.

Table 3.1. Non-Modified and **Q**-Mjodified PNA Oligomers.

PNA Sequence	Identity of X,Y,Z	Duplex Label
GGCA**X**TGCC-Lys LysCCGT**Y**ACGG	**X** = A **Y** = T **X** = **Y** = Q_i	**X_1•X_1** **Q_i-X_1•X_1**
GTAG**X**TCACT-Lys Lys-CATC**Y**AGTGA	**X** = - **Y** = - **X** = **Y** = Q_i **X** = Q_1 **Y** = C	**X_2•X_3** **Q_i-X_2•X_3** **Q_1C-X_2•X_3**
ZGTAGTCACT**X**-Lys Lys-CATCAGTGA**Y**	**X,Y,Z** = Q_1,Q_1,- **X,Y,Z** = -,Q_1,Q_1	**Q_1-X_2•X_3-same** **Q_1-X_2•X_3-opp**
ACACQ_1ACACA-Lys		**Q_1-X_4**

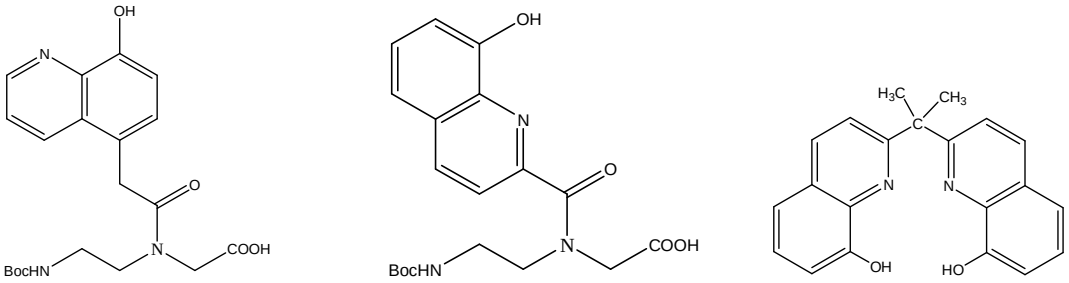

(a) (b) (c)

Scheme 3.1. Chemical structure of (a) 2-(*N*-(*tert*-Butyloxycarbonyl-2-aminoethyl)-2-(8-hydroxyquinolin-5-yl)-acetamido)-acetic acid **Q_1**; (b) 2-(N-(2-(*tert*-butoxycarbonyl-2aminoethyl)-8-hydroxyquinoline-2-carboxamido)-acetic acid **Q_2**; c. 2,2'-isopropylidenedi-8-quinolinol (ipdq).

ITC of Cu^{2+} with Q ligands

We have studied by ITC the Cu^{2+} binding to two ligands, 8-hydroxyquinoline and 2,2'-isopropylidenedi-8-quinolinol (ipdq), which was

synthesized as previously reported (Scheme 3.1).[28,29] These ligands are known to form 2:1 and 1:1 complexes with Cu^{2+}, respectively.[29,30] The ipdq is expected to have a higher affinity for Cu^{2+} than 8-hydroxyquinoline due to the fact it contains two hydroxyquinolines in close proximity of each other. A pH 8.10 100 mM Tris buffer was employed for all the ITC experiments because the complexes formed by metal ions and Tris have been well studied.[11] We refer everywhere in the text to this particular buffer as the "buffer". Acetonitrile or methanol was added to solutions of 8-hydroxyquinoline and ipdq because they have low solubility in water.

The thermodynamic parameters measured by ITC for Cu^{2+} binding to 8-hydroxyquinoline or ipdq are shown in Figure 3.1 and Table 3.2. These apparent thermodynamic parameters have been considered together with information on metal ions interactions with buffer solutions to calculate the absolute stability constants (equation 3.1).[31] The absolute stability constants were calculated based on equation 3.1, where K_{ITC} is obtained from a fit of the ITC isotherm, and α_{Proton} and α_{buffer} account for proton and buffer competition, respectively.[31] The enthalpy was corrected by consideration of $Cu(Tris)_4^{2+}$ complex dissociation and proton transfer (Scheme 3.2).[11]

$$K_{ML} = \alpha_{proton}\alpha_{buffer}K_{ITC} = K_{ITC}(1+K_{HL}[H^+]+\beta_{H2L}[H^+]^2)(1+K_{MB}[B]) \quad (3.1)$$

$$\begin{aligned}
&2^*\ HQ \longrightarrow Q^- + H^+ \\
&Cu(Tris)_4^{2+} \longrightarrow Cu^{2+} + 4Tris \\
&Cu^{2+} + 2Q^- \longrightarrow CuQ_2 \\
&2^*\ H^+ + Tris \longrightarrow TrisH^+ \\
&\hline \\
&Cu(Tris)_4^{2+} + 2HQ \longrightarrow CuQ_2 + 2Tris + 2TrisH^+
\end{aligned} \quad (3.2)$$

Scheme 3.2. Thermodynamic cycles for the enthalpy(ΔH) calculated by consideration of the formation of $Cu(Tris)_4^{2+}$ and proton transfer.

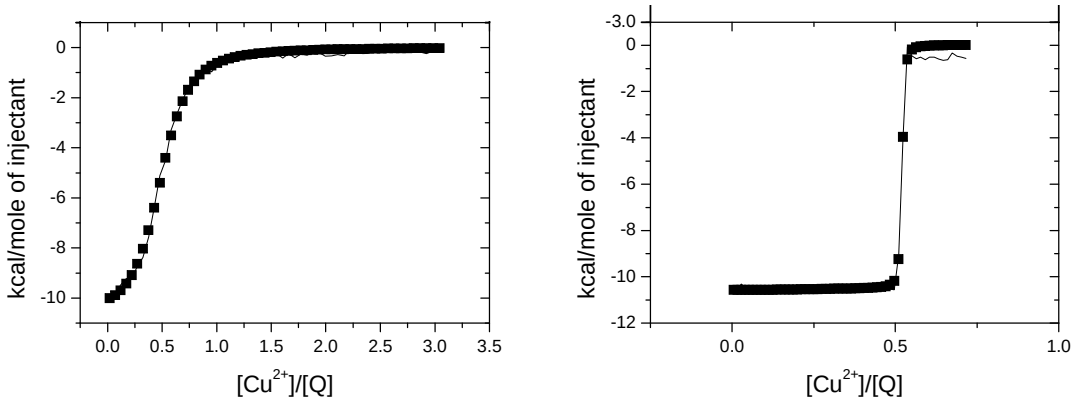

(a) (b)

Figure 3.1. ITC titration of a. 0.03 mM solution of 8-hydroxyquinoline with 0.44mM solution of $Cu(NO_3)_2$, both in 3:1 buffer/acetonitrile; b. 0.2 mM solution of ipdq with 1.47 mM $Cu(NO_3)_2$, both in 1:1 buffer/methanol.

One transition was observed in the ITC titration of 8-hydroxyquinoline with Cu^{2+} at a Cu^{2+}/**Q** ratio of 1:2, which indicates that as expected, Cu^{2+} binds two **Q** ligands. The absolute overall stability constant Logβ determined in the titration is 24.8 and is slightly larger than the one previously reported in the literature, Logβ of 23.0,[32] which was measured by solubility. This small difference may be due to the different methods and models employed for calculation of stability constants. The ITC titration of ipdq with Cu^{2+} showed only one transition at a Cu^{2+}/ipdq ratio of 1:1. The overall stability constant for the [Cu(ipdq)] complex was about four orders of magnitude higher than that of the $[CuQ_2]$, which is attributed to the chelate effect. Comparison of the enthalpy and entropy changes for the formation of the [Cu(ipdq)] and $[CuQ_2]$ complexes indicates that the high binding is entropy-driven.

Table 3.2. Thermodynamic parameters for the binding of Cu^{2+} to 8-hydroxyquinoline, ipdq and **Q**-PNA by ITC[a]

	N	LogK ITC	ΔH ITC (kcal/mol)	Logβ	ΔH (kcal/mol)	ΔS (cal/mol/deg)	ΔG (kcal/mol)
8-HQ	1.98	5.8	-5.7	24.8	-22	40	-34
ipdq	1.95	7.7	-5.4	28.6	-22	57	-39
Q_1-X_4	1.91	7.0	-6.8	27.2	-24	44	-37
Q_1C-X_2•X_3	1.96	6.3	-3.9	25.8	-19	54	-35
Q_1-X_1•X_1	2.02	6.8	-4.3	26.8	-19	60	-37
Q_1-X_2•X_3	2.15	7.9	-4.1	29.0	-19	70	-40
Q_1-X_2•X_2	1.95	7.7	-10.6	28.6	-32	23	-39
Q_1-X_3•X_3	1.98	7.8	-5.9	28.8	-23	54	-39
Q_1-X_2•X_3-same	2.1	7.4	-3.7	28.0	-18	67	-38
Q_1-X_2•X_3-opp	2.0	7.8	-5.9	28.8	-23	54	-39
Q_2-X_2•X_3	1.95	3.6	2.1	20.2	-7	70	-28

a. Assumes two Tris ligands are replaced by one Q in each step. Error ranges for N, LogK and ΔH are 10%, 5% and 20%, respectively.

ITC of Cu^{2+} with non-modified PNA

Cu^{2+} interacts very weakly with natural nucleobase pairs. The very few previously reported binding constants of Cu^{2+} to calf thymus DNA were in the range of Log$K$ 1.60-3.25,[33] which is much smaller than those for complexes of Cu^{2+} with 8-hydroxyquinoline.[32] The ITC titrations of the non-modified PNA duplex **X_2•X_3** with Cu^{2+} showed only mixing heat (Figure 3.2), which indicates that the interaction of Cu^{2+} with the natural base pairs is weaker than that of the $[Cu(Tris)_4]^{2+}$ complex, which is Logβ_4 14.1 and represents an upper limit for the stability constant of complexes of Cu^{2+} with non-modified PNA.[8]

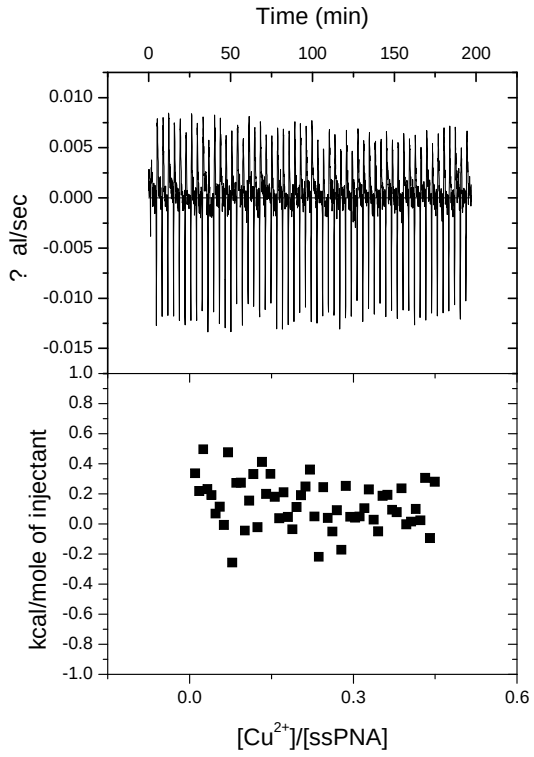

Figure 3.2. ITC titration of 0.03 mM solution of **X_2•X_3** with 0.13mM solution of $Cu(NO_3)_2$, both in buffer.

ITC of Cu^{2+} with Q-PNA

ITC of Cu^{2+} with Q_1-PNA single stand

The ITC titration of Cu^{2+} with the PNA **Q_1-X_4**, which cannot form any Watson-Crick base pairs with itself, allowed us to estimate the effect of the PNA single stand on the interaction of Cu^{2+} with an 8-hydroxyquinoline situated in the middle of the PNA oligomer. This titration showed one transition at a Cu^{2+}/**Q_1** ratio of 1:2 (Figure 3.3a). The absolute stability constant Logβ_2 for the [Cu(**Q_1-X_4**)$_2$] complex was 27.2, which is 2 orders of magnitude larger than that of Cu^{2+} and 8-hydroxyquinoline. We attribute this result to the fact that at 60 μM concentrations PNA after annealing may aggregate by hydrophobic interactions even in the absence of Watson Crick base pairing,[22] thus bringing pairs of **Q_1**

ligands in close proximity of each other and favoring the formation of $[CuQ_2]$ complexes. The comparison of the enthalpy and entropy changes for the formation of the $[Cu(\mathbf{Q_1\text{-}X_4})_2]$ and $[CuQ_2]$ complexes indicates that the higher stability constant of the former complex is entropy-driven. The sensitivity of ITC prevented us from studying by this method the binding of Cu^{2+} to PNA in solutions with concentrations at which the PNA aggregation is unlikely.

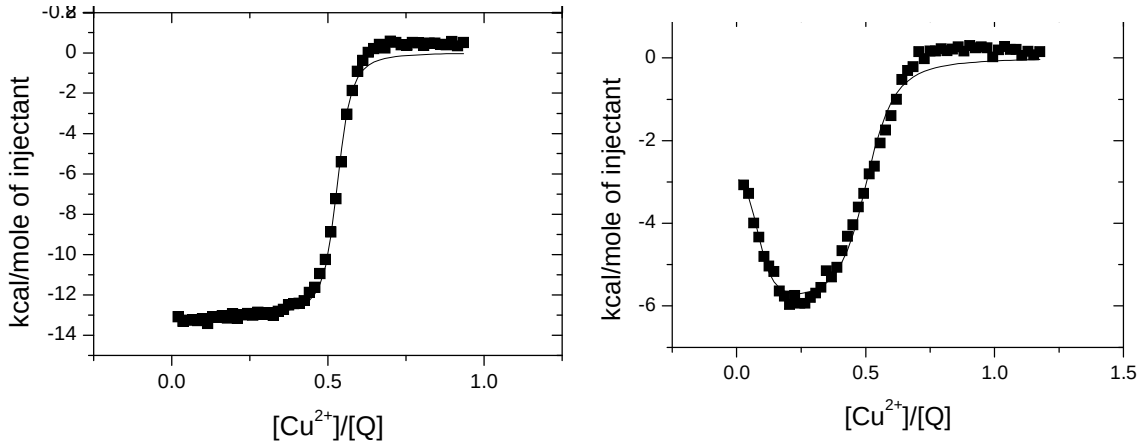

Figure 3.3. ITC titration of a. 0.06 mM solution of $\mathbf{Q_1\text{-}X_4}$ with 0.27 mM solution of $Cu(NO_3)_2$; b. 0.03 mM solution of $\mathbf{Q_1C\text{-}X_2{\bullet}X_3}$ with a 0.34 mM solution of $Cu(NO_3)_2$.

Cu^{2+} Binding to Q-PNA duplexes containing one ligand

The PNA duplex $\mathbf{Q_1C\text{-}X_2{\bullet}X_3}$ contains a central $\mathbf{Q_1}$•C mismatch. Given the high stability constant of $[CuQ_2]$ complexes, we anticipated that in the presence of Cu^{2+} the $\mathbf{Q_1}$ ligands will bulge out of the duplex to form inter-duplex $[CuQ_2]$ complexes that bridge a pair of $\mathbf{Q_1C\text{-}X_2{\bullet}X_3}$ duplexes into a dimer of duplexes. The ITC titration of the PNA duplex $\mathbf{Q_1C\text{-}X_2{\bullet}X_3}$ with Cu^{2+} confirmed the formation of a $[Cu(\mathbf{Q_1C\text{-}X_2{\bullet}X_3})_2]$ complex (Figure 3.3b, Table 3.2). The absolute stability constant of the complex Logβ_2 25.8 is smaller than that measured for the $[Cu(\mathbf{Q_1\text{-}X_4})_2]$ complex (Logβ_2 27.2). Comparison of the enthalpy and entropy changes for the formation of $[Cu(\mathbf{Q_1C\text{-}X_2{\bullet}X_3})_2]$ and $[Cu(\mathbf{Q_1\text{-}X_4})_2]$ complexes

indicates that the determinant of the higher stability constant of the former complex is the entropy, which we attribute to the steric differences between the ss and ds PNA.

The binding isotherm for the titration of the **Q_1C-X_2•X_3** duplex with Cu^{2+} showed a second binding step at Cu^{2+}/**Q_1** ratio of 1:10 with an equilibrium constant comparable to that measured for the formation of the [Cu(**Q_1C-X_2•X_3**)$_2$] complex but with lower enthalpy change (Figure 3.3b). To elucidate the nature of this transition, we did CD titrations of the **Q_1C-X_2•X_3** duplex with Cu^{2+} (Figure 3.4). The CD spectrum of the duplex in the absence of Cu^{2+} and in the presence of 0.1 equivalents Cu^{2+} is typical of a left-handed PNA duplex. However, in the presence of 0.2 equivalents of Cu^{2+} or more, the intensity of the negative CD peak at 255 nm decreased significantly, which indicates that a conformational change occurs in the duplex upon interaction with Cu^{2+}. We conclude that 0.1-0.2 equivalents of Cu^{2+} trigger a conformational change in the PNA, which takes place with an equilibrium constant of Log*K* about 5 and an enthalpy change of -3 kcal/mol.

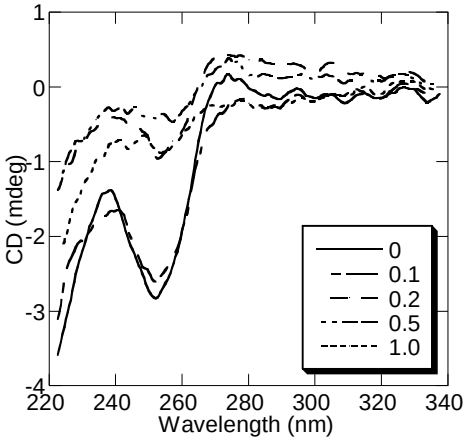

Figure 3.4. CD titration of 10 μM solution of **Q_1C-X_2•X_3** with 0, 0.1, 0.2, 0.5 and 1.0 eq of $Cu(NO_3)_2$ in buffer. The PNA duplex was annealed before the addition of $Cu(NO_3)_2$.

Cu^{2+} binding to Q_1-PNA duplexes that contain a pair of 8-hydroxyquinoline ligands

Previous spectroscopic studies of Cu^{2+} binding to PNA duplexes that contained a central pair of 8-hydroxyquinoline ligands showed that they form [CuQ_2] complexes and that the effect of the metal on the duplex stability depends on the duplex sequence and on the way in which the ligand is attached to the PNA backbone. To put these findings on a quantitative basis, we have conducted ITC titrations of PNA duplexes that contained a pair of ligands either in the center or at the end of the duplex and determined the thermodynamic parameters for metal binding to the Q-PNAs.

The ITC titration of the palindromic duplex **Q_1-X_1•X_1** with Cu^{2+} (Figure 3.5a) showed one transition at a Cu^{2+}/**Q_1** ratio of 1:2, indicating the binding of Cu^{2+} to two **Q_1** ligands. The absolute stability constant of the [CuQ_2] complex formed by **Q_1-X_1•X_1** and Cu^{2+}, Logβ_2 = 26.8, is similar to that of the complex formed by Cu^{2+} and ss **Q_1**-PNA (Logβ_2 = 27.2). This similarity, together with the fact that the melting temperature of the **Q_1-X_1•X_1** duplex in the absence and presence of Cu^{2+} is the same, leads us to hypothesize that the [CuQ_2] complex (*1*) does not function as an alternative base pair, (*2*) has only weak, if any, 诰 stacking interactions with adjacent nucleobase pairs. These two hypotheses are compatible with the existence of a [CuQ_2] complex that bridges pairs of **Q_1-X_1•X_1** duplexes.

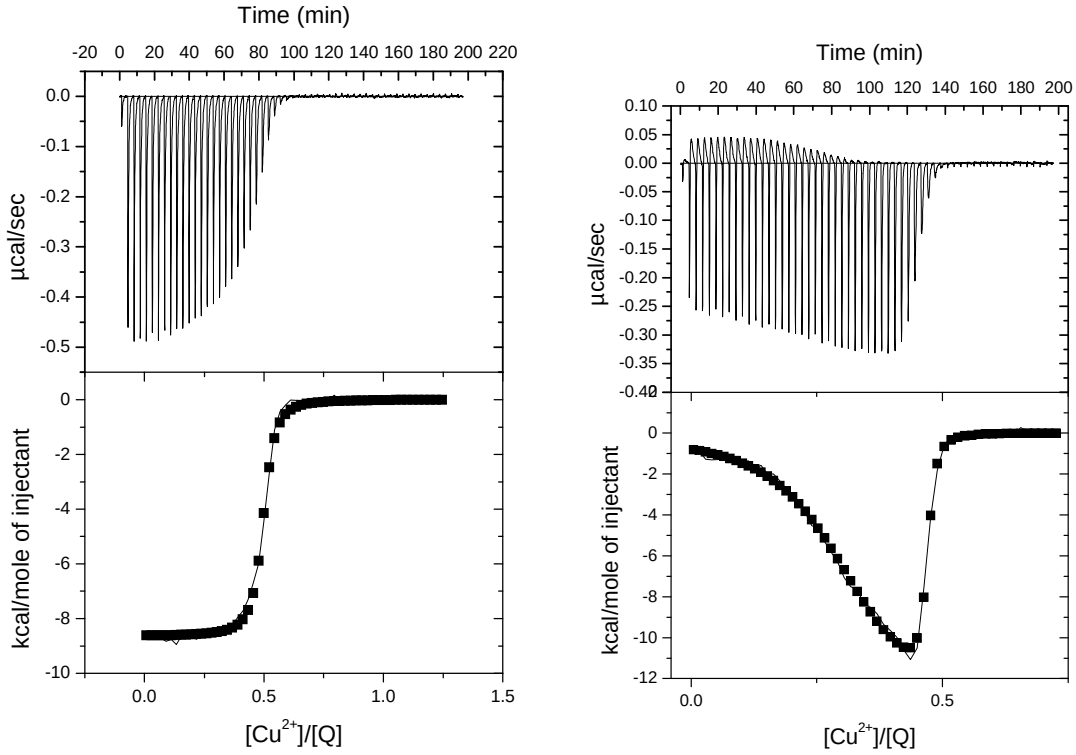

(a) (b)

Figure 3.5. ITC titration of (a) 0.06 mM solution of **Q_1-X_1** with a 0.27 mM solution of $Cu(NO_3)_2$; (b) 0.03 mM solution of **Q_1-X_2•X_3** with 0.29 mM solution of $Cu(NO_3)_2$.

Significantly different from the properties of the palindromic duplex **Q_1-X_1•X_1** in the presence of Cu^{2+}, the binding isotherm of the PNA duplex **Q_1-X_2•X_3** with Cu^{2+} has shown two transitions and was simulated with a two-site binding model (Figure 3.5b and Table 3.2). The transition observed at the Cu^{2+} /**Q_1** ratio of 1:2 corresponds to the formation of a [Cu(**Q_1**)$_2$]. The absolute stability constant for this complex Logβ_2 is 29.0, which is significantly larger than the stability constants for the complexes with [CuQ_2] stoichiometry formed by Cu^{2+} with 8-hydroxyquinoline (25.0), or the palindromic duplex **Q_1-X_1•X_1** (26.9). The higher binding is entropy-driven. This result can be rationalized by the formation of the [CuQ_2] within the **Q_1-X_2•X_3**, with the metal complex playing the role of an alternative base pair and the duplex exerting a supramolecular chelate effect. The result also establishes the fact that the affinity for a given transition metal

ion of the 8-hydroxyquinoline incorporated in PNA duplexes depends on the sequence of the duplex.

A second equilibrium is observed in the binding isotherm at a Cu^{2+}/**Q_1-X_2•X_3** ratio of about 0.25 and it has an apparent equilibrium constant Log$K$ ~ 5, indicating a weaker interaction than that which leads to the complex with Cu^{2+}/**Q_1-X_2•X_3** ratio of 0.5. The formation of a Cu^{2+} complex with more than two 8-hydroxyquinoline ligands is unlikely because no such synthetic complex is known to date. Close examination of the peaks measured at Cu^{2+}/**Q_1** ratios below 0.3 shows the existence of two kinetic phases, namely a fast exothermic phase followed by a slow, endothermic one (Figure 3.6). Our hypothesis is that the binding equilibrium observed for Cu^{2+}/**Q_1** ratios of ~0.25 involves the formation of inter-duplex [CuQ_2] with two **Q_1** ligands buldged out of two different duplexes, a step that involves the exothermic metal coordination and the endothermic duplex reorganization. This step is followed upon further addition of Cu^{2+}, by the transformation of the inter-duplex [CuQ_2] complexes that bridge two **Q_1-X_2•X_3** duplexes into intra-duplex [CuQ_2] ones that play the role of artificial base pairs in the **Q_1-X_2•X_3** duplexes.

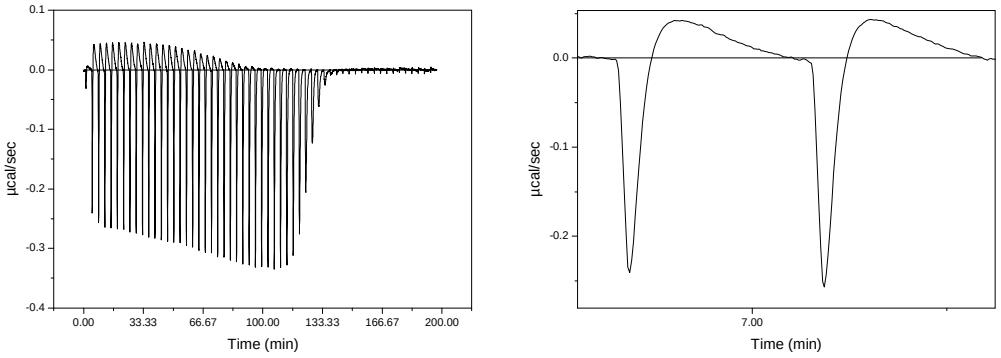

(a) (b)

Figure 3.6. Kinetic steps associated with the binding of Cu^{2+} in the ITC titration of a 30 µM solution of **Q_1-X_2•X_3** with a 0.29 mM solution of $Cu(NO_3)_2$. a. raw data of ITC; b. two injections of the ITC.

ITC of Cu^{2+} with Q_2-PNA duplex

Duplexes **Q_2-X_1•X_1** and **Q_2-X_2•X_3** have the same sequence as **Q_1-X_1•X_1** and **Q_1-X_2•X_3** but the binding of Cu^{2+} to the former two PNAs is much weaker than to the latter two because the ligand **Q_2** is attached to the PNA backbone at a position closer to the coordination site of the ligand and through a shorter linker than **Q_1**. The binding isotherm for titrations of the **Q_2-X_2•X_3** (Figure 3.7a) reveals that the Cu^{2+} binding to **Q_2** has an equilibrium constant Logβ_2 of 20.2, which is several orders of magnitude smaller than the corresponding constant for Cu^{2+} binding to 8-hydroxyquinoline (Logβ_2 = 24.8). The weaker binding of Cu^{2+} to Q_2 is due to the fact that the increase in enthalpy is not compensated by an increase of entropy. The ITC titration of Cu^{2+} with **Q_2-X_1•X_1** (Figure 3.7b) showed only very small peaks comparable with mixing heat, which prevented us from determining the stability constant for the complex formed by Cu^{2+} with **Q_2-X_1•Q_2-X_1**.

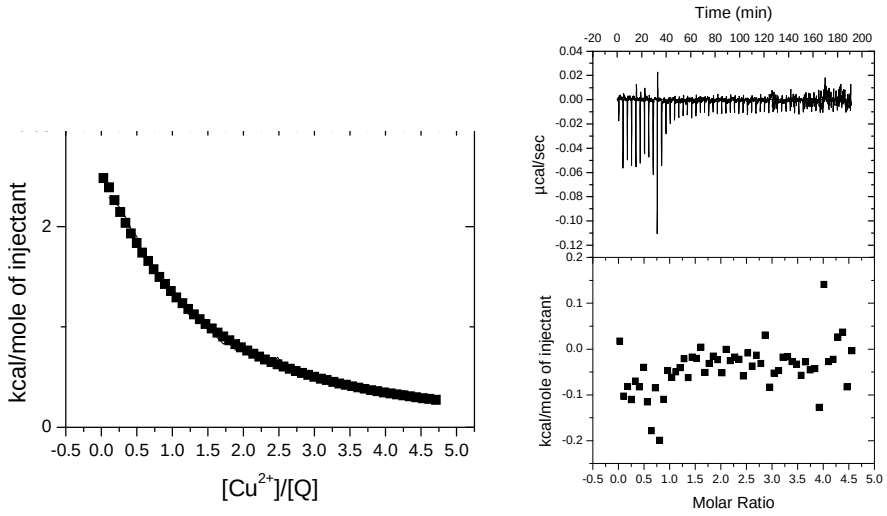

(a) (b)

Figure 3.7: ITC titration of a. 0.03 mM solution of **Q_2-X_2•X_3** with 1.3mM solution of $Cu(NO_3)_2$; b. 0.06 mM solution of **Q_2-X_1**.with 1.2mM solution of $Cu(NO_3)_2$.

ITC of Cu^{2+} with Q_1-PNA duplex with Q_1 at terminal position

We have synthesized two PNAs duplexes which upon Watson Crick hybridization have two **Q_1** ligands situated either at the same end of the duplex, **Q_1-X_2•X_3-same**, or at opposite ends of the duplex, **Q_1-X_2•X_3-opp** (Table 3.1) and studied their interaction with Cu^{2+}. UV titrations of these duplexes with Cu^{2+} clearly indicate the formation of 1:1 complexes in which Cu^{2+} coordinates two 8-hydroxyquinolines (Figure 3.8).

Melting curves of these duplexes showed that they have the same thermal stability but that the effect of Cu^{2+} on the duplex stability on these duplexes is very different (Figure 3.9). While Cu^{2+} does not affect the thermal stability of the **Q_1-X_2•X_3-opp**, it affects significantly the melting curve of the **Q_1-X_2•X_3-same** duplex. Specifically, the absorbance of the **Q_1-X_2•X_3-same** duplex in the presence of one equivalent of Cu^{2+} increases with the temperature but as the increase is not sigmoidal, we could not determine a melting temperature (Figure 3.9). Nevertheless this result is compatible with the formation of a very stable **Q_1-X_2•X_3-same** duplex in the presence of Cu^{2+} when considered together with the facts that (*1*) the melting temperature of a duplex with the same sequence of base pairs as **Q_1-X_2•X_3-same** but a central pair of **Q_1** ligands increases in the presence of one equivalent of Cu^{2+}, and (*2*) the increase of the melting temperature due to Cu^{2+} coordination to a pair of ligands close to the end of the duplex is significantly larger than when the Cu^{2+} coordination to a pair of ligands situated in the center of a duplex.

The CD spectrum of the **Q_1-X_2•X_3-same** is typical of a left handed helix, with negative CD bands at 220 nm and 255 nm and a positive band at 275 nm (Figure 3.10a). A CD titration of the pre-annealed **Q_1-X_2•X_3-same** duplex shows an increase in the intensity of the CD features at 255 nm and 275 nm, which indicates that the duplex undergoes a structural change without a change in its left handedness. In contrast and surprisingly, the **Q_1-X_2•X_3-opp** duplex has a CD spectrum indicative of a right handed duplex although both strands of the duplex have an N-terminus L-Lysine, which is known to induce a preference for left handedness in PNA duplexes (Figure 3.10b). A CD titration of the duplex

with Cu^{2+} shows that upon Cu^{2+} binding the preferred handedness of the duplex is changed from right to left. We hypothesize that these interesting chiral properties of the duplex are due to the fact that in the absence of Cu^{2+}, the amino group of the N-terminal L-Lysine is involved in hydrogen bonding with the 8-hydroxyquinoline situated at the C-terminus of the opposite strand of the duplex, and that upon Cu^{2+} coordination to 8-hydroxyquinoline and consequent destruction of these bonds, the L-Lysine induces as usually a preference for left handedness to the duplex.

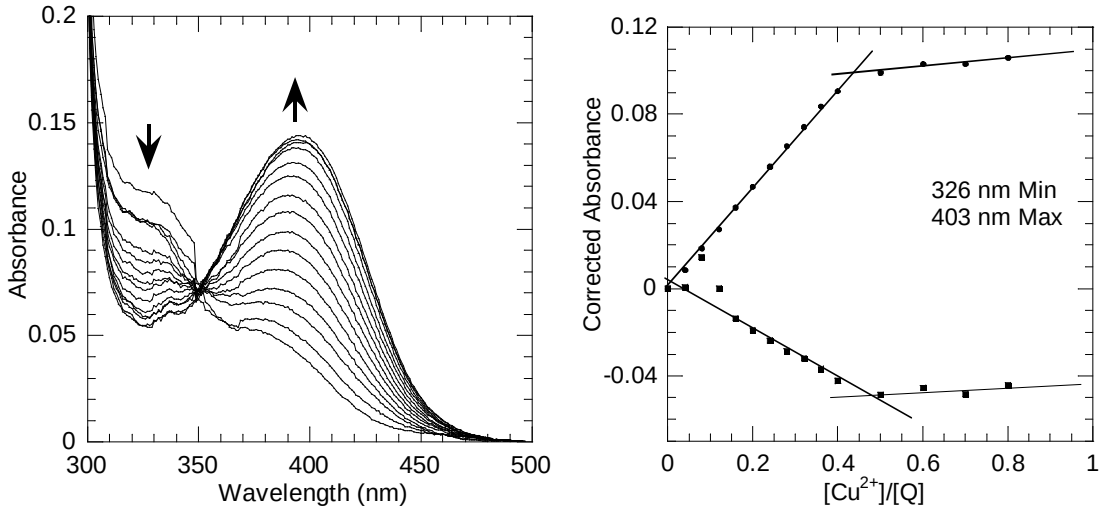

Figure 3.8: Spectrophotometric titration of a 25 μM solution of **Q_1-X_2•X_3-same** with a 2 mM solution of $Cu(NO_3)_2$. The titration curves in (b) are at 326 nm (squares) and 403 nm (circles).

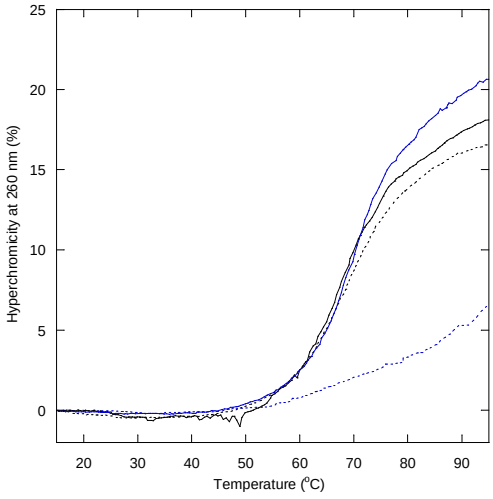

Figure 3.9: Melting curves of 5 μM solution of **Q_1-X_2•X_3-same** (dotted lines) and **Q_1-X_2•X_3-opp** without (solid lines) and with 1.0 eq. (blue) $Cu(NO_3)_2$ in buffer.

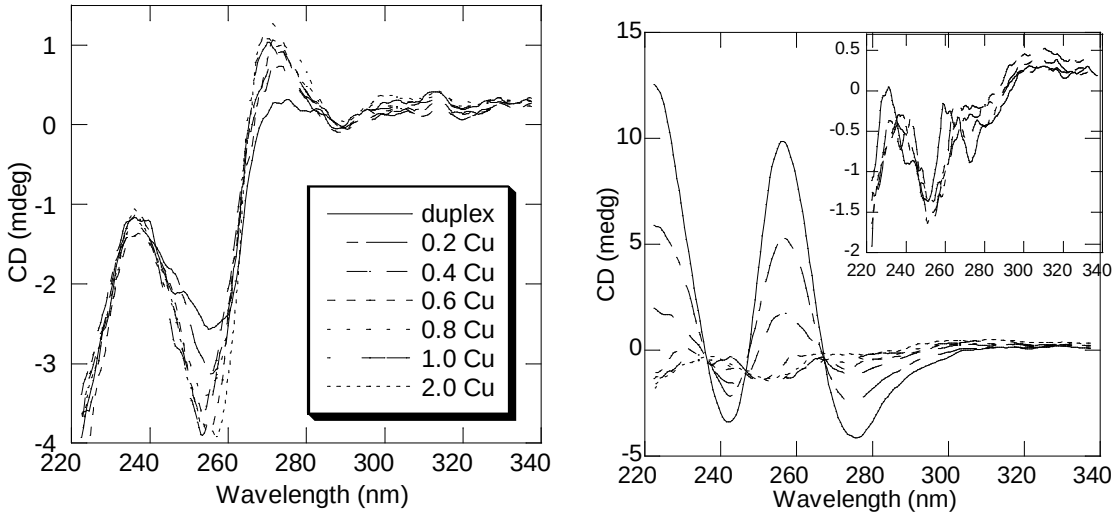

(a) (b)

Figure 3.10. CD titration of 10 μM solution of pre-annealed duplex **Q_1-X_2•X_3-same** (a) and **Q_1-X_2•X_3-opp** (b) with $Cu(NO_3)_2$. The number of Cu^{2+} equivalents added to the solution of duplexes is specified in the inset of Figure 8, next to the line type for each spectrum. These line types apply to both figures. The inset in figure 9b shows an expanded view of the CD spectra of **Q_1-X_2•X_3-opp** annealed in the presence of 0.5-1.0 equivalents of Cu^{2+}.

The binding isotherms obtained in direct and reverse ITC titrations of the **Q_1-X_2•X_3-same** and **Q_1-X_2•X_3-opp** with Cu^{2+} are shown in Figures 3.11 and 3.12 respectively. All the isotherms show the formation of $[CuQ_2]$ with the **Q_1-X_2•X_3-same** and **Q_1-X_2•X_3-opp** complexes in solutions in which the Cu^{2+}/Q-PNA duplexes ratio is 1:1. The absolute stability constants for these complexes, $Log\beta_2$ are 28.0 and 28.8**,** respectively, are significantly larger than the stability constants for the $[CuQ_2]$ complex formed with the free 8-hydroxyquinoline (24.8) but smaller than for the same complex formed with the PNA duplex **Q_1-X_2•X_3** that has a central pair of 8-hydroxyquinoline ligands (29.0). The high affinity of Cu^{2+} with **Q_1-X_2•X_3-same** is attributed to the chelate effect, which is comparable to that manifested in the formation of $[CuQ_2]$ complexes between Cu^{2+} and **Q_1-X_2:X_3**. However, the high stability constant $[CuQ_2]$ complex formed

with the **Q_1-X_2•X_3-opp** is surprising because Cu^{2+} is most likely to coordinate **Q_1** ligands from two different duplexes. Interestingly, both the direct and reversed titrations of the **Q_1-X_2•X_3-opp** reveal a second transition at a ratio of Cu^{2+}/**Q_1** ratio of ~0.3, as it was observed in the ITC titration of **Q_1-X_2•X_3** with Cu^{2+}.

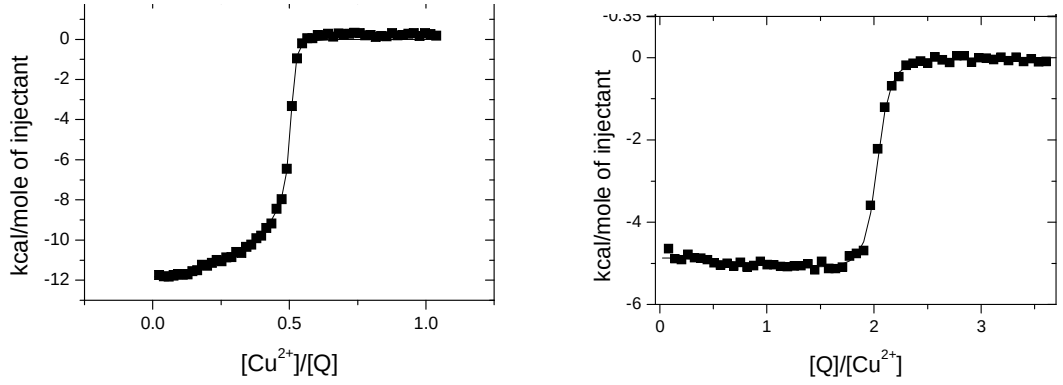

(a) (b)

Figure 3.11. ITC titration at 25°C of (a) 30 μM **Q_1-X_2•X_3-opp** with 0.30 mM $Cu(NO_3)_2$; and (b) 23 μM $Cu(NO_3)_2$ with 0.40 mM **Q_1-X_2•X_3-opp**.

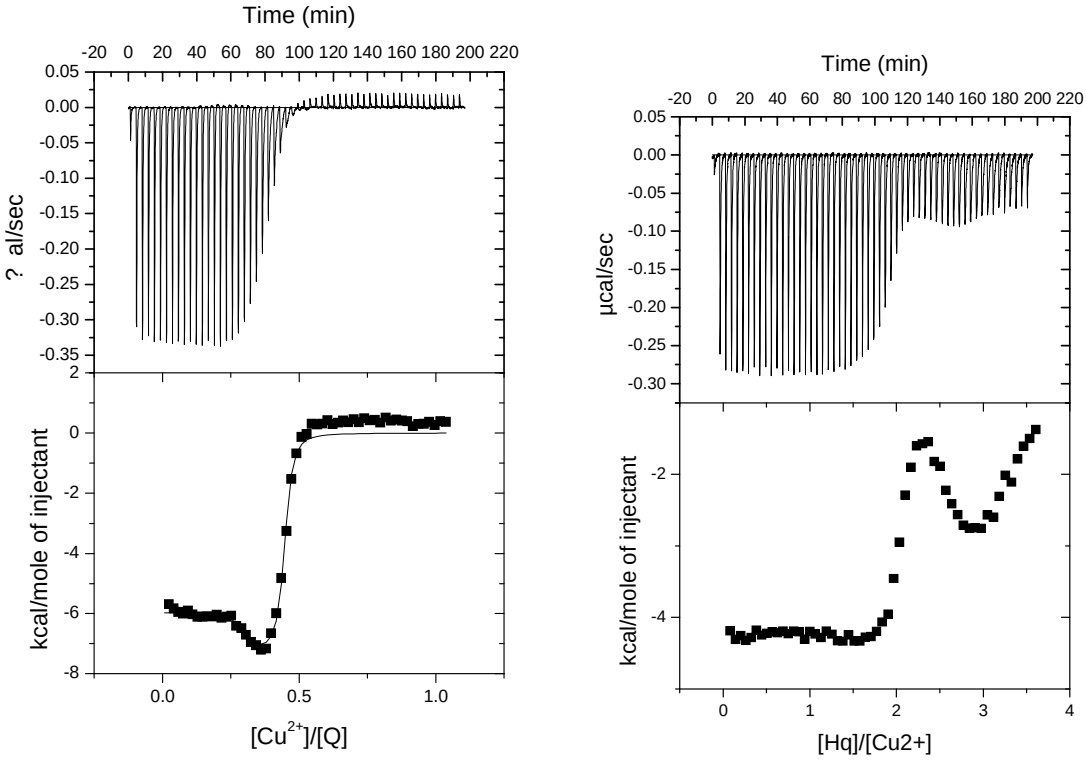

(a) (b)

Figure 3.12. ITC titration of (a) 0.03mM solution of **Q_1-X_2•X_3-same** with 0.30 mM solution of $Cu(NO_3)_2$; (b) 0.023 mM solution of $Cu(NO_3)_2$ with 0.40 mM **Q_1-X_2•X_3-same**, both in buffer.

3.2.2 ITC Titrations of Bpy ligands and Bpy-containing PNAs with Ni^{2+} and Cu^{2+}

PNA Sequences

The Bpy-modified PNA oligomers synthesized for this study are listed in Table 3.3. A pair of 2,2'-bipyridine (**Bpy**) PNA monomers (Scheme 3.3) was inserted into the middle of a complementary PNA oligomer **X_2•X_3** to create the **Bpy**–containing PNA duplex **Bpy-X_2•X_3**. Similarly, a triplet of **Bpy** ligands was inserted into the middle of a PNA triplex to create the **Bpy**–containing PNA triplex **Bpy-X_5•X_4•X_5**.

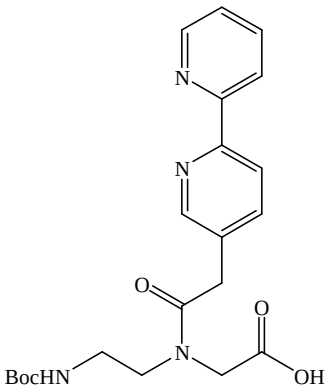

Scheme 3.3. Chemical structure of (a) 2-(N-(2-(tert-butoxycarbonyl)ethyl)-2-(6-(pyridin-2-yl)pyridin-3-yl)acetamido)acetic acid (**Bpy**).

Table 3.3. Bpy-modified PNAs

Name	PNA Sequence
Bpy-X_2•X_3	GTAG**Bpy**TCACT-Lys

	LysCATC**Bpy**AGTGA
Bpy-X_5•X_4•X_5	AcTTTTT**Bpy**TTTT-Lys LysAAAAA**Bpy**AAAAAc AcTTTTT**Bpy**TTTT-Lys

ITC Titrations of 2,2′-Bipyridine with Ni^{2+} and Cu^{2+}

The interactions of Ni^{2+} and Cu^{2+} with 2-2′-bipyridine (**Bpy**) were studied by ITC titrations. The binding isotherm for the titration of **Bpy** with Ni^{2+} shows one transition at a Ni^{2+}/**Bpy** ratio of 1:3 (Figure 3.13a), which indicates the formation of the $[Ni(Bpy)_3]$ complex. The binding isotherm for the titration of **Bpy** with Cu^{2+} shows also one transition but at Cu^{2+}/**Bpy** ratio of 1:1 (Figure 3.13b), which indicates the formation of [Cu(Bpy)] complex in which the other coordination sites of Cu^{2+} are occupied by solvent or buffer molecules.

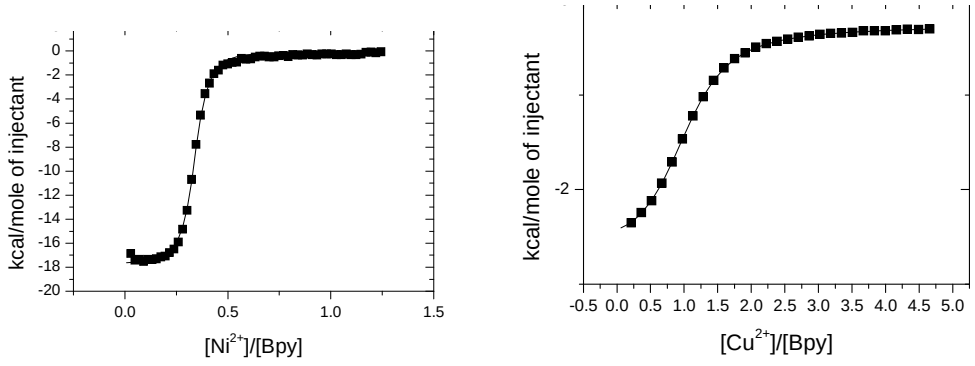

(a) (b)

Figure 3.13. ITC titration of a. 0.06 mM 2,2′-Bipyridine with 0.36 mM $Ni(NO_3)_2$; b. 0.1 mM 2,2′-Bipyridine with 4.41mM $Cu(NO_3)_2$, .

The thermodynamic parameters for these complexes are listed in Tables 3.4 and 3.5. The stability constants independent of buffers and pH were calculated based on equation 3.1,[31] using the binding constant for Ni^{2+} complexes with Tris of (Log β_1 =2.63, Log β_2 =4.5) and Cu^{2+} and Tris (Log β_1

=3.95, Log β_1 =7.63, Log β_2 =11.10, Log β_3 =14.1)[8]. The enthalpy was corrected assuming that the $Ni(Tris)_2^{2+}$, $Ni(Tris)^{2+}$ and $Cu(Tris)_4^{2+}$ complexes, which exist in the pH 8.10 Tris buffer solution dissociate according to Schemes 3.4 and 3.5.[11]

$$\begin{aligned} 82\% \quad & Ni(Tris)_2^{2+} \longrightarrow Ni^{2+} + 2Tris \\ 17\% \quad & Ni(Tris)^{2+} \longrightarrow Ni^{2+} + Tris \\ & Ni^{2+} + 3Bpy \longrightarrow Ni(Bpy)_3^{2+} \end{aligned} \qquad (3.4)$$

$$0.82Ni(Tris)_2^{2+} + 0.18Ni(Tris)^{2+} + 3Bpy \longrightarrow Ni(Bpy)_3^{2+} + 1.82Tris$$

Scheme 3.4. Thermodynamic cycle based on which the enthalpy (ΔH) for the formation of $Ni(Bpy)_3^{2+}$ was calculated

$$\begin{aligned} & Cu(Tris)_4^{2+} \longrightarrow Cu(Tris)_2^{2+} + 2Tris \\ & Cu(Tris)_2^{2+} + Bpy \longrightarrow Cu(Tris)(Bpy)^{2+} \end{aligned} \qquad (3.5)$$

$$Cu(Tris)_4^{2+} + Bpy \longrightarrow Cu(Tris)_2(Bpy)^{2+} + 2Tris$$

Scheme 3.5. Thermodynamic cycle based on which the enthalpy (ΔH) for the formation of $Cu(Tris)_2(Bpy)^{2+}$ was calculated by consideration of the formation of $Cu(Tris)_4^{2+}$.

The stability constants that we have measured for $Ni(Bpy)_3$, Logβ_3 = 21.3, and Cu(Bpy), Logβ_1 =9.4, are slightly larger than the values reported in the literature of 20.5 and 8.52, respectively.[8] We attribute this difference to the fact that the earlier reported constants were measured by potentiometric titration rather than ITC. The enthalpy values for $Ni(Bpy)_3$ and Cu(Bpy) are close to the corresponding literature values.

Table 3.4. Thermodynamic parameters for [Ni(**Bpy**)$_N$] complexes measured by ITC.[ab]

	N	LogK_{ITC}	ΔH_{ITC} (kcal/mol)	Logβ	ΔH (kcal/mol)	ΔS (cal/mol/deg)	ΔG (kcal/mol)
Bpy	3.0	6.2	-5.9	21.3	-24	17	-29
Bpy-X_5:X_4:X_5	3.02	4.7	-0.9	16.8	-9	47	-23
Bpy-X_2:X_3	2.07	7.0	-1.2	16.6	-9	47	-23

a. Error ranges for N, LogK and ΔH are 10%, 5% and 20% respectively.
b. Assumes one Tris ligand is replaced by one Bpy for the first and second step. No Tris ligand is replaced by the third Bpy.

Table 3.5 : Thermodynamic parameters of Cu^{2+} with **Bpy** and **Bpy**-PNA by ITC.[ab]

	N	LogK ITC	ΔH ITC (kcal/mol)	Logβ	ΔH (kcal/mol)	ΔS (cal/mol/deg)	ΔG (kcal/mol)
Bpy-X_5:X_4:X_5	3.23	4.2	-0.7	22.6	-18	44	-31
Bpy-X_2:X_3	1.98	4.8	0.7	19.7	-17	34	-27
B	1.02	4.9	-2.4	9.4	-12	3	-13

a. Error ranges for N, LogK and ΔH are 10%, 5% and 20% respectively.
b. Assumes two Tris ligand is replaced by one Bpy for the first and second step.

ITC Titrations of Bpy-PNA duplexes with Ni^{2+} and Cu^{2+}

ITC titrations of the PNA duplex **Bpy-X_2•X_3** with Ni^{2+} or Cu^{2+} led to the thermodynamic parameters listed in Table 3.4 and 3.5. The binding isotherms were simulated assuming a two-site binding model. The transitions observed at a M^{2+}/**Bpy** ratio of 1:2 indicates the formation of a [M(**Bpy**)$_2$]$^{2+}$ complex. This

result is different from the observation of a $Ni(Bpy)_3$ or a $[Cu(\mathbf{Bpy})]^{2+}$ complex in the titrations of the free **Bpy** ligand with Ni^{2+} or Cu^{2+}, respectively. The thermodynamic parameters for the formation of these $[M(\mathbf{Bpy})_2]$ complexes have been obtained using the thermodynamic cycles shown in Schemes 3.6 and 3.7.[11] The stability constants for the $[M(\mathbf{Bpy})_2]^{2+}$ complexes formed by Ni^{2+} and Cu^{2+} with the PNA duplex **Bpy-X_2•X_3** are 16.6 and 19.7 respectively. These values are significantly larger than the corresponding values for the complexes with free Bpy, $Log\beta_2$ = 14.0 and 14.3, respectively.[8]. We attribute the observation of $M(\mathbf{Bpy})_2$ complexes and the relatively large values of their stability constants to a duplex-induced supramolecular chelate effect.

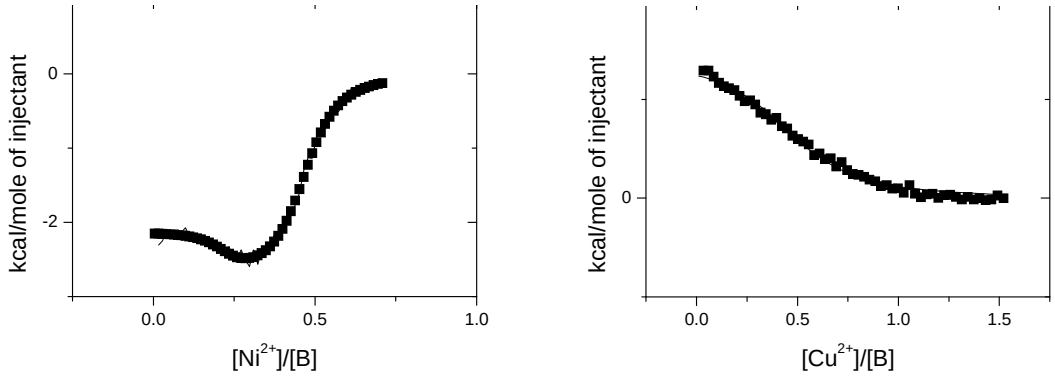

(a) (b)

Figure 3.14. ITC titration of a. 0.06 mM **Bpy-X_2•X_3** with 0.41mM $Ni(NO_3)_2$; b. 0.06 mM **Bpy-X_2•X_3** with 0.88 mM $Cu(NO_3)_2$.

$$82\%\quad Ni(Tris)_2^{2+} \longrightarrow Ni^{2+} + 2Tris$$

$$17\%\quad Ni(Tris)^{2+} \longrightarrow Ni^{2+} + Tris$$

$$Ni^{2+} + 2Bpy \longrightarrow Ni(Bpy)_2^{2+} \qquad (3.6)$$

$$0.82Ni(Tris)_2^{2+} + 0.18Ni(Tris)^{2+} + 2Bpy \longrightarrow Ni(Bpy)_2^{2+} + 1.82Tris$$

Scheme 3.6. Thermodynamic cycle for the calculation of the formation enthalpy (ΔH) for $[Ni(\mathbf{Bpy})_2]^{2+}$.

$$Cu(Tris)_4^{2+} \longrightarrow Cu^{2+} + 4Tris$$

$$Cu^{2+} + 2Bpy \longrightarrow Cu(Bpy)_2^{2+} \qquad (3.7)$$

$$Cu(Tris)_4^{2+} + 2Bpy \longrightarrow Cu(Bpy)_2^{2+} + 4Tris$$

Scheme 3.7. Thermodynamic cycle for the calculation of the formation enthalpy (ΔH) for $[Cu(\mathbf{Bpy})_2]^{2+}$.

The corrected enthalpy value for the complex formed between Ni^{2+} and **Bpy-X_2•X_3** is -9 kcal/mol, which is significantly smaller than the value reported for the $Ni(Bpy)_2$ complex with the free Bpy ligand (-19.0 kcal/mol).[8] We attribute this difference to the steric interaction between the tetrahedrally-distorted $Ni(Bpy)_2$ and the neighboring nucleobase pairs in the PNA duplex. In contrast, the corrected enthalpy value for the complex formed between Cu^{2+} with **Bpy-X_2•X_3** is -17 kcal/mol, which is similar to the reported value for the $Cu(Bpy)_2$ complex with the free Bpy ligand (-17.0 kcal/mol).[8]

The equilibrium observed at low Ni^{2+}/Bpy ratio has a weak equilibrium constant and it may be due to a conformational change of the PNA duplex.

ITC Titrations of the Bpy-PNA Triplex with Ni^{2+} and Cu^{2+}

The results of ITC titrations of PNA triplexes **Bpy-X_5•X_4•X_5** with Ni^{2+} and Cu^{2+} are shown in Figure 3.15. In both cases, a transition is observed at M^{2+}/**Bpy** ratio of 1:3, which indicates the formation of $[M(Bpy)_3]^{2+}$ complexes with the PNA triplex. The thermodynamic parameters are listed in Tables 3.4 and 3.5. The corrected stability constants independent of buffers and pH were calculated similarly.[11] The absolute stability constant of the $Ni(Bpy)_3$ complex with the PNA triplex is Logβ_3 16.8, which is significantly lower than the value reported for the $Ni(Bpy)_3$ complex with free Bpy (Logβ_3=20.5). The corrected enthalpy for the formation of the $Ni(Bpy)_3$ complex with the PNA triplex is -9 kcal/mol, which is significantly less negative than the value for the $Ni(Bpy)_3$ complex with free Bpy (-28.2)[8]. We attribute the differences between the stability constants and enthalpy values to the unfavorable steric interations between the octahedral $Ni(Bpy)_3$ complex and the PNA triplex in which the triplets of nucleobases are planar. This finding suggests that the binding affinity of the triplex for Ni^{2+} is dominated not by the entropic supramolecuar chelate effect, but by the enthalpic steric effect.

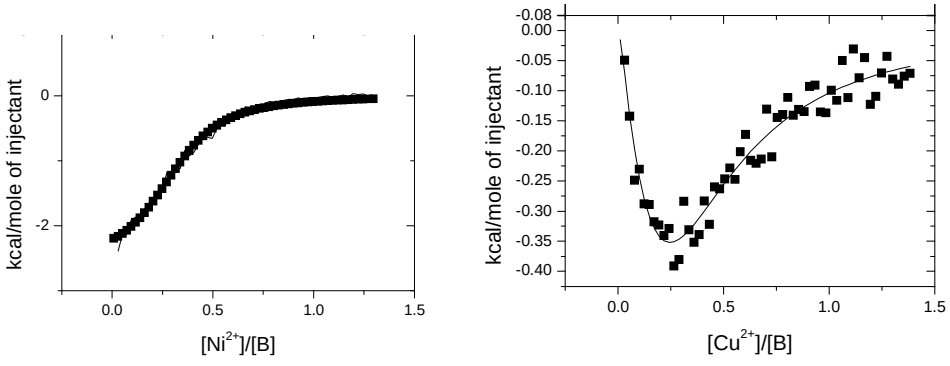

(a) (b)

Figure 3.15. ITC titration of a. 0.04 mM **Bpy-X_5•X_4•X_5** with 0.75 mM $Ni(NO_3)_2$; b. 0.03 mM **Bpy-X_5•X_4•X_5** with 0.60 mM $Cu(NO_3)_2$.

3.3 Discussion

Nucleic acids duplexes and triplexes can be used as scaffolds for transition metal ions. A strategy developed and used in the recent decade to achieve this goal is to substitute one or more nucleobases with ligands to create a site with high affinity for transition metal ions at a specific position in the nucleic acid duplex or triplex. The control over the position and nature of the transition metal ions is a particularly advantage of this strategy because it allows one to design and synthesize arrays of transition metal ions with diverse geometric and electronic properties. While the strategy for metal incorporation can be summed up as the exploitation of the differences between the affinity of ligands and nucleobase pairs for transition metal ions, quantitative knowledge of the thermodynamics of metal binding to ligand-modified nucleic acids can enable one to fine tune the design of the hybrid nucleic acid-inorganic molecules to the extent needed for answering specific fundamental questions or for practical applications.

As can be seen in Table 3.6, there is a relationship between the stability constants of the $[CuQ_2]$ complexes formed with Q-PNA duplexes and the increase in the melting temperature of the duplexes induced by one equivalent of Cu^{2+}. This relationship represents direct experimental support to the strategy of metal incorporation in nucleic acid duplexes through ligand modification, which was previously based on knowledge of the stability constants of metal complexes with ligands outside the nucleic acid context. The results of the ITC titrations presented above put on a quantitative basis several other conclusions that we and others have reached indirectly in previous studies of ligand-modified nucleic acids.

Table 3.6. Stability constants for complexes formed by Cu^{2+} and Q-PNA and melting temperature T_m(°C)* of **Q**-PNA measured in the absence and presence of Cu^{2+}

	Logβ	T_m(no metal)	T_m(1eq. Cu^{2+})	ΔT_m
Q_1-X_2•X_3	29.0	46	>79	>33
Q_1-X_3•X_3	28.8	-	>79	>33
Q_1-X_2•X_2	28.6	-	72	>33
Q_1-X_1•X_1	26.8	74	>79	>5
Q_2-X_2•X_3	20.2	38	37	-1

* T_m values were measured for 5 μM solutions of PNA duplexes in pH 7.0 10 mM sodium phosphate buffer.

In our previous study of a PNA duplex containing a pair of 8-hydroxyquinoline ligands, we concluded based on the results of melting curves, UV titrations, and EPR spectroscopy that the PNA duplex exerts a supramolecular chelate effect on the Cu^{2+} binding to the Q-PNA to form a [CuQ_2] complex that plays the role of alternative base pair. The current study showed that the stability constant for the [CuQ_2] complex formed between the **Q_1-X_2•X_3** and Cu^{2+} (Logβ_2 = 29.0) is much larger than that for the complex formed with the free 8-hydroxyquinoline (24.8). The enthalpy changes for the formation of the two complexes are similar but the entropy change for the formation of the former complex is much larger than for the latter one. Thus, the supramolecular chelate effect induced by PNA duplexes on metal coordination to the pair of ligands incorporated in the PNAs is entropy driven. We also note that the stability constants of the [CuQ_2] complex formed with the **Q_1-X_2•X_3** duplex that has the **Q_1** ligands at the centre of the duplex has a higher stability constant than that of the complex formed with the **Q_1-X_2•X_3-same** duplex that has the **Q_1** ligands at the end of the duplex. This difference can be explained by a stronger supramolecular chelate effect when the metal complex is flanked by Watson

Crick nucleobase pairs on both sides than when the complex has neighboring Watson-Crick base pairs on one side only.

In another study of 8-hydroxyquinoline PNAs, we have found out that the linker between the ligand and the PNA backbone influences the steric interactions between the metal complex formed with the PNA and the PNA duplex. In the current study we found that the stability constant of the $[CuQ_2]$ complex formed between Cu^{2+} and the **Q_2-X_2•X_3** duplex, which contains an 8-hhydroxyquinoline connected to the backbone through a very short linker close to the coordination site, is much lower than that for the $[CuQ_2]$ complex with the free ligand Q. This difference is primarily due to the less negative enthalpy change for the formation of the former complex. It is the difference in enthalpy change that also causes the difference between the stability constants for the complexes formed by Cu^{2+} with **Q_2-X_2•X_3** and **Q_1-X_2•X_3**, although the duplex **X_2•X_3** exerts a chelate effect in both cases.

We have examined several properties of the PNA that influence the stability constants of complexes, namely the PNA sequence and the position of the ligand in the PNA duplex. First, our current study showed that the stability constants of the $[CuQ_2]$ complex formed with duplexes **Q_1-X_2•X_3** and **Q_1-X_1•X_1**, which both have the same pair of 8-hydroxyquinoline ligands situated in the center of the duplex, are significantly different. The duplex **Q_1-X_2•X_3** has four and five Watson Crick base pairs on each side of the Q ligands, while the duplex **Q_1-X_1•X_1** has the same four base pairs on each side of the Q ligands. We hypothesize that the difference in sequence causes differences in the secondary structure of the PNA, which in turn affect the stability of the complexes they form with Cu^{2+}. Second, this study sheds light on the effect of mismatches in the ligand-containing PNA duplexes on the binding affinity of the ligands they contain. In a previous study of Q-PNA, we discovered that in the presence of Cu^{2+}, PNA duplexes can be formed from 8-hydroxyquinoline-containing PNA oligomers that are not fully complementary and that the thermal stability of these duplexes is comparable to that of the fully complementary PNA duplexes

with similar length and related sequence.[7] In the current study, we have measured the stability constants of complexes of Cu^{2+} with two different PNA oligomers that can form such duplexes with four mismatches, namely **Q_1-X_2•X_2** and **Q_1-X_3•X_3**, and found that these constants are similar, Logβ_2 ~ 29, and only slightly smaller than the stability constant for the [CuQ_2] complex with the closely related, fully Watson Crick complementary **Q_1-X_2•X_3** PNA duplex. This result indicates that the metal complex exerts a "reverse" chelate effect on the PNA strands, bringing them in close proximity of each other and thus favoring the formation of the PNA duplex. Of course, some degree of Watson Crick complementarity between the PNA strands is necessary to observe the chelate and reverse chelate effect. Single strands of PNA that contain exclusively A and C nucleobases besides the Q ligands do not show cooperative melting and the stability constant of the [CuQ_2] complex that such a ss PNA strand, namely **Q_1-X_4**, is Logβ_2 27.2, which is significantly smaller than the same constant for [CuQ_2] complexes with the fully complementary **Q_1-X_2•X_3** or partly complementary **Q_1-X_2•X_2** and **Q_1-X_3•X_3** duplexes.

An unexpected result of the current ITC study is the observation of a binding process between Cu^{2+} and the duplexes **Q_1C-X_2•X_3**, **Q_1-X_2•X_3** or **Q_1-X_2•X_3-same** in solutions in which the Cu^{2+}/**Q_1** ratio is smaller than 0.5 (see Figure 3.3b, 3.5b. 3.12a, 3.16). These transitions have relatively low apparent equilibrium constants, i.e Log$K$ ~ 5, and an enthalpy change that is less negative than the enthalpy change for the formation of [CuQ_2] complexes at Cu^{2+}/**Q_1** ratio of 0.5. The UV titrations of these duplexes do not show features that can be attributed to any other complex of Cu^{2+} than [Cu(**Q_1**)$_2$]. Hence we hypothesize that the transition at Cu^{2+}/**Q_1** < 0.5 is due to the formation of an inter-duplex [CuQ_2] complex and it involves a conformational change of the PNA duplex. CD spectroscopy results show the CD peak observed for the **Q_1-X_2•X_3** duplex at 260 nm shifts to 255 nm and its intensity increases upon Cu^{2+} binding to the pre-annealed duplex (Figure 3.16b), which is indicative of a conformational change of the duplex. The hypothesis that a conformational change occurs in the

formation of the inter-duplex [CuQ_2] complex is supported by the observation of two kinetic steps in the heat effect associated with the Cu^{2+} injections for which the Cu^{2+}/**Q_1** ratio in solution is lower than 0.5. Two kinetic steps have been previously observed in ITC titrations of ovotransferrin[34] or human serum transferrin[35] with ferric ions as well as in ITC titrations of apoazurin with Cu^{2+}.[36] The fast initial exothermic phase observed for the binding of ferric ions to transferrins was attributed to "contact binding". The kinetic phases observed for Cu^{2+} binding to apoazurin were attributed to the exothermic formation of an intermediate complex and the endothermic rearrangement of the intermediate to the final product. In the latter study, the heat peaks measured for each single injection have been integrated and simulated using a two-step kinetic model to obtain the kinetic and thermodynamic parameters for each step. We are in the process of using similar methods to analyze the data measured for Cu^{2+} binding to Q-PNA.

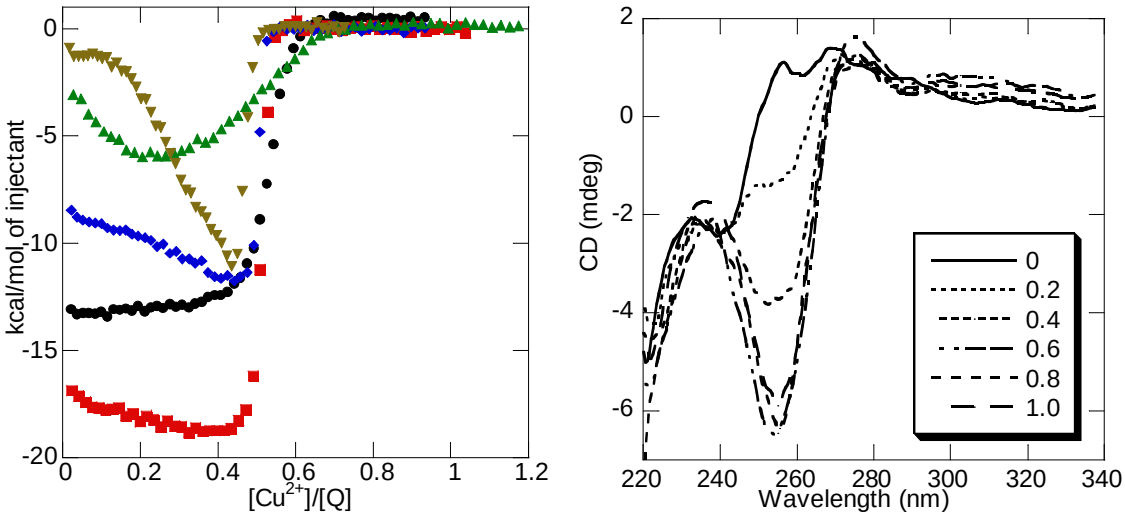

(a) (b)

Figure 3.16. (a) ITC titrations of **Q_1-X_4** (black), **Q_1-X_2•X_2** (red), **Q_1-X_3•X_3** (blue), **Q_1C-X_2•X_3** (green) and **Q_1-X_2•X_3** (brown) with Cu^{2+} in buffer. The stability constants of the [CuQ_2] complexes formed with these duplexes are **27.2**, **28.0**, **28.8**, **25.8**, and **29.0**, respectively. (b) CD titration of a 10 μM solution of pre-annealed **Q_1-X_2•X_3** duplex in the absence and presence of 0.2 - 1.0 eq. $Cu(NO_3)_2$.

Another unexpected result of this study is that the PNA duplex **Q_1-X_2•X_3-opp**, which has L-lysine at the C-end of each of its two PNA strands, adopts a right handed conformation (Figure 3.10b). We attribute this effect to hydrogen bonding between each of the two L-lysines and the 8-hydroxyquinoline situated at the N-end of the opposite strand of the duplex. Metal coordination to the 8-hydroxyquinoline "frees" the L-Lysine from its interaction with the 8-hydroxyquinoine and allows it to exert its well know induction of left handedness in the duplex. This result lends support to the previously proposed mechanism for chiral induction by L-lysine through hydrogen bonding between L-Lysine and adjacent nucleobases or peptide bonds in the PNA. We have already identified such hydrogen bonds in the high resolution crystal structure of the palindromic **X_1·X_1** PNA duplex To the best of our knowledge, this strategy for switching the preferred handedness of a PNA duplex was not reported before. We are in the process of verifying this hypothesis by testing the effect of the pH on the handedness of the PNA duplex **Q_1-X_2•X_3-opp**.

In conclusion, thermodynamic parameters of metal ions with ligand-containing PNA including Cu^{2+} with **Q**-PNA, Ni^{2+} and Cu^{2+} with **Bpy**-PNA have been studied by ITC. This study established that the previously proposed supramolecular chelate effect on metal binding to PNA duplexes exists and it is entropy-driven. Another major factor that influences the binding affinity of ligand-containing PNA for transition metal ions is the steric interaction between the metal complex and the PNA. Last but not least, the sequence of the PNA, the base pair mismatches, and the position of ligands in the PNA also influence the stability constants of metal complexes formed with ligand-modified PNAs.

3.4 Experiments

PNA Synthesis

PNA oligomers were synthesized using the Boc-protection strategy. PNA monomers were bought from ASM Research Chemicals and used without further purification. After cleavage, PNA was precipitated using ethyl ether and was purified by reversed-phase HPLC using a C18 silica column on a Waters 600 Controller and Pump. Absorbance was measured with a Waters 2996 Photodiode Array Detector. Characterization of the oligomers was performed by MALDI-TOF mass spectrometry on an Applied Biosystems Voyager Biospectrometry Workstation with Delayed Extraction and an R-cyano-4-hydroxycinnamic acid matrix (10 mg/mL in 1:1 water: acetonitrile, 0.1% TFA). MALDI-TOF calculated/found for (Xi + H)+ m/z **X_1** 2314.3/2314.6, **Q_1-X_1** 2600.5/2600.2, **Q_2-X_1** 2586.5/2586.5, **X_2** 2579.6/2579.8, **X_3** 2588.6/2588.7, **Q_1-X_2** 2865.8/2866.0, **Q_1-X_3** 2874.8/2875.0, **Q_2-X_2** 2851.8/2850.6, **Q_2-X_3** 2860.8/2860.8, **C-X_3** 2839.8/2839.2 , **Q_1-X_2-same** 2864.9/2864.5**, Q_1-X_3-same** 2873.9/2873.2**, Q_1-X_2-opp** 2864.9/2864.5, **Q_1-X_3-opp** 2873.9/2873.2, **Q_1-X_4** 2811.9/2811.5, **Bpy-X_2** 2875.9/2875.5, **Bpy-X_3** 2884.9/2890.5, **Bpy-X_4** 2962.0/2962.7, **Bpy-X_5** 2880.9/2880.4.

Isothermal Titration Calorimetry

$Cu(NO_3)_2$ and $Ni(NO_3)_2$ were obtained from Alfa Aesar and were 99.999% pure. 8-Hydroxyquinoline, 2,2-bipyridine and Tris(hydroxymethyl)-aminomethane (Tris) were obtained from Aldrich and was 99%, 99% and 99.9+% pure respectively. Tris buffer solutions were made by dissolving calculated amounts of salt in Nanopure water, and adjusting to the desired pH with HCl. The concentration of $Cu(NO_3)_2$ and $Ni(NO_3)_2$ was standardized by Cu^{2+}-Na_2EDTA and Ni^{2+}-Na_2EDTA ITC experiments.

A MicroCal VP-ITC was used for all ITC experiments. All ITC experiments were conducted at 25 ^oC and 100mM Tris buffer (pH=8.1) was used as buffer

unless specified. All PNAs were annealed before the ITC. A solution was placed in the cell (volume 1.4616 mL) and the titrant solution (about 281.5 μl) was in a syringe with the stirring speed at 300 rpm. Typically 58 injections of 5 μL each and 210s apart were made. The integrated peaks of the heat were plotted as a function of the molar ratio. With MicroCal Origin, the binding isotherms were simulated according to a one-site-binding or two-site-binding model, giving values of stoichiometry, the enthalpy of binding (ΔH) and the binding constant (K). The absolute values of enthalpy and stability constants were calculated by consideration of metal buffer interaction and possible proton transfer.[31] The free energy (ΔG) and entropy (ΔS) values were calculated based on the following equations of $\Delta G=-RTlnK$ and $\Delta G=\Delta H-T\Delta S$. Based on MicroCal manual of EDTA-$CaCl_2$ test kit, for the same ITC experiment with the same reagent, the error ranges of N, *K* and H are 5%, 20% and 10% respectively.

CD Spectroscopy

CD spectra were measured for 10 μM PNA duplex concentration in specific buffer solutions. In the case where complementary PNA strands were used, solutions were equimolar in the two strands. CD measurements were conducted on a JASCO J-715 spectropolarimeter equipped with a thermoelectrically controlled, single-cell holder. CD spectra were collected using bandwidth 1 nm, response time 1 s, speed 100 nm/min, sensitivity 20 mdeg, and scan accumulation 16.

UV-Vis Spectroscopy.

UV-vis experiments were performed on a Varian Cary 3 spectrophotometer with programmable temperature block, in 10 mm quartz cells. PNA stock solutions were prepared with nanopure water and were stored at -18 °C. The concentration of PNA oligomers was determined by UV absorption at 95 °C using the sum of the extinction coefficients of the constituent nucleosides ϵ_{260} taken from the literature. The extinction coefficient for 8-hydroxyquinoline and

2,2-bipyridine ϵ_{260} was determined from the slope of the calibration curve A_{260} versus concentration. PNA solutions for melting curves and titrations had concentrations in the micromolar range (5-25) and were prepared in pH 8.1 100 mM Tris buffer. UV-vis titrations were carried out by addition of standard 0.5-2 mM $Cu(NO_3)_2$ solutions in Tris to PNA solutions. The absorbance A after each addition was corrected for dilution and for the contribution of $Cu(NO_3)_2$ and PNA.

UV melting curves were recorded in the temperature range 15-95 °C for both cooling and heating modes, at a rate of 1 °C/min. Prior to the measurement of the melting profiles, the solutions were kept at 95 °C for at least 10 min. Melting curves were measured at 260 nm. T_m is the inflection point of a sigmoidal function used to fit the melting curve.

Reference

(1) Mueller, J. *Eur. J. Inorg. Chem.* **2008**, 3749-3763.
(2) He, W.; Franzini, R. M.; Achim, C. *Prog. Inorg. Chem.* **2007**, *55*, 545-611.
(3) Clever, G. H.; Kaul, C.; Carell, T. *Angew. Chem., Int. Ed.* **2007**, *46*, 6226-6236.
(4) Tanaka, K.; Shionoya, M. *J. Org. Chem.* **1999**, *64*, 5002-5003.
(5) Popescu, D.-L.; Parolin, T. J.; Achim, C. *J. Am. Chem. Soc.* **2003**, *125*, 6354-6355.
(6) Franzini, R. M.; Watson, R. M.; Patra, G. K.; Breece, R. M.; Tierney, D. L.; Hendrich, M. P.; Achim, C. *Inorg. Chem.* **2006**, *45*, 9798-9811.
(7) Watson, R. M.; Skorik, Y. A.; Patra, G. K.; Achim, C. *J. Am. Chem. Soc.* **2005**, *127*, 14628-14639.
(8) Martell, A. E.; Smith, R. M. *Critical Stability Constants, Vol. 2.*; Plenum Press: New York and London, 1975.
(9) Tanaka, K.; Yamada, Y.; Shionoya, M. *J. Am. Chem. Soc.* **2002**, *124*, 8802-8803.
(10) Jelesarov, I.; Bosshard, H. R. *J. Mol. Recognit.* **1999**, *12*, 3-18.
(11) Zhang, Y.; Akilesh, S.; Wilcox, D. E. *Inorg. Chem.* **2000**, *39*, 3057-3064.
(12) Wilcox, D. E. *Inorg. Chim. Acta* **2008**, *361*, 857-867.
(13) Wu, J.; Du, F.; Zhang, P.; Khan, I. A.; Chen, J.; Liang, Y. *J. Inorg. Biochem.* **2005**, *99*, 1145-1154.
(14) Wettig, S. D.; Wood, D. O.; Lee, J. S. *J. Inorg. Biochem.* **2003**, *94*, 94-99.
(15) Engman, K. C.; Sandin, P.; Osborne, S.; Brown, T.; Billeter, M.; Lincoln, P.; Norden, B.; Albinsson, B.; Wilhelmsson, L. M. *Nucleic Acids Res.* **2004**, *32*, 5087-5095.
(16) Ramstad, T.; Hadden, C. E.; Martin, G. E.; Speaker, S. M.; Teagarden, D. L.; Thamann, T. J. *Int. J. Pharm.* **2005**, *296*, 55-63.
(17) Myszka, D. G. *Curr. Opin. Biotechnol.* **1997**, *8*, 50-57.
(18) Green, D. B.; Lane, J.; Wing, R. M. *Appl. Spectrosc.* **1987**, *41*, 847-851.
(19) Wiesner, P.; Kayser, H. *J. Biochem. Mol. Toxicol.* **2000**, *14*, 221-230.
(20) Bruylants, G.; Wouters, J.; Michaux, C. *Curr. Med. Chem.* **2005**, *12*, 2011-2020.
(21) Horn, J. R.; Russell, D.; Lewis, E. A.; Murphy, K. P. *Biochemistry* **2001**, *40*, 1774-1778.
(22) Ratilainen, T.; Holmen, A.; Tuite, E.; Haaima, G.; Christensen, L.; Nielsen, P. E.; Norden, B. *Biochemistry* **1998**, *37*, 12331-12342.
(23) Puglisi, J. D.; Tinoco, I. *Method Enzymol.* **1989**, *180*, 304-325.
(24) Marky, L. A.; Breslauer, K. J. *Biopolymers* **1987**, *26*, 1601-1620.
(25) Turnbull, W. B.; Daranas, A. H. *J. Am. Chem. Soc.* **2003**, *125*, 14859-14866.
(26) Li, J.; Swanson, R. V.; Simon, M. I.; Weis, R. M. *Biochemistry* **1995**, *34*, 14626-36.

(27) Sigurskjold, B. W.; Berland, C. R.; Svensson, B. *Biochemistry* **1994**, *33*, 10191-9.
(28) Yamamoto, Y.; Miura, A.; Kawamata, A.; Miura, M.; Takei, S. *Bull. Chem. Soc. Jpn.* **1978**, *51*, 3489-95.
(29) Deraeve, C.; Boldron, C.; Maraval, A.; Mazarguil, H.; Gornitzka, H.; Vendier, L.; Pitie, M.; Meunier, B. *Chem.--Eur. J.* **2008**, *14*, 682-696.
(30) Palenik, G. J. *Acta Cryst.* **1964**, *17*, 687-95.
(31) Grossoehme, N. E.; Spuches, A. M.; Wilcox, D. E. *J. Biol. Inorg. Chem.* **2010**, *15*, 1183-1191.
(32) Fresco, J.; Freiser, H. *Analytical Chemistry* **1964**, *36*, 372-375.
(33) Izatt, R. M.; Christensen, J. J.; Rytting, J. H. *Chem. Rev.* **1971**, *71*, 439-82.
(34) Lin, L. N.; Mason, A. B.; Woodworth, R. C.; Brandts, J. F. *Biochemistry* **1991**, *30*, 11660-11669.
(35) Lin, L. N.; Mason, A. B.; Woodworth, R. C.; Brandts, J. F. *Biochemistry* **1993**, *32*, 9398-9406.
(36) Blasie, C. A.; Berg, J. M. *J. Am. Chem. Soc.* **2003**, *125*, 6866-6867.

Chapter 4 Metal-Containing PNA Triplexes

4.1 Introduction

DNA triplexes have received considerable interest due to its potential biological role in transcription regulation and homologous recombination and potential applications in therapeutics.[1] In DNA triplexes, a third, homopyrimidine strand binds to a duplex, which comprises a homopurine (A or G) and a homopyrimidine (C or T) strand (for example, see triplex $\mathbf{X_2 \bullet X_1 \bullet X_2}$ in Table 4.1). Depending on the relative orientation of the third homopyrimidine strand with respect to the homopurine strand, the DNA triplexes can be parallel or antiparallel ($\mathbf{X_4 \bullet X_3 \bullet X_5}$ and $\mathbf{X_4 \bullet X_3 \bullet X_4}$ triplexes in Table 4.1). In parallel triplexes, the third homopyrimidine strand binds in a parallel manner to the homopurine strand of the duplex by Hoogsteen base pairing. In antiparallel triplexes, it is possible, albeit it is rare, that a third homopyrimidine strand binds in an antiparallel orientation to the homopurine strand by reverse Hoogsteen base pairing.[1,2] Melting of DNA triplexes is typically stepwise, with the dissociation of the third strand bound through Hoogsteen or reverse Hoogsteen base pairing taking place at a lower temperature than the dissociation of the Watson-Crick duplex (Scheme 4.1).[3] In LNA and PNA, a highly cooperative transition from triplex directly to single strands was also observed.[4,5]

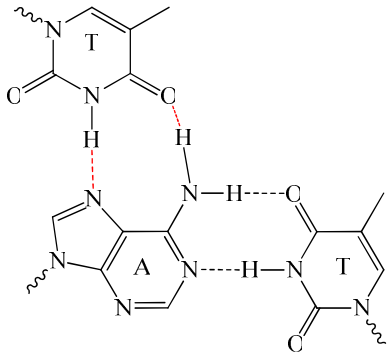

Scheme 4.1. Cartoon representation of a T•A•T triplet in the parallel triplex motif. Watson-Crick and Hoogsteen hydrogen bonds are shown as dotted black and red lines, respectively.

PNA is a synthetic analog of DNA which binds to DNA with higher affinity due to the substitution of negatively charged phosphodiester backbone with a neutral pseudopeptide one.[6] Two homopyrimidine PNA strands and a homopurine DNA strand can form triplexes with very high thermal stability.[7] The crystal structure of a PNA/DNA triplex showed that the triplex adopts P-form helix.[8] The formation of homoPNA triplexes from homo-A and homo-T PNA oligomers was also reported.[5] Our previous studies have shown that both parallel and antiparallel PNA triplexes can form and that the triplexes with parallel orientation are slightly more stable than the antiparallel triplexes.

Metal ions have been incorporated into several DNA triplexes (*1*) by coordination to triplets of either the natural nucleobase[9] or of ligands [10,11] or (*2*) by attachment of a metal complex to one of the oligonucleotide strands of the triplex.[12,13] Melting curves of DNA triplexes in which the metal ion coordinated to a triplet of nucleobases or ligands showed an increase in the transition temperature of the triplex-to-duplex and/or duplex-to-single strand transition, which correlated with the coordination mode of the metal to the triplet, i.e. to two or to three members of the triplet.[9,11]

Previous research in our lab indicated that metal ions can be incorporated into PNA duplexes by substitution of natural base pairs with ligands such as 2,2'-bipyridine(**Bpy**) and 8-hydroxyquinoline which have high affinity with metal ions.[14-16] In this chapter, we describe the extension of this strategy for metal ion incorporation in PNA duplexes to PNA triplexes. The most common coordination number of metal complexes is six. This number can be attained by binding to the metal ion of three bidentate ligands. Hence, we incorporate a bidentate ligand on each of the three PNA oligomers of a triplex to create a high affinity metal binding site.

4.2 Result and Discussion

We have synthesized five PNA oligomers with the sequences shown in Table 4.1. PNAs $\mathbf{X_1}$ and $\mathbf{X_2}$ are homo-A or T oligomers, respectively, and can form a PNA triplex $\mathbf{X_2 \bullet X_1 \bullet X_2}$, which differs from the PNA triplex reported by Nielsen et al. only in the fact that the three single strands have their N-end acetylated and that the homo-A strand has an L-lysine rather than a L-glycine at the C-end.[5] The PNA strands $\mathbf{X_3}$, $\mathbf{X_4}$ and $\mathbf{X_5}$ contain a central bipyridine **Bpy** ligand and could form an antiparallel triplex $\mathbf{X_4 \bullet X_3 \bullet X_4}$ or a parallel triplex $\mathbf{X_4 \bullet X_3 \bullet X_5}$, that each includes nine AT_2 triplets besides the Tris(bipyridine) coordination site.

Table 4.1. PNA sequences

	PNA sequences	Triplex type
$\mathbf{X_1}$	LysAAAAAAAAAAAc	
$\mathbf{X_2}$	LysTTTTTTTTTTAc	
$\mathbf{X_4}$ $\mathbf{X_3}$ $\mathbf{X_4}$	AcTTTTT**Bpy**TTTTLys LysAAAAA**Bpy**AAAAAc AcTTTTT**Bpy**TTTTLys	Antiparallel
$\mathbf{X_4}$ $\mathbf{X_3}$ $\mathbf{X_5}$	AcTTTTT**Bpy**TTTTLys LysAAAAA**Bpy**AAAAAc LysTTTTT**Bpy**TTTTAc	Parallel

Job plots can be used to determine the stoichiometry of association complexes, including those constituted of nucleic acid strands.[11,17,18] We have used this method to determine the stoichiometry of the complex formed by non-modified and Bpy-modified homo-A and homo-T PNA strands. The homo-A ($\mathbf{X_1}$) and -T ($\mathbf{X_2}$) PNA oligomers had maximum absorbance at about 254 and 270 nm, respectively (Figure 4.1a). The Job plots for mixtures of $\mathbf{X_1}$ and $\mathbf{X_2}$ or for mixtures of **Bpy**-containing PNA oligomers $\mathbf{X_3}$ and $\mathbf{X_4}$ in the absence or presence of Ni^{2+} have one inflection point at the $\mathbf{X_i/X_{i+1}}$ ratio ~1:2, indicating the formation of the PNA triplex $\mathbf{X_{i+1} \bullet X_i \bullet X_{i+1}}$ (i = 1 or 3, Figure 4.1b).

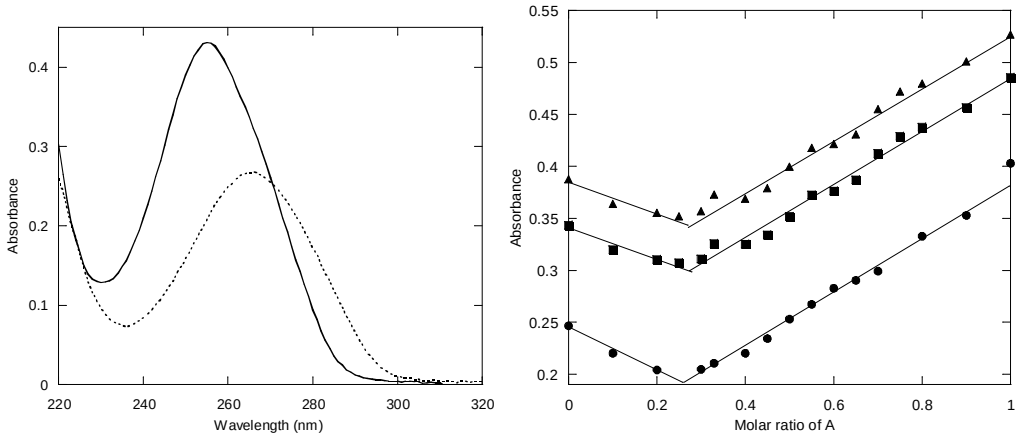

(a) (b)

Figure 4.1. (a) Absorbance spectra of 3.6 μM solutions of $\mathbf{X_1}$ and $\mathbf{X_2}$ (dotted line) in pH 7.0 10 mM NaPi buffer at 25 °C; (b) Job plots for 3.6 μM ss PNA solutions monitored at 260 nm: (top) $\mathbf{X_1}$ and $\mathbf{X_2}$; (middle) $\mathbf{X_3}$ and $\mathbf{X_4}$; (bottom) $\mathbf{X_3}$ and $\mathbf{X_4}$ in the presence of 4.8 μM Ni^{2+}. Absorbance of top two curves was shifted up by 0.05 and 0.10 for clarity purposes.

Melting curves measured by UV spectroscopy for the PNA triplexes $\mathbf{X_4 \bullet X_3 \bullet X_4}$ and $\mathbf{X_4 \bullet X_3 \bullet X_5}$ in the absence of metal ions are shown in Figure 4.2; the corresponding melting temperatures are shown in Table 4.2. The melting temperature T_m of triplex $\mathbf{X_2 \bullet X_1 \bullet X_2}$ is 67 °C, which is less than the value of 76°C reported by Nielsen et al. for a similar triplex.[5] This difference in melting temperature may be due to the fact that the C-end amino acid of the triplexes are different in our and Nielsen's study. Also, our PNA triplex has N-terminus acetylation while Nielsen's does not.

Replacement of one central AT_2 triplet with a triplet of **Bpy** ligands decreased the melting temperature to 41 and 43°C for the antiparallel $\mathbf{X_4 \bullet X_3 \bullet X_4}$ and parallel $\mathbf{X_4 \bullet X_3 \bullet X_5}$ triplexes, respectively, which is likely due to the absence of hydrogen bonding between the **Bpy** ligands and structural perturbations of the duplex induced by the nucleobase substitution.

The melting temperature of the **Bpy**-modified antiparallel $\mathbf{X_4 \bullet X_3 \bullet X_4}$ and parallel $\mathbf{X_4 \bullet X_3 \bullet X_5}$ triplexes measured in the presence of one equivalent Ni^{2+}, Co^{2+} or Cu^{2+} was higher than in the absence of the metal ions by ~20°C, ~10°C

and 2-5°C. This increase of the thermal stability of ligand-modified PNA triplexes in the presence of metal ions is similar to the one we have observed for ligand-containing PNA duplexes in the presence of metal ions and is attributed to the contribution of coordination bonds to the triplex/duplex stabilization. We consider the steric interactions between the metal complex and the adjacent nucleobase triplets the cause for the fact that the melting temperature of the Bpy-modified triplexes in the presence of metal ions is still lower than the melting temperature of the non-modified PNA triplex $\mathbf{X_2 \bullet X_1 \bullet X_2}$. This cause-effect relationship is corroborated by the fact that the decrease in the temperature-induced hyperchromicity parallels the lowering in the metal ion effect on the triplex melting temperature, i.e. Ni^{2+} > Co^{2+} > Cu^{2+} (Figure 4.2) indicative of an increasing interference of the metal complex with the nucleobase stacking in the order Ni^{2+} > Co^{2+} > Cu^{2+}. Our previous investigations of metal-containing PNA duplexes showed a correlation between the change in melting temperature induced by the metal ions and the stability constants of the complex formed by the same metal ion and ligands.[16,19]

Similarly, in the current research, Ni^{2+} determined the largest increase in melting temperature, which is consistent with Ni^{2+} being the M^{2+} ion of the three with the highest stability constant for $[M(Bpy)_3]^{2+}$, namely $\text{Log}\beta_3 = 20.2$.[20] The effect of Co^{2+} and Cu^{2+} on the melting temperature of the PNA triplex is smaller as are the stability constants of $[Co(Bpy)_3]^{2+}$ ($\text{Log}\beta_3 = 15.9$) and $[Cu(Bpy)_3]^{2+}$ ($\text{Log}\ \beta_3 = 16.9$).[20]

It is noteworthy that all melting curves of non-modified and ligand-modified PNA triplexes in the absence and presence of metal ions display one transition, i.e. their dissociation into single strands is a one-step, cooperative process. This is in contrast to the common two-step melting observed for DNA triplexes,[3] but it is similar to the one observed for a LNA[4] and for PNA triplexes[5]

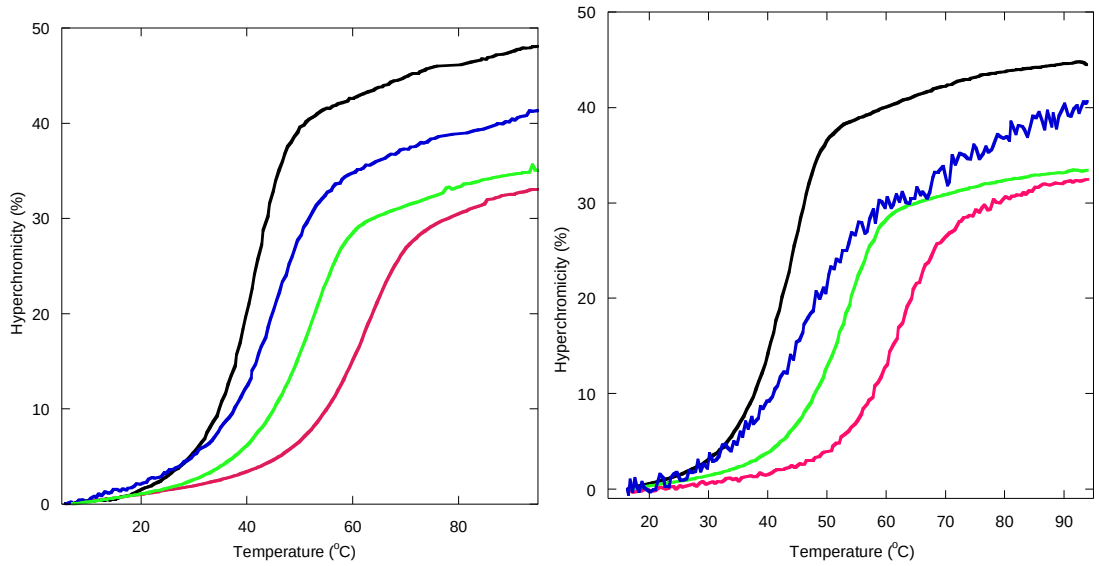

a b

Figure 4.2. Melting curve of (a) **X_4•X_3•X_4** or (b) **X_4•X_3•X_5** in the absence (black) or in the presence of Ni^{2+}(red), Co^{2+}(green) or Cu^{2+}(blue). Solutions were 5 μM in triplex PNA in pH 7.0 10 mM sodium phosphate buffer. If present, the concentration of the transition metal ion was also 5 μM.

Table 4.2. Melting temperature (°C)* of PNA triplexes in the absence of presence of metal ions.

	X_2•X_1•X_2	**X_4•X_3•X_4**	**X_4•X_3•X_5**	$Log\beta_3^{20}$
no metal	67	41	43	
Ni^{2+}	-	61	62	20.2
Co^{2+}		51	52	15.9
Cu^{2+}	-	46	45	16.9

*The precision for the T_m is ±1°C.

The ITC titration of **X_1** with **X_2** showed a one-step transition with a log K of 7.52 (Figure 4.3). Hence we conclude that the relative contributions of the Hoogsteen and Watson-Crick hydrogen bonds to the formation of the triplex are similar. The enthalpy change for the triplex formation is -44.3 kcal/mol, less than the enthalpy change of -63 kcal/mol previously reported for the ten base pair PNA duplex LysTCACTAGATG•LysCATCTAGTGA.[21]

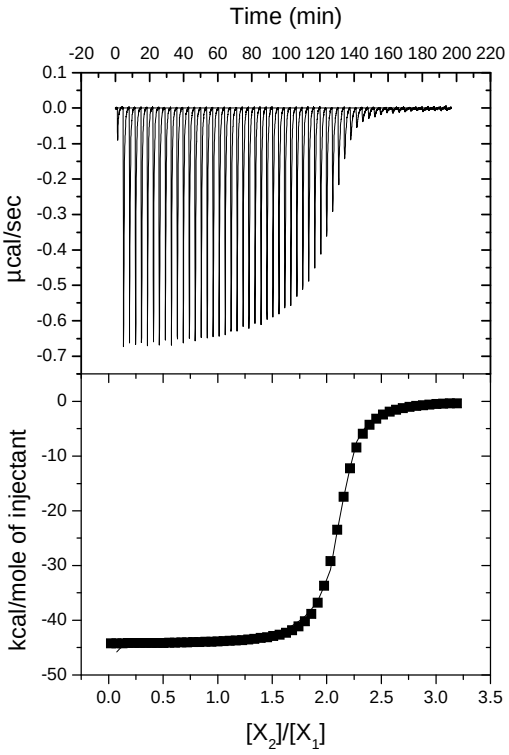

Figure 4.3. ITC titration of a 6.5 μM solution of $\mathbf{X_1}$ with a 100 μM solution of $\mathbf{X_2}$ in pH 7.0 10mM NaPi buffer.

The Ni^{2+}, Co^{2+} and Cu^{2+} binding to the annealed PNA triplex $\mathbf{X_4 \bullet X_3 \bullet X_4}$ was studied by UV titrations (Figure 4.4). The UV spectrum of the PNA triplex $\mathbf{X_4 \bullet X_3 \bullet X_4}$ is dominated by the broad absorption band at 262 nm due to the π–π^* transitions of the nucleobases. The two π–π^* bands of **Bpy** at 235 nm and 245 nm shifted in the presence of M^{2+} to 280 nm and 295-320 nm, respectively, which indicated that the metal ions coordinate to **Bpy**.[22,23] For PNA triplex $\mathbf{X_4 \bullet X_3 \bullet X_4}$, the titration curves at 274, 313 and 276, 312 nm for Ni^{2+} and Co^{2+} had an inflection point at a M^{2+}/ssPNA ratio of 0.3, which indicates the formation of $[Ni(\mathbf{Bpy})_3]^{2+}$ and $[Co(\mathbf{Bpy})_3]^{2+}$ complexes (Figure 4.4 ab). Titration of the same triplex with Cu^{2+} led to a titration curve at 279 and 316 nm with two inflection points at Cu^{2+}/ssPNA ratios of 0.3 and 0.7 (Figure 4.4c), indicating that a $[Cu(\mathbf{Bpy})_3]^{2+}$ forms and transforms into complex(es) with fewer Bpy ligands in the presence of excess Cu^{2+}.

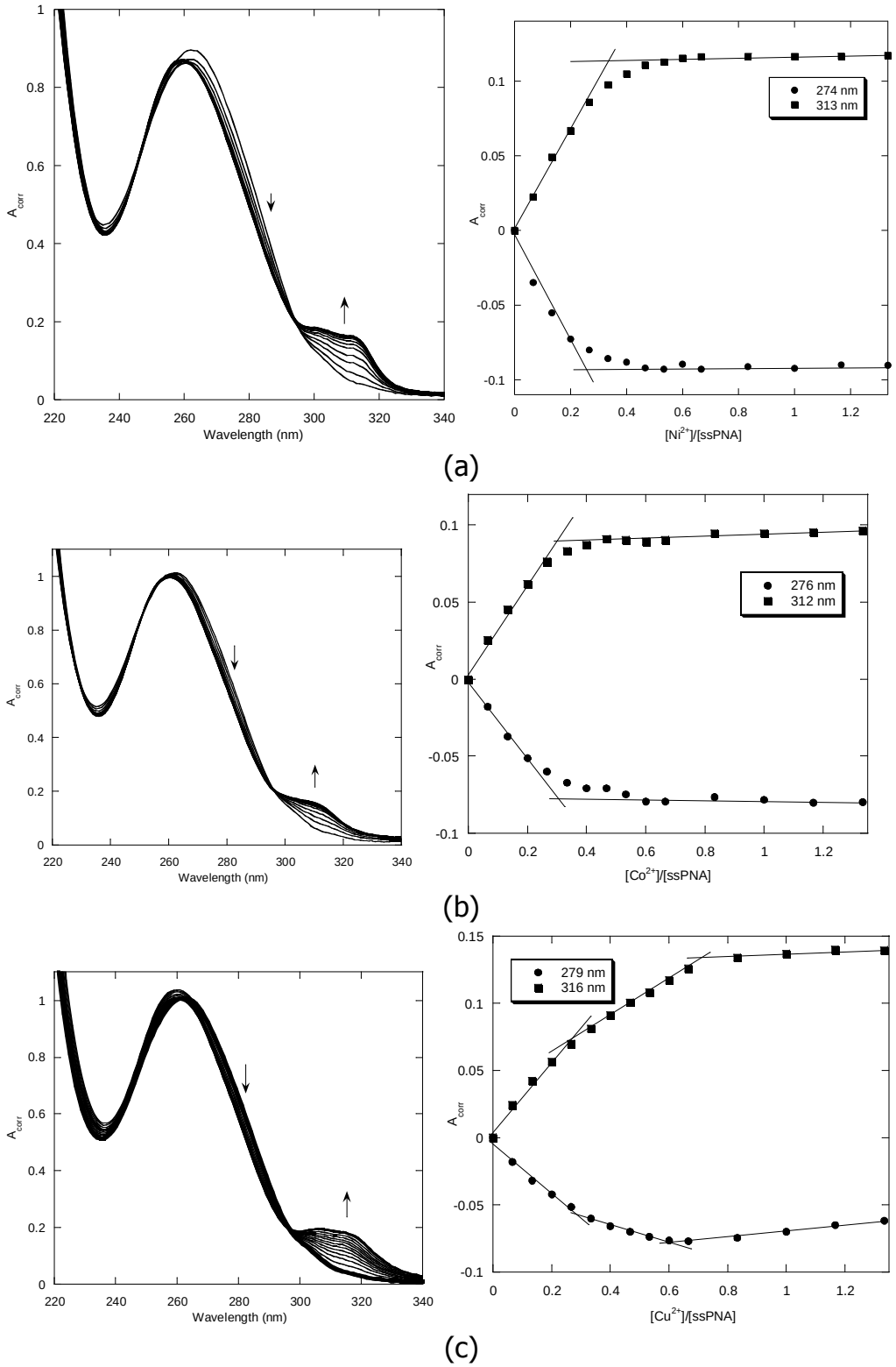

Figure 4.4. Spectrophotometric titration of a 5 μM **X_4•X_3•X_4** solution in pH 7.0 10 mM sodium phosphate solution with 500 μM solutions of $Ni(NO_3)_2$ (a), $Co(NO_3)_2$ (b) or $Cu(NO_3)_2$ (c).

CD spectra of PNA duplexes[14] and triplexes[5] are different from each other and can be used to distinguish the two types of structures. The CD spectrum of a solution of **X_3** and **X_4** in a 1:2 ratio is indicative of a PNA triplex (Figure 4.5). Upon addition of one equivalent of Ni^{2+} to this solution, the intensity of the spectrum characteristic of a triplex decreased. We tentatively attribute this decrease to steric interactions between the $[Ni(Bpy)_3]^{2+}$ and the rest of the **X_3**·**X_4**·**X_4** triplex that may weaken the transmission of the chiral induction effect of the C-end L-Lysine. A similar large decrease in the intensity of the CD spectrum was observed for a non-modified DNA triplex upon Fe^{3+} coordination.[10] Evidence for the Fe^{3+} binding to the DNA in this previous report came from UV titrations and ESI mass spectrometry.[10]

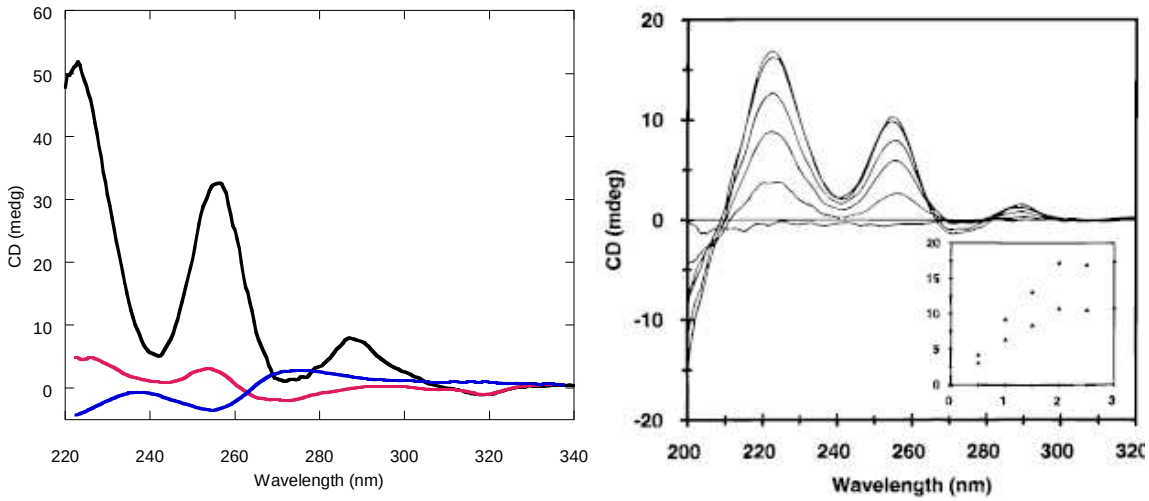

(a) (b)

Figure 4.5. CD spectra of a. a solution containing **X_3** and **X_4** in a 1:2 ratio; a solution containing Ni^{2+}, **X_3** and **X_4** in a 1:1:2 ratio (red); PNA nature duplex LysTCACTAGATG:LysCATCTAGTGA (blue). The concentration of duplex and triplex was 10 μM and all samples were made in pH 7.0 10 mM sodium phosphate buffer at 20 °C; b. CD spectrum of PNA triplex reported by Nielsen et al.

In the current research, electrospray ionization mass spectrometry (ESI MS) was employed to confirm the formation of metal-containing PNA triplexes. This method has been used in the past to verify the formation of DNA triplexes.[10] Mass spectrograms for solutions containing M^{2+} (M = Ni, Co, Cu) and the triplex $\mathbf{X_3 \cdot X_4 \cdot X_4}$ in a 1:1 ratio are shown in Figures 4.6a-c. The dominant peak observed for the Ni^{2+} solution is $[\mathbf{X_4 \bullet X_3 \bullet X_4}+Ni]^{5+}$ (Table 4.3), which confirms the formation of a Ni^{2+}-containing PNA triplex. The mass spectrograms for solutions containing Co^{2+} or Cu^{2+} also confirm the formation of the M^{2+}-containing triplexes with these metal ions but they also show peaks corresponding to dissociation fragments, namely $[\mathbf{X_4}\text{-Co-Na}]^{2+}$, $[\mathbf{X_3}\text{-Co}]^{3+}$, $[\mathbf{X_4}\text{-Cu}]^{2+}$ and dsPNA $[\mathbf{X_3 \bullet X_4}\text{-Co}]^{3+}$, $[\mathbf{X_3 \bullet X_4}\text{-Cu}]^{3+}$. These observations suggest that either the triplexes co-exist in solution with complexes of Co^{2+} or Cu^{2+} with one or two strands of the triplex or that in the conditions of the electrospray experiment, the triplex can dissociate to generate such complexes.

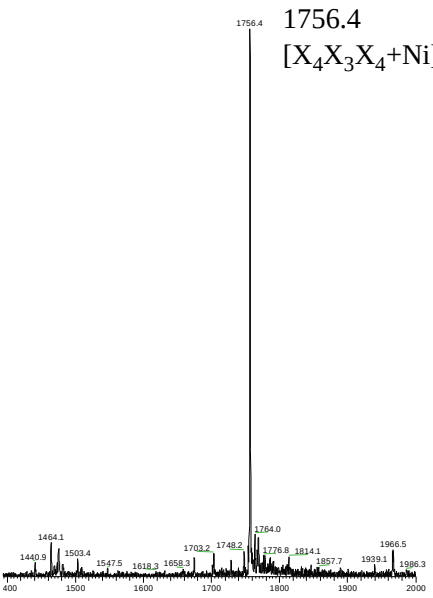

(a)

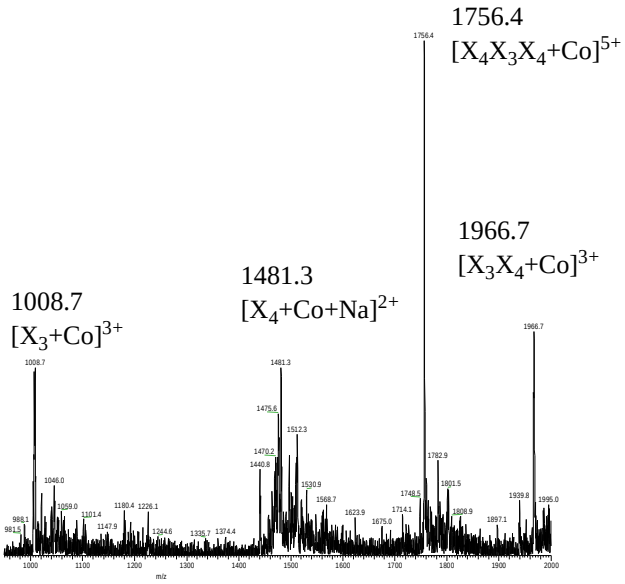

(b)

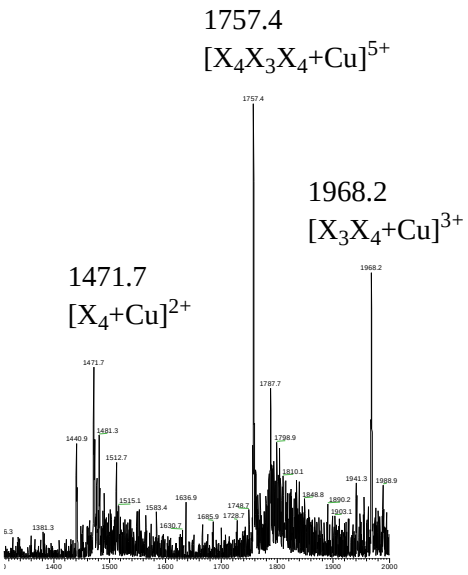

(c)

Figure 4.6. Mas spectrograms of aqueous solutions containing: (a) Ni^{2+}: **X_3: X_4** = 1:1:2 ; (b) Co^{2+}: **X_3: X_4** = 1:1:2; (c) Cu^{2+}: **X_3: X_4** = 1:1:2.The concentration of **X_3** was 40 μM and all samples were in water.

Table 4.3. Molecular weight of metal-containing PNA triplexes.

$[M+H]/[M+5H]^{5+}$	M_{obs}	PNA
8780.5/1756.9	1756.4	[**X₄•X₃•X₄** +Ni]
8780.7/1756.4	1756.4	[**X₄•X₃•X₄** +Co]
8785.4/1757.4	1757.4	[**X₄•X₃•X₄** +Cu]

Electron paramagnetic resonance (EPR) is an important spectroscopic method to investigate structural details of complexes of metal ions with unpaired electrons. We have studied the coordination of Cu^{2+} to 8-hydroxyquinoline- and 2,2-bipyridine-containing PNA duplexes by EPR spectroscopy.[15,16] Due to the similarity of the EPR parameters of Cu^{2+} complexes with 1-3 Bpy ligands, it is not straightforward to make an assignment of the number of coordinated Bpys and their relative orientation in the complexes. The Figure 4.7b shows that one could distinguish based on the A_3/g_3 ratio the cis-[$Cu(Bpy)_2$]

We have obtained EPR spectra for the single strand **X₄** (T_4BpyT5) in the presence of 1/3 and ½ equivalents of Cu^{2+} in pH 7.0 10 mM sodium phosphate buffer with 25% glycerol (Figure 4.7). These Cu^{2+}/**X₄** ratios correspond to Cu^{2+}/Bpy ratios of 1:3 and 1:2, respectively. We have also obtained spectra for solutions containing Cu^{2+} and the PNA triplex **X₄·X₃·X₄** in a 1:1 and 2:1 ratio, which correspond to Cu^{2+}/Bpy ratios of 1:3 and 2:3, respectively.

Simulations of the EPR spectra with an S = 1/2 spin Hamiltonian that includes hyperfine parameters for $^{63,65}Cu^{2+}$ (I = 3/2) led to the parameters shown in Table 4.4, which are compared with the EPR parameters previously reported for copper bipyridine complexes (Table 4.5).[24-26] We have plotted the

A_3 versus g_3 values for these complexes because the correlation between these two parameters has been used in the past to elucidate the coordination of Cu^{2+} in copper-proteins. This plot indicates that the coordination of Cu^{2+} is not cis-[Cu(**Bpy**)$_2$] and supports the fact that the number of coordinated **Bpy**s is higher for the solutions in which the Cu^{2+}/**Bpy** ratio is 1:3, i.e. Cu^{2+}/**X$_4$** is 1:3 or Cu^{2+}/**X$_4$·X$_3$·X$_4$** triplex is 1:1, than in solutions in which the Cu^{2+}/**Bpy** ratio is higher than 1:3. The g_3/A_3 values for solutions Cu^{2+}/**X$_4$** is 1:3 or Cu^{2+}/**X$_4$·X$_3$·X$_4$** triplex are close to those measured for [Cu(**Bpy**)$_3$]$^{2+}$ complexes but as the g_3/A_3 values are also close to those for trans-[Cu(**Bpy**)$_2$]$^{2+}$ complexes, we cannot decide based on this experiment what is the Cu^{2+} coordination.

The EPR parameters for Cu^{2+}/**X$_4$·X$_3$·X$_4$** = 2:1 and Cu^{2+}?**X$_4$** =1:2 are close to those measured for [Cu(**Bpy)**]$^{2+}$,[26] suggesting that in both cases Cu^{2+} coordinates to only one **Bpy**.

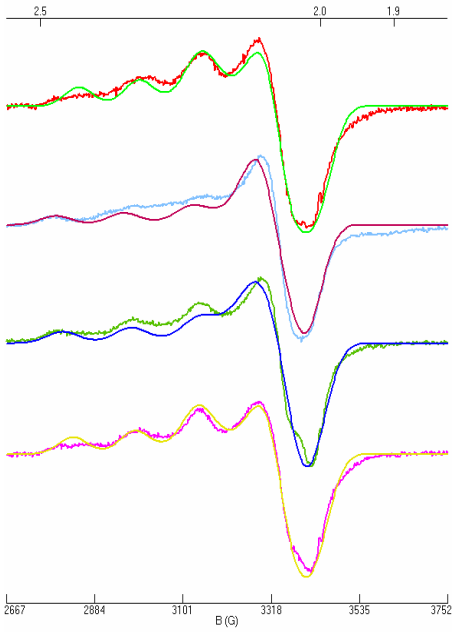

(a)

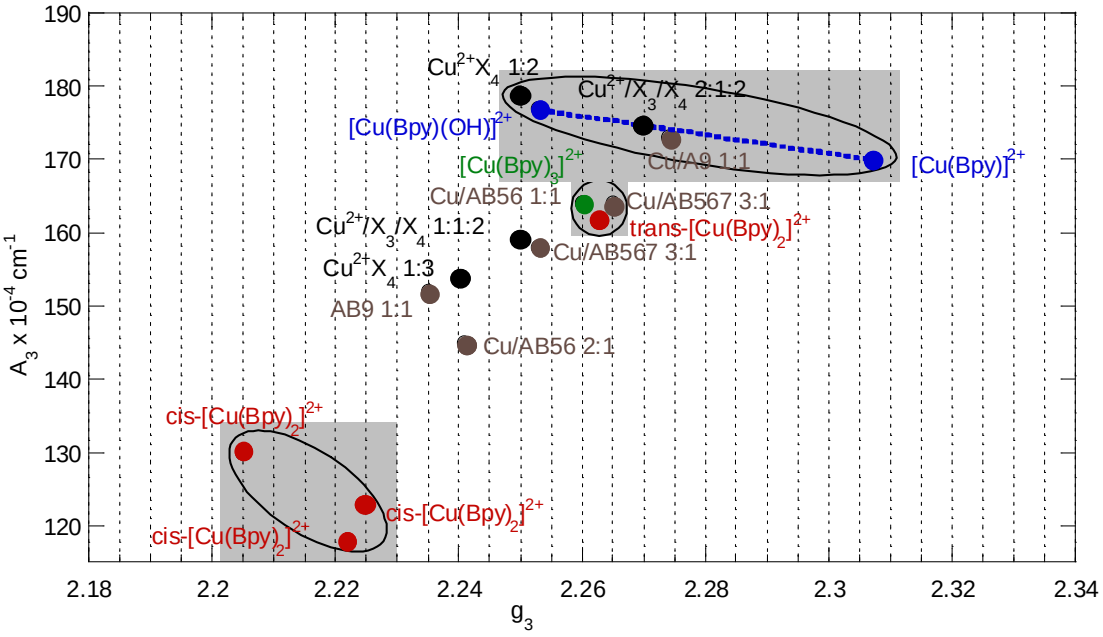

(b)

Figure 4.7. Perpendicular mode X-band EPR spectrum of a 100 μM from top to bottom, Cu^{2+}: **X_3: X_4** =1:1:2; Cu^{2+}: **X_3: X_4** =2:1:2; Cu^{2+}: **X_4** =1:2; Cu^{2+}: **X_4** =1:3 solution in pH 7.0 10 mM sodium phosphate buffer with 25% glycerol and simulation using the parameters given in Table 4.4), T 8 K, frequency 9.62 GHz, microwave power 0.02 mW, modulation amplitude 6.676 G.

Table 4.4. EPR Parameters for copper complexes with Bpy-PNA

	Cu^{2+}:**X₃:X₄**		Cu^{2+}:**X₄**	
	1:1:2	2:1:2	1:2	1:3
g_1	2.11	2.07	2.05	2.12
g_2	2.03	2.06	2.08	2.03
g_3	2.24	2.27	2.25	2.25
A_3 x10^{-4} cm^{-1}	154	175	179	159

Table 4.5. EPR parameters of $[Cu(Bpy)_n]^{2+}$ complexes

Species	g_3	A_3 x10^{-4} cm^{-1}	Solvent	Reference
$[Cu(Bpy)_3]^{2+}$	2.260	164	Aq	26
Trans-$[Cu(Bpy)_2]^{2+}$	2.263	162	Aq	26
cis-$[Cu(Bpy)_2]^{2+}$	2.225	123	60:40 EtOH-H_2O	24
cis-$[Cu(Bpy)_2]^{2+}$	2.222	118	60:40 EtOH-H_2O pH 2.2	25
cis-$[Cu(Bpy)_2]^{2+}$	2.205	130	60:40 EtOH-H_2O pH 2-7	26
$[Cu(Bpy)]^{2+}$	2.307	170	Aq pH 5.1	26
$[Cu(Bpy)(OH)]^{+}$	2.253	177	Aq	26

In conclusion, the incorporation of metal ions in PNA triplexes is observed and confirmed by Job-plot, ITC, UV-titrations, CD spectrum and ESI. The formations of Ni-tsPNA and Co-tsPNA are stable. EPR results show that in the PNA triplex, the coordination environment of Cu^{2+} is similar to those of $[Cu(\mathbf{Bpy})_3]^{2+}$ and trans-$[Cu(\mathbf{Bpy})_2]^{2+}$.

4.3 Experiments

Materials. Bpy monomer was prepared according to reported methods.[15] All other reagents were obtained from commercially available sources, were of

analytical grade quality, and were used without further purification. A Finnegan Mattson instrument was used for electrospray mass spectrometry (ES-MS). An Applied Biosystems Voyager Biospectrometry Workstation with Delayed Extraction was used for MALDI-TOF mass spectrometry.

Solid-Phase Synthesis, Purification and Characterization of PNA

PNA oligomers were synthesized using the Boc-protection strategy. PNA monomers were purchased from ASM Research Chemicals and used without further purification. After cleavage, PNA was precipitated using ethyl ether and was purified by reversed-phase HPLC using a C18 silica column on a Waters 600 Controller and Pump. Absorbance was measured with a Waters 2996 Photodiode Array Detector. Characterization of the oligomers was performed by MALDI-ToF mass spectrometry on an Applied Biosystems Voyager Biospectrometry Workstation with Delayed Extraction and an R-cyano-4-hydroxycinnamic acid matrix (10 mg/mL in 1:1 water: acetonitrile, 0.1% TFA). MALDI-TOF calculated/found for (Xi + H)+ m/z $\mathbf{X_1}$ 2940.9/2940.4, $\mathbf{X_2}$ 2850.8/2850.0, $\mathbf{X_3}$ 2962.0/2961.2, $\mathbf{X_4}$ 2880.9/2880.3, $\mathbf{X_5}$ 2880.9/2880.7.

Physical Methods. CD Spectroscopy. CD spectra were measured in pH 7.0 10 mM sodium phosphate buffer solutions. CD measurements were conducted on a JASCO J-715 spectropolarimeter equipped with a thermoelectrically controlled, single-cell holder. CD spectra were collected using bandwidth 1 nm, response time 1 s, speed 100 nm/min, sensitivity 20 mdeg, and scan accumulation 16.

UV-Vis Spectroscopy. UV-vis experiments were performed on a Varian Cary 3 spectrophotometer with programmable temperature block, in 10 mm quartz cells. PNA stock solutions were prepared with nanopure water and were stored at -18 °C. The concentration of PNA oligomers was determined by UV absorption at 95 °C using the sum of the extinction coefficients of the constituent nucleosides ε_{260} taken from the literature. The extinction coefficient for 2,2-bipyridine was determined from the slope of the calibration curve A_{260} versus concentration. PNA solutions for melting curves and titrations had concentrations in the micromolar range and were prepared in pH 7.0 10 mM phosphate buffer. UV-vis

titrations were carried out by addition of standard 0.5 mM metal ions solutions in water to PNA solutions. The absorbance A after each addition was corrected for dilution and for the contribution of metal ions and PNA.

UV melting curves were recorded in the temperature range 5-95 °C for both cooling and heating modes, at the rate of 1 °C/min. Prior to the measurement of the melting profiles, the solutions were kept at 95 °C for at least 10 min. Melting curves were measured at 260 nm. T_m is the inflection point of a sigmoidal function used to fit the melting curve. All measurements were performed at least in triplicate.

ITC. A MicroCal VP-ITC was used for all ITC experiments. A solution was placed in the cell (volume 1.4616 mL) and the titrant solution (about 281.5 μl) in a syringe with the stirring speed at 300 rpm. Typically 58 injections of 5 μL each and 210s or 600s apart were made. The integrated peaks of the heat were plotted as a function of the molar ratio. With MicroCal Origin, the binding isotherms were simulated to a one-site-binding model, giving values of stoichiometry, the enthalpy of binding (ΔH) and the binding constant (K). The free energy (ΔG) and entropy (ΔS) values were calculated based on the following equations of $\Delta G=-RTlnK$ and $\Delta G=\Delta H-T\Delta S$.

EPR Spectroscopy. EPR spectra were recorded on an X-band (9 GHz) Bruker ESP 300 spectrometer equipped with an Oxford ESR 910 cryostat. The microwave frequency was calibrated with a frequency counter and the magnetic field with a NMR gaussmeter. The temperature was calibrated using devices from Lake Shore Cryonics. Spectra were collected under nonsaturating conditions. Samples were prepared in pH 7.0 10 mM sodium phosphate buffer with 25% glycerol as glassing agent. Samples containing PNA and Cu^{2+} in appropriate molar ratio were heated at 95 °C for 10 min, slowly cooled to room temperature, and then transferred into EPR tubes and frozen. EPR spectra were simulated using the program SpinCount written by Prof. Michael P. Hendrich.[27] Spin quantitation was done relative to a 0.499 mM Na_2[Cu(edta)] strandard, the copper concentration of which was determined by plasma emission spectroscopy.

References

(1) Wang, E.; Feigon, J. In *Hand Book of Nucleic Acids Structure*; Neidle, S., Ed.; Oxford University Press: 1998, p 355-388.
(2) Frankkamenetskii, M. D.; Mirkin, S. M. *Annu. Rev. Biochem.* **1995**, *64*, 65-95.
(3) Plum, G. E.; Park, Y. W.; Singleton, S. F.; Dervan, P. B.; Breslauer, K. J. *Proc. Natl. Acad. Sci.* **1990**, *87*, 9436-9440.
(4) Rahman, S. M. A.; Seki, S.; Obika, S.; Haitani, S.; Miyashita, K.; Imanishi, T. *Angew. Chem., Int. Ed.* **2007**, *46*, 4306-4309.
(5) Wittung, P.; Nielsen, P.; Norden, B. *J. Am. Chem. Soc.* **1997**, *119*, 3189-3190.
(6) Nielsen, P. E.; Egholm, M.; Berg, R. H.; Buchardt, O. *Science* **1991**, *254*, 1497-500.
(7) Egholm, M.; Buchardt, O.; Nielsen, P. E.; Berg, R. H. *J. Am. Chem. Soc.* **1992**, *114*, 1895-1897.
(8) Betts, L.; Josey, J. A.; Veal, J. M.; Jordan, S. R. *Science* **1995**, *270*, 1838-1841.
(9) Ihara, T.; Ishii, T.; Araki, N.; Wilson, A. W.; Jyo, A. *J. Am. Chem. Soc.* **2009**, *131*, 3826-3827.
(10) Takezawa, Y.; Maeda, W.; Tanaka, K.; Shionoya, M. *Angew. Chem., Int. Ed.* **2009**, *48*, 1081-4.
(11) Tanaka, K.; Yamada, Y.; Shionoya, M. *J. Am. Chem. Soc.* **2002**, *124*, 8802-8803.
(12) Sharma, S. K.; McLaughlin, L. W. *J. Inorg. Biochem.* **2004**, *98*, 1570-1577.
(13) Wiederholt, K.; McLaughlin, L. W. *Nucleic Acids Res.* **1999**, *27*, 2487-2493.
(14) Popescu, D.-L.; Parolin, T. J.; Achim, C. *J. Am. Chem. Soc.* **2003**, *125*, 6354-6355.
(15) Franzini, R. M.; Watson, R. M.; Patra, G. K.; Breece, R. M.; Tierney, D. L.; Hendrich, M. P.; Achim, C. *Inorg. Chem.* **2006**, *45*, 9798-9811.
(16) Watson, R. M.; Skorik, Y. A.; Patra, G. K.; Achim, C. *J. Am. Chem. Soc.* **2005**, *127*, 14628-14639.
(17) Kettle, S. F. In *Physical Inorganic Chemistry-A Coordination Chemistry Approach*; Oxford University Press: 1998, p 78-79.
(18) Pilch, D. S.; Breslauer, K. J. *Proc. Natl. Acad. Sci. U. S. A.* **1994**, *91*, 9332-6.
(19) Ma, Z.; Skorik, Y. A.; Achim, C. *Inorg. Chem.*, submitted.
(20) Martell, A. E.; Smith, R. M. *Critical Stability Constants, Vol. 2.*; Plenum Press: New York and London, 1975.
(21) Ratilainen, T.; Holmen, A.; Tuite, E.; Haaima, G.; Christensen, L.; Nielsen, P. E.; Norden, B. *Biochemistry* **1998**, *37*, 12331-12342.
(22) Jorgensen, C. K. *Adv. Chem. Phys.* **1963**, *5*, 33-146.
(23) Sone, K.; Krumholz, P.; Stammreich, H. *J. Am. Chem. Soc.* **1955**, *77*, 777-80.
(24) Noack, M.; Gordon, G. *J. Chem. Phys.* **1968**, *48*, 2689-99.

(25) Marov, I. N.; Belyaeva, V. K.; Smirnova, E. B.; Dolmanova, I. F. *Inorg. Chem.* **1978**, *17*, 1667-9.
(26) Garribba, E.; Micera, G.; Sanna, D.; Strinna-Erre, L. *Inorg. Chim. Acta* **2000**, *299*, 253-261.
(27) Hendrich, M. P.; Petasis, D.; Arciero, D. M.; Hooper, A. B. *J. Am. Chem. Soc.* **2001**, *123*, 2997-3005.

Chapter 5 Structure of Q-modified PNA

5.1 Introduction

The incorporation of metal ions into nucleic acids has attracted intense attention during the past decade due to its potential applications in molecular electronics.[1-3] In particular, DNA has been employed as a scaffold for transition metal ions because of the diversity of accessible structures it can form, such as duplexes, triplexes, quadruplexes, or hairpins. The diversity of topologies of these structures may be exploited in the future to attain novel electronic and magnetic properties and possibly fabricate DNA-based nanodevices. In addition to DNA, other nucleic acid analogues such as peptide nucleic acid (PNA)[4-6] and glycol nucleic acid (GNA) have been used as metal scaffolds.[7]

Although a variety of metal ions has been selectively incorporated into nucleic acids, there is limited information regarding the structure of metal-containing nucleic acids. Three crystal structures have been reported to date. Schultz reported a crystal structure of a DNA duplex containing a Dipic-Cu^{2+}-Py DNA alternative base pair. Cu^{2+} adopts a distorted octahedral coordination in this duplex.[8] Meggers reported the crystal structure of an (*S*)-GNA duplex with two Cu^{2+}-hydroxypyridone base pairs.[9] Very recently, Muller reported a NMR solution structure of a DNA duplex with three consecutive Ag^{+}-imidazole nucleotides.[10]

Our research focus is on the synthesis of metal-containing PNA. PNA is one of the best synthetic analogues of DNA due to its advantages of higher stability, higher specificity and resistance to enzyme degradations.[11] In our past research, transition metal ions such as Ni^{2+} and Cu^{2+} have been incorporated into the 2,2-bipyridine(**Bpy**)- and 8-hydroxyquinoline(**Q**)-modified PNA duplexes.[4-6] In terms of structural characterization of PNA, a NMR solution structure of PNA duplex, a structure of a γ-modified PNA duplex, and a crystal structure of a PNA duplex with or without **Bpy** modifications have been reported.[12-14] Interestingly,

in the **Bpy**-modified PNA duplex, the two **Bpy** ligands of the **Bpy**-modified PNA duplex were bulged out of the duplex. This phenomenon is related to the fact that the two bipyridines of a duplex can not form hydrogen bonding with each other.

In addition to **Bpy**, **Q** has found to be a good ligand for metal incorporation in PNA. Cu^{2+} forms complexes with Q that have high stability constant, are square planar and neutral. EPR spectra of Cu^{2+}-containing Q-PNA duplexes have confirmed that the [Cu**Q**$_2$] complex formed with the PNA duplexes has a square-planar geometry similar to that determined by X-ray crystallography for the synthetic [CuQ_2] complex. The Cu**Q**$_2$ complex in PNA would be better accommodated in the duplex if it had a cis-structure (Figure 5.1a). However, all the crystal structures of [Cu**Q**$_2$] complexes showed a trans-structure (Figure 5.1b).[15]

In order to better understand the coordination of Cu^{2+} with Q-PNA duplexes, we present in this chapter EPR spectra of Cu^{2+}-containing Q-PNA duplexes and compare them to the spectra of trans-[Cu**Q**$_2$] and of a recently reported synthetic complex, $Cu_2(ipdq)_2$ (ipdq=2,2'-isopropylidenedi-8-quinolinol, see Figure 5.1c) in which the Cu^{2+}coordination is cis-[CuQ_2] because the two **Q** ligands are connected to each other. We also analyze the crystal structure of a 9-base pair PNA duplex with a central **Q** ligand (H-GGCA**Q**TGCC-Lys-NH_2) obtained in the presence of excess Cu^{2+}.

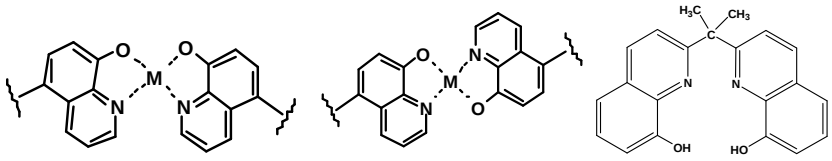

a b c

Figure 5.1. Structure of a. cis-CuQ_2; b. trans-CuQ_2; c.ipdq.

5.2 Results and Discussions

The crystal structure of a Cu^{2+}-coordinated Q-PNA

Crystals of a 9-base pair PNA with a central **Q** (GGCA**Q**TGCC-Lys-NH_2) ligand modification were obtained in the presence of excess Cu^{2+} in solutions in pH 4 acetate buffer. The crystal structure contains duplexes in which the **Q** ligands are bulged out of the duplex and form by π-stacking inter-duplex dimers (Figure 5.2b). Five Cu^{2+} ions are coordinated to each duplex, with three of the Cu^{2+} ions forming an inter-duplex trinuclear Cu^{2+} complex coordinated to the pair of **Q** ligands and two Cu^{2+} ions being coordinated to the guanines situated close to each end of the duplex.

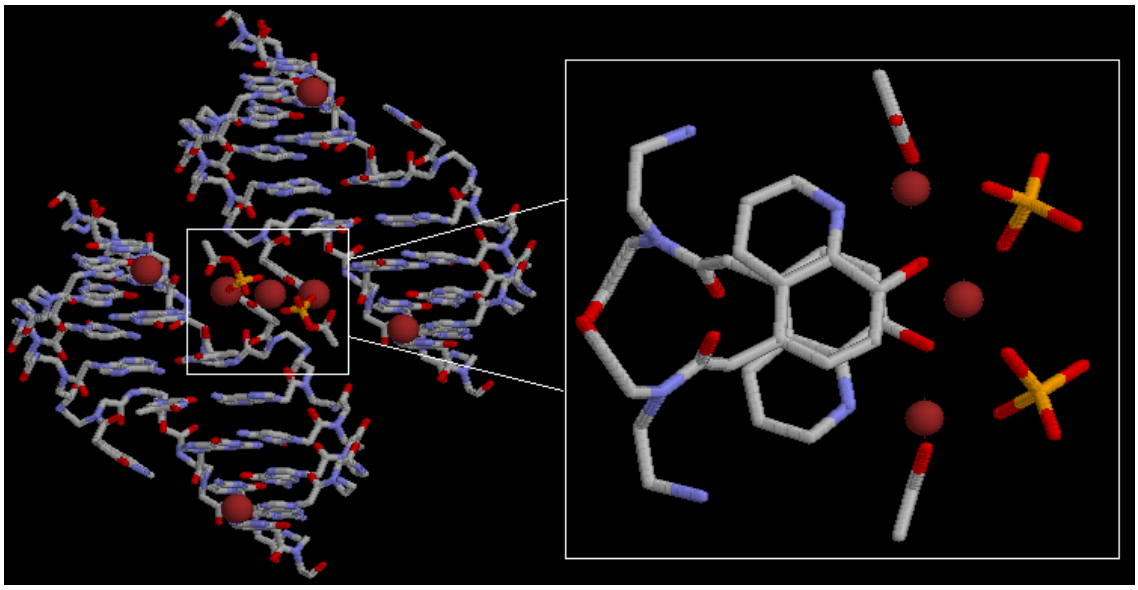

Figure 5.2. Pair of Q-PNA duplexes and expanded view (left) and tri-Cu^{2+} center (right) in the in the **HQ**-9-base pair PNA crystal.

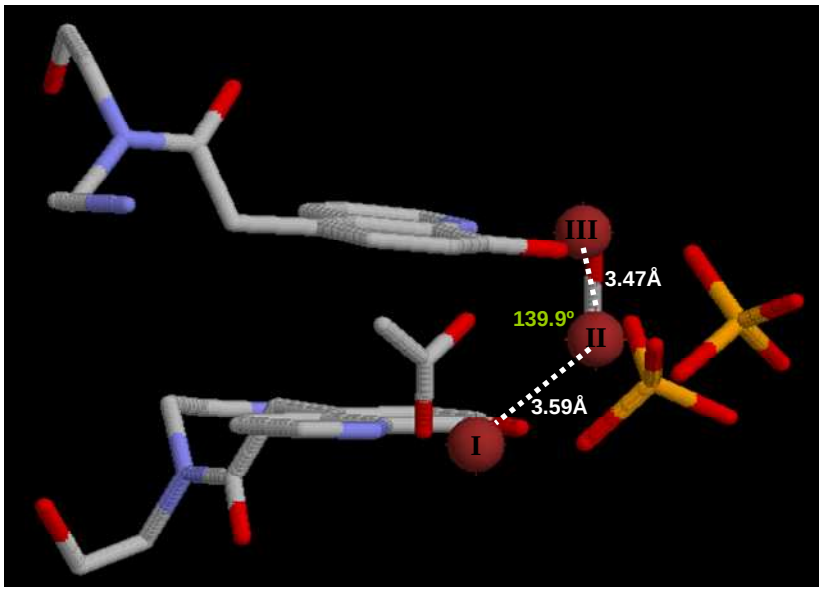

Figure 5.3. Three **HQ**-coordinated Cu^{2+} ions I (close to duplex AB), II (central) and III (close to duplex XY) in the **HQ**-9-base pair PNA crystal.

The two outer Cu^{2+} ions of the trinuclear cluster have identical square planar coordination formed by the oxygen and nitrogen atoms of one **Q** ligand, and one oxygen atom from a μ_1-acetate and another one from a phosphate group (Figure 5.4). These four donor atoms are almost coplanar. The central Cu^{2+} ion has a tetrahedral coordination geometry of four oxygen atoms, two of which belong to the **Q** ligands and two originate from acetate groups (Figure 5.5). The pairwise Cu-Cu distance in this cluster is ~3.5 Å (Figure 5.3).

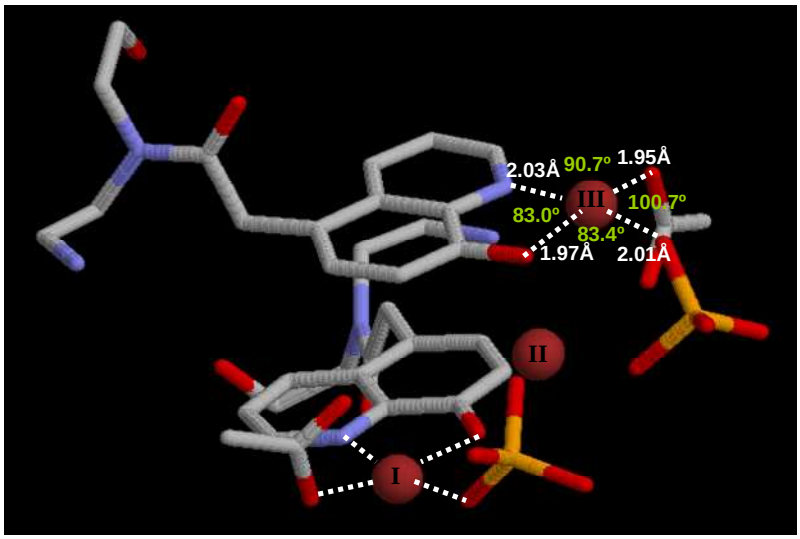

Figure 5.4. Square planar coordination of terminal Cu^{2+} ions of the trinuclear cluster.

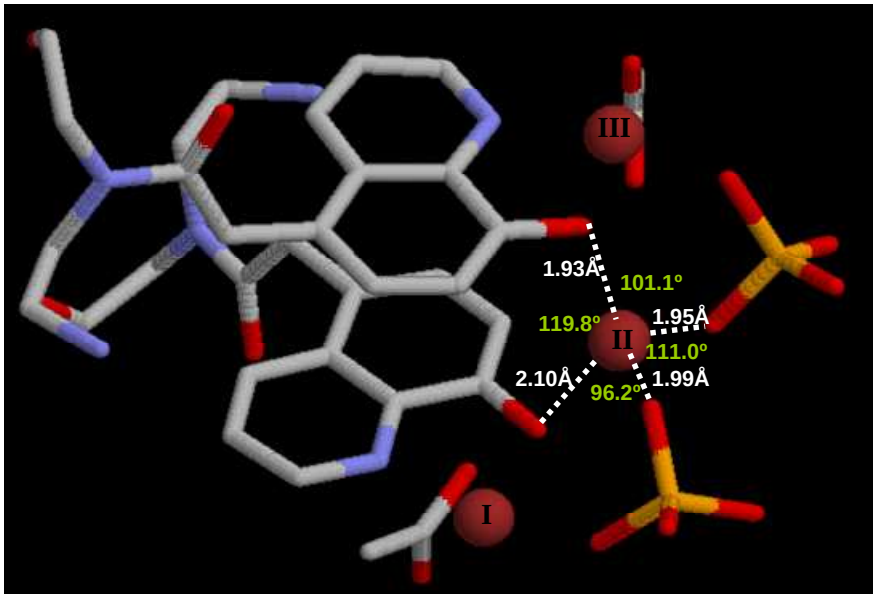

Figure 5.5. Tetrahedral coordination of central Cu^{2+} ion of the trinuclear cluster.

The helical parameters for the Cu^{2+}-coordinated **Q-**PNA duplex are similar to those of the unmodified 6-base pair PNA[16] and of the Bpy-modified 9-base pair PNA[12] and are indicative of a characteristic P-form helix (Table 5.1). The twist in the Cu^{2+}-coordinated, Q-PNA is comparable to that observed for the 6-base pair PNA. The duplex (with the central **Q** eliminated during calculation) has an overall smaller displacement (5.49 Å) and a larger inclination (8.84º) with respect to the global axis than those of the unmodified 6 base pair PNA crystal (8.3 Å and 0.3º, respectively). These parameter changes are similar to those previously observed for the Bipy-PNA duplex and cause the duplex to be slightly compressed along the duplex axis and to have a larger twist around the modification site (Table 5.2).

The two half-duplexes that flank the Q ligands have identical helical parameters except for the tilt angle, which has opposite sign in the two halves (Table 5.1). The rise and displacement are comparable to those of a non-modified PNA,[16] while the inclination and tilt are large. The twist for the two half-segments is smaller than for a non-modified PNA, suggesting a more unwound

helix. As shown in Figure 5.6, the overall helix kink angle of the duplex is 46.65º, which is slightly smaller than that measured for the Bpy-PNA duplex (53.99º).[12]

Table 5.1. Helical parameters calculated from half-segments or the whole duplex of **Q**-9-base pair PNA.

Duplex	**Helical sense**	**Disp. (Å)**	**Rise (Å)**	**Inclination (º)**	**Tilt (º)**	**Twist* (º)**	**Propeller (º)**
Q-9-base pair duplex							
half 1 (line [a])	R	7.26	3.25	5.05	6.90	17.67	-7.83
half 2 (line)	R	7.26	3.25	5.05	-6.90	17.67	-7.83
whole (Q deleted, mini)	R	5.49	3.04	8.84	0.00	**19.09**	-7.60
6mer[16]	R	8.3	3.2	0.3	1.0	19.8	/
Bpy-9-base pair[12]							
half 1 (line)	R	-4.01	4.08	-24.81	5.54	20.24	-5.62
half 2 (line)	R	-4.00	4.08	-24.81	-5.54	20.24	-5.62
whole (bipy deleted, mini)	R	-3.27	3.66	-20.03	0.0	**20.45**	-5.65

[a] line indicates that a linear helical axis is chosen, while mini indicates that a curvilinear helical axis is chosen when calculating helical parameters.

Table 5.2. Stepwise rise and twist values of the **Q**-9-base pair (The **Q** between T and A is eliminated)

BP interval	**Rise (Å)**	**Tilt (º)**
G/G	3.8	18.85
C/G	3.29	17.52
A/C	2.18	18.46
T/A	**2.75**	**43.05**
G/T	2.18	18.46
C/G	3.29	17.52
C/C	3.8	18.85

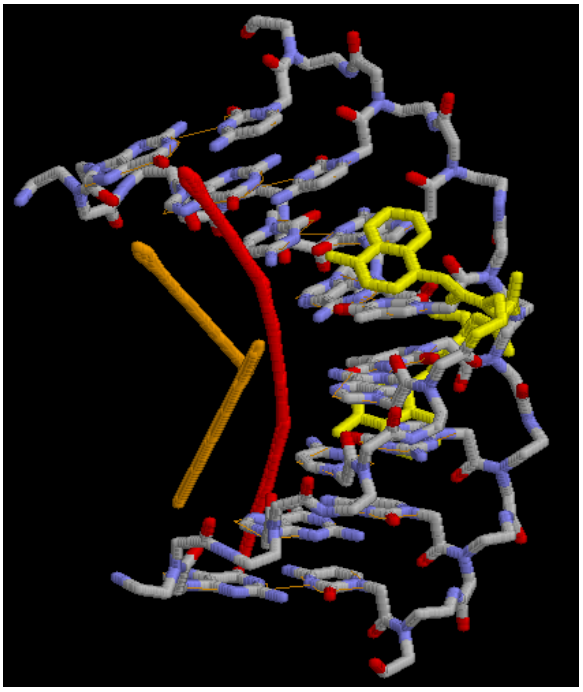

Figure 5.6. The curvilinear global axis of the **HQ**-9-base pair (red) and linear global axis of the two half-segments (orange). The **HQ** ligands are labeled in yellow.

EPR of Cu^{2+}-Q-PNA, CuQ_2 and $Cu_2(ipdq)_2$

The compound $Cu_2(ipdq)_2$ was synthesized according to reported methods.[17,18] We have measured the crystal structure of this complex (Figure 5.7).

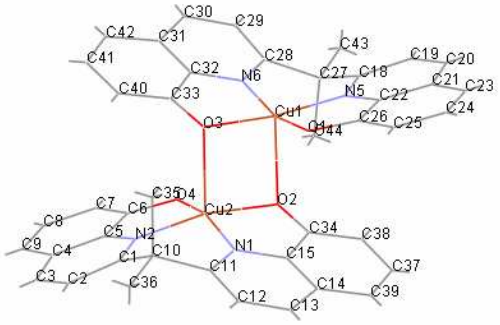

Figure 5.7. Crystal structures of $Cu_2(ipdq)_2$.

The EPR spectrum of $Cu_2(ipdq)_2$ in acetonitrile was recorded and compared to EPR spectra of 1:1 solutions of Cu^{2+} and the palindromic duplex

(GGCA**Q**TGCC-Lys-NH_2)$_2$ (Figure 5.8 and Table 5.3). All the EPR spectra show g values $g_1 \sim g_2 < g_3$ typical of an axial Cu^{2+}coordination, such as square planar or axially-distorted octahedral, suggesting that Cu^{2+} coordinates to a pair of 8-hydroxyquinolines. The superhyperfine structure of EPR spectra observed for Cu^{2+} complexes with both ipdq and with the duplex (GGCAQTGCC-Lys-NH_2) indicates that two nitrogens are coordinated to Cu^{2+}. These spectral features support the coordination of Cu^{2+} to two 8-hydroxyquinolines. However, the similarity of g and A values for these complexes and for [CuQ_2] prevented us from ascertaining that the CuQ_2 complexes formed with the Q-PNA duplex is cis- or trans.

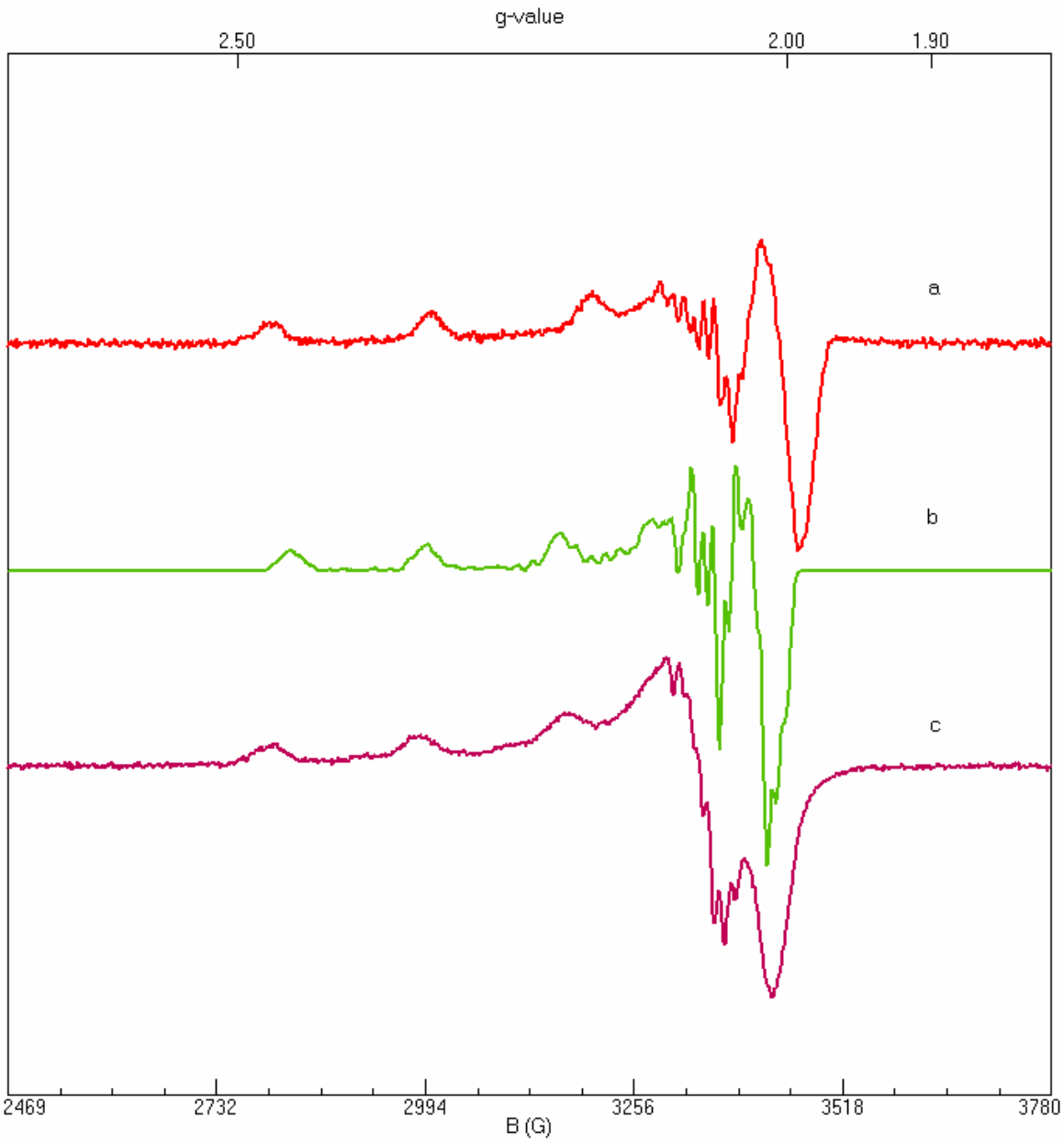

Figure 5.8. Perpendicular mode X-band EPR spectrum of a. 1:2 Cu^{2+} and GGCA**Q**TGCC-Lys-NH_2 in pH 7.0 10 mM sodium phosphate buffer with 25% glycerol; b. simulated EPR of Cu$\mathbf{Q}_2$ using parameters listed in Table 5.3; c. $Cu_2(ipdq)_2$ solution in 1:1 acetonitrile and pH 7.0 10 mM sodium phosphate buffer with 25% glycerol. T 20 K, frequency 9.65 GHz, microwave power 0.02 mW, modulation amplitude 6.676 G.

Table 5.3. EPR Parameters for $[CuQ_2]$ complexes

	[Cu(ipdq)] MeCN	Cu+ Q-PNA	$[CuQ_2]$[19]
g_1	2.06	2.06	2.06
g_2	2.05	2.05	2.06
g_3	2.24	2.22	2.24
A_1 (MHz)	72	72	72
A_1 (MHz)	80	80	72
A_1 (MHz)	560	611	530
A_{1N} (MHz)	39	39	39
A_{2N} (MHz)	32	32	33
A_{3N} (MHz)	36	36	33

In summary, a crystal structure of a 9-base pair PNA with a central **Q** ligand modification is obtained in the presence of excess Cu^{2+}. Due to the unfavorable condition of crystallization at pH 4.0 and with excess Cu^{2+}, metal coordination is outside the PNA duplex. An unusual Cu trinuclear cluster bridges two duplexes and excess Cu^{2+} is coordinated to terminal nucleobases. The similarity between the EPR parameters for the $[CuQ_2]$ complexes with 8-hydroxyquinoline and ipdq precluded us from distinguishing between the possible cis- or trans-geometry of the complex formed by Cu^{2+} with Q-modified PNA duplexes.

5.3 Experiments

Materials

All reagents were obtained from commercially available sources, were of analytical grade quality, and were used without further purification. ^1H NMR spectra were recorded on a Bruker Cryospec WM 300. A Finnegan Mattson instrument was used for electrospray mass spectrometry (ES-MS). An Applied Biosystems Voyager Biospectrometry Workstation with Delayed Extraction was used for MALDI-TOF mass spectrometry.

Synthesis of $Cu_2(ipdq)_2$

The synthesis of ipdq and $Cu_2(ipdq)_2$ was according to the reported methods.[17,18]

EPR Spectroscopy.

EPR spectra were recorded on an X-band (9 GHz) Bruker ESP 300 spectrometer equipped with an Oxford ESR 910 cryostat. The microwave frequency was calibrated with a frequency counter and the magnetic field with a NMR gaussmeter. The temperature was calibrated using devices from Lake Shore Cryonics. Spectra were collected under nonsaturating conditions. Samples were prepared in pH 7.0 10 mM sodium phosphate buffer with 25% glycerol as glassing agent. Samples containing PNA and Cu^{2+} in appropriate molar ratio were heated at 95 °C for 10 min, slowly cooled to room temperature, and then transferred into EPR tubes and frozen. EPR spectra were simulated using the program SpinCount written by Prof. Michael P. Hendrich.[20] Spin quantitation was done relative to a 0.499 mM Na_2[Cu(edta)] standard, the copper concentration of which was determined by plasma emission spectroscopy.

References

(1) Mueller, J. *Eur. J. Inorg. Chem.* **2008**, 3749-3763.
(2) He, W.; Franzini, R. M.; Achim, C. *Prog. Inorg. Chem.* **2007**, *55*, 545-611.
(3) Clever, G. H.; Kaul, C.; Carell, T. *Angew. Chem. Int. Ed.* **2007**, *46*, 6226-6236.
(4) Franzini, R. M.; Watson, R. M.; Patra, G. K.; Breece, R. M.; Tierney, D. L.; Hendrich, M. P.; Achim, C. *Inorg. Chem.* **2006**, *45*, 9798-9811.
(5) Watson, R. M.; Skorik, Y.; Patra, G. K.; Achim, C. *J. Am. Chem. Soc.* **2005**, *127*, 14628-14639.
(6) Popescu, D.-L.; Parolin, T. J.; Achim, C. *J. Am. Chem. Soc.* **2003**, *125*, 6354-6355.
(7) Meggers, E.; Zhang, L. *Acc. Chem. Res.* **2010**, *43*, 1092-1102.
(8) Atwell, S.; Meggers, E.; Spraggon, G.; Schultz, P. G. *J. Am. Chem. Soc.* **2001**, *123*, 12364-12367.
(9) Schlegel, M. K.; Essen, L. O.; Meggers, E. *J. Am. Chem. Soc.* **2008**, *130*, 8158-+.
(10) Johannsen, S.; Megger, N.; Bohme, D.; Sigel, R. K. O.; Muller, J. *Nature Chem.* **2010**, *2*, 229-234.
(11) Nielsen, P. E.; Egholm, M.; Berg, R. H.; Buchardt, O. *Science* **1991**, *254*, 1497-500.
(12) Yeh, J. I.; Pohl, E.; Truan, D.; He, W.; Sheldrick, G. M.; Du, S. C.; Achim, C. *Chem.--Eur. J.* **2010**, *16*, 11867-11875.
(13) He, W.; Crawford, M. J.; Rapireddy, S.; Madrid, M.; Gil, R. R.; Ly, D. H.; Achim, C. *Mol. Biosyst.* **2010**, *6*, 1619-1629.
(14) He, W.; Hatcher, E.; Balaeff, A.; Beratan, D. N.; Gil, R. R.; Madrid, M.; Achim, C. *J. Am. Chem. Soc.* **2008**, *130*, 13264-13273.
(15) Palenik, G. J. *Acta Cryst.* **1964**, *17*, 687-95.
(16) Rasmussen, H.; Kastrup, J. S.; Nielsen, J. N.; Nielsen, J. M.; Nielsen, P. E. *Nat. Struct. Biol.* **1997**, *4*, 98-101.
(17) Deraeve, C.; Boldron, C.; Maraval, A.; Mazarguil, H.; Gornitzka, H.; Vendier, L.; Pitie, M.; Meunier, B. *Chem.--Eur. J.* **2008**, *14*, 682-696.
(18) Yamamoto, Y.; Miura, A.; Kawamata, A.; Miura, M.; Takei, S. *Bull. Chem. Soc. Jpn.* **1978**, *51*, 3489-95.
(19) Walker, F. A.; Sigel, H.; McCormick, D. B. *Inorg. Chem.* **1972**, *11*, 2756-63.
(20) Hendrich, M. P.; Petasis, D.; Arciero, D. M.; Hooper, A. B. *J. Am. Chem. Soc.* **2001**, *123*, 2997-3005.